MICROSTRUCTURAL CHARACTERIZATION OF SIMULATED PLASTIC-BONDED EXPLOSIVES

By

JOHN DAVID YEAGER

A dissertation submitted in partial fulfillment of
the requirements for the degree of

DOCTOR OF PHILOSOPHY

WASHINGTON STATE UNIVERSITY
School of Mechanical and Materials Engineering

AUGUST 2011

To the Faculty of Washington State University:

The members of the Committee appointed to examine the dissertation of JOHN DAVID YEAGER find it satisfactory and recommend that it be accepted.

_____
David F. Bahr, Ph.D., Chair

_____
David P. Field, Ph.D.

_____
Daniel E. Hooks, Ph.D.

_____
Indranath Dutta, Ph. D.

ACKNOWLEDGEMENTS

I have been fortunate in love and life and would like to acknowledge several people and groups. First, and most importantly, I must thank my wife for her love and support over the years. Adria, you are amazing. Second, I want to thank Dr. Bahr for his guidance and support over the years, as well as for his friendship. I also wish to thank Dan Hooks and Kyle Ramos for endless discussion, collaboration and advice. I'd also like to thank several other people from Los Alamos National Laboratory. In particular, I'd like to thank Andrew Dattelbaum for use of his lab space as well as assistance with ellipsometry measurements and analysis. Cheng Liu, Philip Rae, Bruce Orler, Dana Dattelbaum, Brian Jensen, Sheng Luo, Tim Pierce, and Tate Hamilton all contributed to this dissertation in ways ranging from sample preparation to experiment planning to funding. I have been fortunate to work at Los Alamos National Laboratory over the last few years while completing this thesis and should acknowledge several facilities. This work benefited from the use of the Lujan Neutron Scattering Center at LANSCE funded by the DOE Office of Basic Energy Sciences and Los Alamos National Laboratory under DOE Contract DE-AC52-06NA25396. This work was performed, in part, at the Center for Integrated Nanotechnologies, a U.S. Department of Energy, Office of Basic Energy Sciences user facility. Los Alamos National Laboratory, an affirmative action equal opportunity employer, is operated by Los Alamos National Security, LLC, for the National Nuclear Security Administration of the U.S. Department of Energy under contract DE-AC52-06NA25396.

MICROSTRUCTURAL CHARACTERIZATION OF SIMULATED

PLASTIC-BONDED EXPLOSIVES

Abstract

by John David Yeager, Ph.D.
Washington State University
August 2011

Chair: David F. Bahr

Plastic-bonded explosives (PBX) are highly complex molecular composites. Recent mechanical investigations of PBX properties, in particular deformation and failure under uniaxial and cyclic loading, have revealed microstructure-dependent fracture behavior. A methodology of characterizing the relationship between microstructure and mechanical properties of PBX materials has been developed and tested on simulated materials with particular focus on the interface. Synchrotron X-ray studies of molecular crystals, explosive binders and formulated simulant composites revealed some intriguing possibilities in real-time observation of cracks, bubbles, delamination, and void collapse during high-speed loading events. A surface energy and thermomechanical study of several molecular crystals, including explosives, and potential binder candidates revealed thermodynamic interactions were not likely to be more important than mechanical properties for insensitive explosives. Ellipsometry and neutron reflectometry were used to identify the interfacial structure of polymer-acetaminophen (an explosive simulant) composites. The crystal-polymer interfacial structure was altered by inclusion of a plasticizing agent – an important result considering the commonality of plasticizing polymers in PBX formulation. The difference in interfacial properties was also observed

mechanically with nanoindentation. Specifically, the plasticizer inhibited formation of a large, diffuse interface / interphase and resulted in a composite which was more likely to experience film delamination than the non-plasticized composite. The difference in mechanical behavior caused by the difference in interfacial structure has important implications for crack initiation and explosive sensitivity. Additionally, certain crystal-binder composites were investigated with a new delamination test, which, while preliminary, resulted in additional insights into fracture behavior. The methodology presented herein provides a pathway for studying PBXs, or similar composites, from the nano-scale to the macro-scale, both in terms of structure and processing, and shows important relationships between interfacial properties and mechanical behavior.

TABLE OF CONTENTS

ACKNOWLEDGEMENTS. III
ABSTRACT. IV
LIST OF TABLES. VIII
LIST OF FIGURES. IX

CHAPTER ONE: INTRODUCTION TO PLASTIC-BONDED EXPLOSIVES 1

1.1 Motivation 1

1.2 Background and Literature 2

1.3 Research Objectives 15

1.4 Overview of Thesis Organization 16

CHAPTER TWO: HIGH-SPEED X-RAY PHASE CONTRAST IMAGING FOR ANALYSIS OF SIMULATED PLASTIC-BONDED EXPLOSIVE MICROSTRUCTURE 22

2.1 Introduction 22

2.2 Sample Preparation 25

2.3 X-Ray Characterization Experiments 27

2.4 Results 30

2.5 Implications for Dynamic Experiments 40

2.6 Conclusions 42

CHAPTER THREE: SURFACE ENERGY, CALCULATED WORK OF ADHESION, AND THERMAL PROPERTIES FOR SEVERAL BINDERS AND CRYSTALS 45

3.1 Introduction 45

3.2 Materials and Methods 49

3.3 Results 54

3.4 Discussion 57

3.5 Conclusions 63

CHAPTER FOUR: EXAMINING CHEMICAL STRUCTURE AT THE INTERFACE BETWEEN POLYMER BINDERS & PHARMACEUTICAL CRYSTALS 67

4.1 Introduction.....67

4.2 Experimental Methods.....71

4.3 Results 76

4.4 Discussion 92

4.5 Conclusions 94

CHAPTER FIVE: MECHANICAL CHARACTERIZATION OF SIMULATED PLASTIC-BONDED EXPLOSIVE MATERIALS 98

5.1 Introduction.....98

5.2 Experimental.....101

5.3 Results & Discussion.....103

5.4 Conclusions 115

CHAPTER SIX: SUMMARY AND CONCLUSIONS 119

6.1 Microstructural Characterization.....119

6.2 Linking Structure and Chemistry to Mechanical Properties 120

6.3 Future Applications to PBX Formulations and Similar Composites 122

LIST OF TABLES

Table 2.1 List of Formulated Samples for PCI Study. 27

Table 3.1 Chemical structures and as-received form of fluoropolymers investigated..... 50

Table 3.2 Summary of test liquids & reference solids, energies in dyn/cm..... 53

Table 3.3 Thermodynamic properties of fluorinated homopolymers.. 56

Table 3.4 Summary of DSC results of the binders..... 56

Table 3.5 Advancing contact angles of test liquids on the binder films.. 57

Table 3.6 Surface energy of the polymer binders and work of adhesion to explosives... 58

Table 3.7 Experimentally determined surface energies from this study compared with literature values..... 59

Table 4.1 Dip-coating parameters and optical constants determined by ellipsometry..... 78

Table 4.2 Model parameters used for Estane – Acetaminophen samples……..... 80

Table 4.3 Data fitting parameters for the composite NR samples along with the goodness of fit..... 86

LIST OF FIGURES

Figure 1.1 Chemical structure of three common explosives used in plastic-bonded explosive formulations 3

Figure 1.2. Microstructure and distribution of particle sizes for PBX 9501.....5

Figure 1.3. Flowchart for absorption of mechanical and electrical energy in solid explosives, illustrating creation of hot spots and subsequent ignition in the absence of quenching.....6

Figure 1.4. Micrographs of PBX 9501, with crack highlighted.....8

Figure 1.5. Layered composite processed with and without annealing, showing the reflected neutron signal (left), the corresponding polymer chain geometry (middle), and the layer profile (right).....13

Figure 2.1. Microstructure of PBX 9501, showing a wide distribution of particle sizes and variability in crystal integrity.....23

Figure 2.2. Schematic of the experimental setup for PCI at APS 32ID-B.....29

Figure 2.3. PCI at the crystal edge for sucrose and acetaminophen 30

Figure 2.4. PCI within the bulk of PMMA and Estane, showing cracking and voids respectively. 31

Figure 2.5. Bicrystal interface resulting from bonding with water.....32

Figure 2.6. Crystal-epoxy-crystal interface observed by PCI in ENG-2. 33

Figure 2.7. ENG-3 sample characterized with absorption microtomography and synchrotron PCI. 34

Figure 2.8. X-ray tomography slice compared with optical microscopy and synchrotron PCI from specified locations in specimen PBS-1. 36

Figure 2.9. Non-doped and doped PBS samples observed by PCI. 38

Figure 2.10. Thin PBS samples observed by PCI. 39

Figure 3.1. Crystal structure of TATB shown parallel to the *ab*-plane (a), and perpendicular to the *ab*-plane.....47

Figure 3.2. A typical deionized water droplet on Kel-F 3700 film, illustrating the surface energies and work of adhesion from Eq. (3.1). 52

Figure 3.3. DSC data of ‘‘as-received” binder samples. 55

Figure 3.4 Wa between the studied binders and four molecular crystals 62

Figure 4.1. The chemical structures of Estane, acetaminophen, a dimer of sulfamerazine showing hydrogen bonding, and hydroxypropylcellulose. 70

Figure 4.2. Polarized light micrograph of the Estane film coating polycrystalline acetaminophen.. 73

Figure 4.3. Change in amplitude and phase of polarized light reflected from the Estane 5703 sample at 70°, along with the model fit. 77

Figure 4.4. Change in amplitude and phase of polarized light reflected at 70° from the acetaminophen-cellulose system, along with two models. 82

Figure 4.5. Partial FTIR spectra of nitroplasticized Estane, acetaminophen, and the layered sample. 83

Figure 4.6. Reflectivity vs. momentum transfer vector Q for the sample with NP/Estane coating acetaminophen.....85

Figure 4.7. Scattering length density profile for the Estane-acetaminophen layered sample, showing a thin layer of acetaminophen intermixing with the polymer 88

Figure 4.8. Scattering length density profile for the NP/Estane-acetaminophen layered sample, showing a thin layer of acetaminophen mixing with plasticizer at the interface .89

Figure 4.9. Scattering length density profile for the HPC-acetaminophen layered sample, showing chemistry as a function of depth into the sample. 90

Figure 4.10. Scattering length density profile for the HPC-sulfamerazine layered sample, showing chemistry as a function of depth into the sample. 91

Figure 5.1. Schematic of how nanoindentation can be used to understand crystal-crystal interactions in an idealized manner.....100

Figure 5.2. Schematic of island delamination test 101

Figure 5.3. Elastic modulus as a function of indentation depth and contact radius for Estane and plasticized Estane coating acetaminophen 104

Figure 5.4. Hardness as a function of indentation depth and contact radius for Estane and plasticized Estane coating acetaminophen.....104

Figure 5.5. Elastic modulus of composites re-plotted from Fig. 5.3, and plotted again with the Estane curve artificially offset to match initial increase in modulus 106

Figure 5.6. Post-indentation microscopy of NP/Estane-acetaminophen.....108

Figure 5.7. Post-indentation microscopy of Estane-acetaminophen.....110

Figure 5.8. Polarized light micrographs of Berkovich indents to 2000nm in the 400nm plasticized Estane film 111

Figure 5.9. Tensile strain along the longitudinal direction mapped over photographs of the Kel-F 800-glass sample at specified points in the loading history. 112

Figure 5.10. Tensile strain along the longitudinal direction mapped over photographs of the NP/Estane-acetaminophen sample at specified points in the loading history.....114

CHAPTER ONE

INTRODUCTION TO PLASTIC-BONDED EXPLOSIVES

This chapter presents an overview of plastic-bonded explosives, covering both historical and recent characterization of the microstructure and microstructural effects on mechanical and detonative properties. A brief outline of the rest of the dissertation is included in the last section.

1.1 Motivation

The goal of this project was to develop a methodology for characterizing the microstructure of plastic-bonded explosives (PBX) and similar molecular composites, and to relate such structure to mechanical properties, with particular attention to material failure. PBXs are composite materials designed for reliable use in industrial and military applications. They consist of highly loaded explosive crystals (often exceeding 85% by weight) in a compliant polymer matrix, commonly referred to as the "binder." The binder serves not only to provide physical stability to the explosive crystals but also to reduce sensitivity to mechanical or thermal insult. Understanding and predicting detonation and failure mechanisms in PBXs is a key area of research for the Department of Energy (DOE) and the Department of Defense (DoD). Defects within crystals, at the crystal-binder interface, in the partially-dissolved crystal-binder region, or within the binder itself may all contribute to "hot spot" formation and initiate deflagration or detonation in off-normal conditions. The microstructure of the PBX, and in particular the crystal-binder interface, plays an important role in failure. Defects, in particular voids and cracks, are important to understand not only for hot spot formation but also for explosive reliability and performance. A mesoscale interpretation of the microstructure and its contribution to PBX

properties is necessary to inform damage and mechanical behavior models and to design better explosives for future use. This project investigates the microstructural contributions to quasi-static PBX behavior, with focus on the crystal-binder interface. PBXs are difficult to study at the micro- or nano-scale with conventional techniques due to the complexity of the microstructure and the sensitivity of the materials. A successful characterization of the PBXs would involve the use of unique, innovative methods to gather information. This project uses state of the art characterization techniques in concert with novel mechanical testing to investigate the structure-properties relationship in these materials in an effort to more accurately predict material failure and to understand the fundamental behavior of explosives.

1.2 Background and Literature

1.2.1 Overview of Plastic-Bonded Explosives

Plastic-bonded explosives were originally developed to provide superior properties to conventional explosives such as TNT. Specifically, chemical stability, energy content, resistance to ignition (i.e. sensitivity) and ease of manufacture were all essential criteria for the new line of explosives [1]. Many early PBX's used cyclotrimethylene-trinitramine (RDX) or cyclotetramethylene-tetranitramine (HMX), which exhibited excellent chemical stability and energy density. More recent formulations use triaminotrinitrobenzene (TATB) because it is normally more insensitive, but under certain conditions TATB can exhibit thermal anisotropy and decreased mechanical and chemical stability [2]. The chemical structures of the three listed explosives are shown in Figure 1.1.

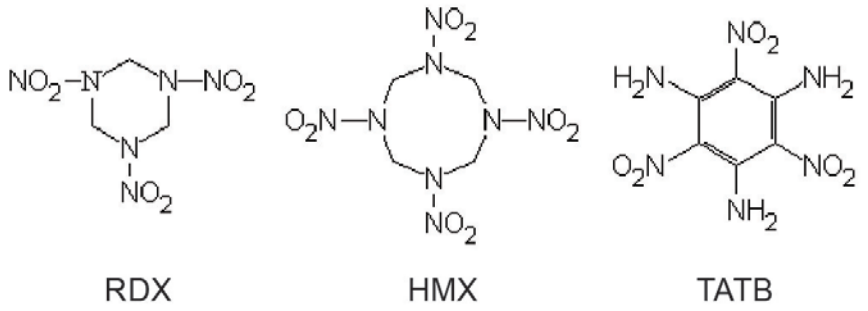

Figure 1.1 Chemical structure of three common explosives used in PBX formulations [3].

A judicious choice of binder can alleviate some of these sensitivity concerns and in general can allow for safe machining and handling of all explosive crystals. The ideal binder would be compliant enough to accommodate strain without detonation, provide mechanical stability, remain chemically stable in multiple environments and over time, all while avoiding negation of the useful explosive properties of the crystals. Early binders were somewhat energetic themselves in order to increase payload upon detonation, usually incorporating nitro- molecular groups. However, these nitropolymers tended to increase sensitivity and in most cases the resulting PBX's were deemed too unsafe for production [1].

Choosing a specific polymer for a binder is more complex than one might initially imagine [2]. Thermosets are often ruled out due to their insoluble cross-linking nature. Most elastomers exhibit suitable compliance for consideration, providing that the glass transition temperature (Tg) is lower than the operating temperature for the explosive. Fluorinated polymers have high chemical stability over a large range of temperatures, but the same characteristics which make them desirable from a safety standpoint can make them undesirable to manufacture – for example, polytetrafluoroethylene (PTFE) has excellent stability but a high melt viscosity and low

solubility in the usual solvents. Copolymerization is often used to adjust the problematic properties of the desired polymer. Additives also are commonly found in the binder, especially plasticizers to increase the compliance. For example, the binder in PBX 9501 (95% HMX, 5% binder by weight) is a copolymer (polyurethane and polyester) called Estane which is mixed with the nitroplasticizer bis-(2,2-dinitropropyl) acetal / formal (BDNPA/F) [4]. The nitroplasticizer increases the strain-to-failure for the PBX as well as contributing slightly to the energy density. However, simply attempting to create certain PBX properties by choosing an apparently suitable binder is not enough. Polymers which fail catastrophically via shear localization can sensitize the PBX, as well as those which exhibit low thermal conductivity or melting points [5]. Other binders have shown a tendency to create electrostatic discharges or other unexpected phenomena which increase sensitivity of the explosive [6]. In general, choosing an appropriate binder for a specific explosive is time-consuming and expensive, requiring exhaustive sensitivity testing prior to approval for manufacture [1].

Typical PBX processing begins with mixing explosive crystals in water, creating a suspension. The crystals are generally in the micron size range. Particle size and distribution has been shown to have an effect on PBX sensitivity and varies for each explosive [7, 8]. For example, PBX 9501 has a 3:1 ratio of coarse to fine HMX particles, while 9502 has a much narrower distribution of TATB crystals [9]. The dissolved polymer binder is then added to the suspension along with any other additives necessary for formulation. After some agitation and heating steps, the remaining solvent is drawn off, which allows for the binder to evenly coat the explosive crystals. The resulting polymer-coated-crystals act similarly to granules of molding powder, and hot isostatic or hydrostatic pressing is often used to form the explosive powder into useful shapes

such as cylinders or disks. The exact methodology of the process can have important effects on PBX density, which in turn influences the explosive characteristics of the PBX as well as the resistance to mechanical destabilization under stress [4]. A microstructure of a typical PBX manufactured in this method is shown in Figure 1.2.

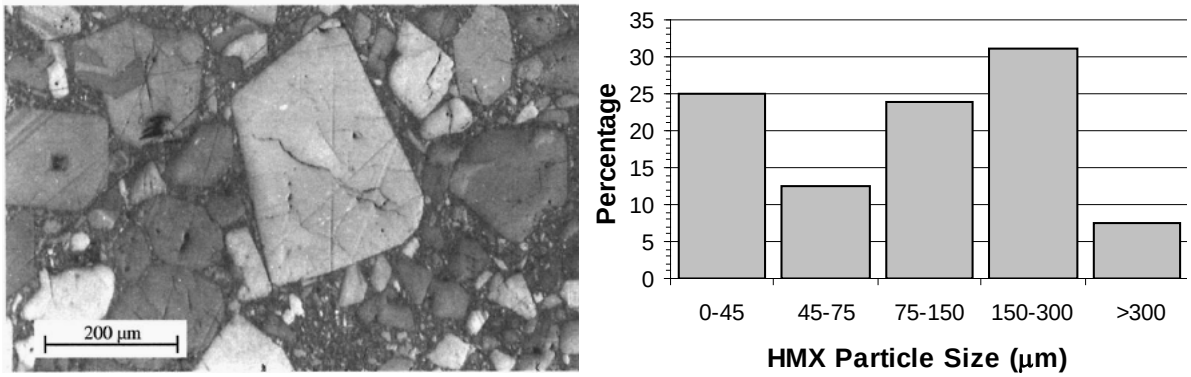

Figure 1.2. Microstructure and distribution of particle sizes for PBX 9501 [10]

Most PBX's are highly loaded (>85%) as illustrated in the figure. The figure shows PBX 9501, which is composed of 95% HMX crystals, 2.5% Estane binder, and 2.5% BDNPA/F nitroplasticizer by weight [2]. The high loading is desirable for maximizing energy content, though a balance must be found between energy and handling safety.

1.2.2 Microstructural Effects on Sensitivity and Performance

Sensitivity of a plastic-bonded explosive is often the defining safety characteristic and can loosely be described as how easily the PBX undergoes initiation of detonation. Material heterogeneity and damage define the initial conditions for which shock initiation processes are thought to occur. Additionally, non-shock processes including material failure, aging, and thermal reaction by deflagration are thought to initiate, progress, and be substantially influenced

by the chemistry and microstructure of the composite. Here, the physical processes thought to influence the initiation of deflagration and detonation are discussed. Usually the shock-induced detonation of an explosive is attributed to the formation of "hot spots," or local thermal zones which have much higher temperatures than the surrounding areas [5, 6, 11, 12]. Non-shock initiation may begin by similar mechanisms but this area is less well-understood. Field *et al* excellently summarized the principal theorized mechanisms for formation of hot spots, which in many cases form in regions of anisotropy, such as voids or dislocation pile-ups [5]. Other localized heating mechanisms include electrostatic discharge, cracking, adiabatic shear, and viscous binder heating due to grain motion under small mechanical loads. In general, ignition has been found to result from conversion of electrical or mechanical energy into thermal. Mellor created generalized flowcharts for initiation of explosives, which are reproduced here for clarity and trimmed for brevity in Figure 1.3.

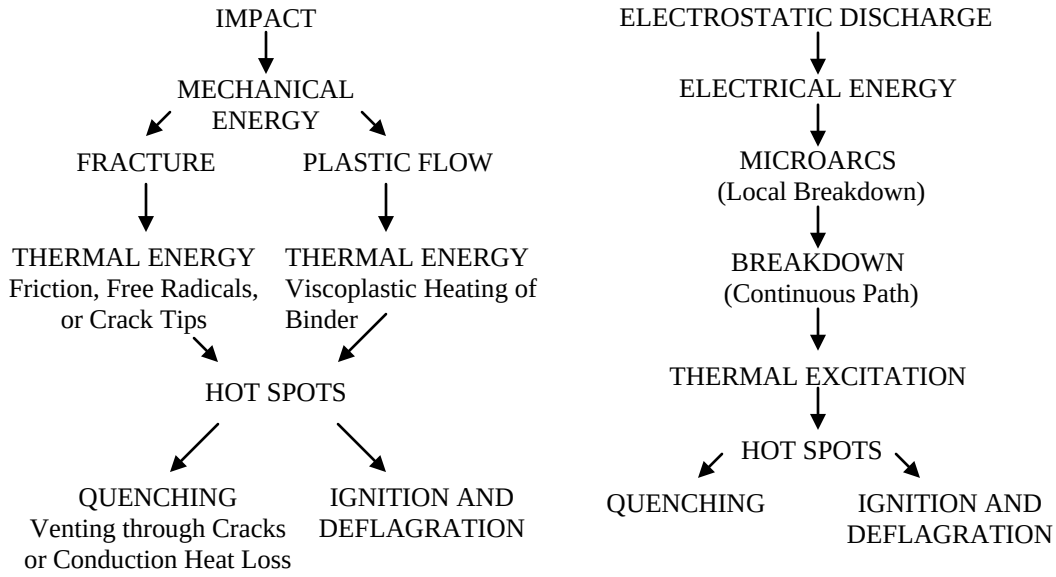

Figure 1.3. Flowchart for absorption of mechanical and electrical energy in solid explosives, illustrating creation of hot spots and subsequent ignition in the absence of quenching [6].

Field makes the important distinction between hot spots and *critical* hot spots, stating that the size and temperature of the hot spots are of crucial importance. Events which create localized hot zones may not necessarily be a danger to crystal ignition alone, though these subcritical events can add together to sensitize the explosive. For example, a crack propagating through a crystal may not cause ignition, but the two new faces of the crystal may subsequently rub under small mechanical stress and create enough friction to ignite. Indeed, Dienes modeled shear crack growth and found that the frictional heating resulting from cracking was the main contributor to low-pressure ignition [13]. However, this view is hardly a consensus. In general, any mechanism which generates hot spots presents a safety risk in handling PBX materials. Several researchers have attempted to quantify the critical size, temperature and duration of hot spots necessary for ignition; in particular, the work of Bowden and Yoffe has been of use and even validated by other experimental results [5]. They found that hot spots needed to be micron sized (~0.1 – 10μm), have temperatures of 400-500°C, and last for 10 – 1000 μs [14]. If one parameter is too low, the others must correspondingly be higher in order to cause ignition.

Crack formation is especially troubling for plastic-bonded explosives. Palmer investigated a variety of PBX formulations with tensile testing, finding a wide range of responses [15]. PBX 9501 and X-0298 are examples of explosives containing relatively large (150 μm avg.) HMX crystals in a soft, plasticized matrix, which exhibited ductile failure via stable crack growth. By contrast, a PBX made from micronized HMX in a polyethylene matrix snapped in a brittle manner. PBX's with micronized HMX particles tended to have higher tensile strengths than more coarsely distributed samples for the same binder. Palmer found that crack propagation

through the crystals was rare and generally confined to the stiff-binder samples, whereas interfacial crack growth tended to be the dominant failure mode. Rae continued Palmer's work on crack growth, and two micrographs from Rae's studies are shown in Figure 1.4 [16]. Fig. 1.4a highlights the growth of a crack along the interface (bold line) as well as the start of an interfacial crack on the right side of the largest crystal, while Fig. 1.4b confirms the interfacial nature of crack propagation.

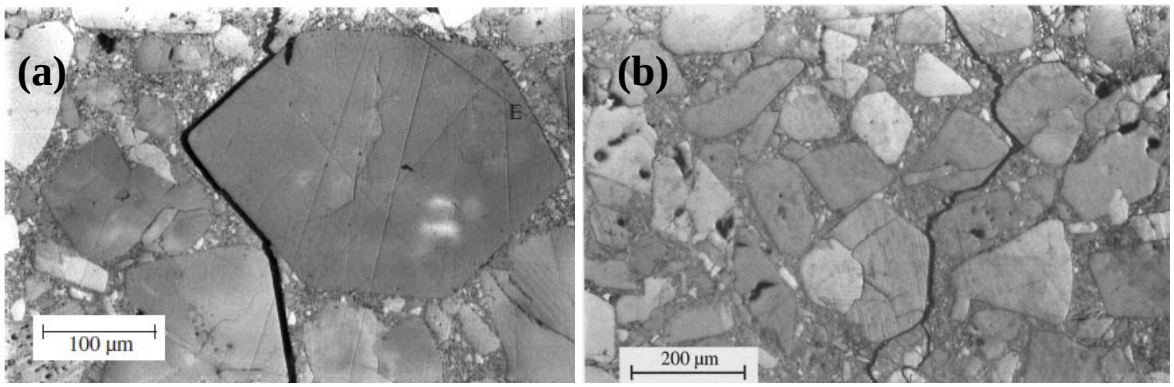

Figure 1.4. Micrographs of PBX 9501, with crack highlighted.

(a) Interfacial fracture along large crystal, with "E" as the start of another interfacial crack [16].

(b) Evidence of widespread interfacial fracture throughout the PBX [10].

Considering Dienes' finding that shear cracking in the crystal is the most sensitizing method of hot spot formation, interfacial failure may seem relatively safe by comparison. However, the cracking does create what are essentially large defects or voids. These regions of anisotropy are analogous to porosity in the PBX, which both increases sensitivity and deplanarizes the explosive front [17]. At best, more care must be taken when handling these damaged explosives.

At worst, the explosive may ignite at unexpectedly low temperatures or pressures, and certainly when employed intentionally will explode differently than designed.

1.2.3 Characterizing the Interface

Adhesion between the binder and the particles is one of the defining parameters in strain-to-failure and fracture toughness in particle-reinforced composites [18]. In some traditional composites, the fracture toughness may be increased by having poor adhesion between the fibers or particles and the matrix due to crack deflection [19]. Strong adhesion will increase the tensile strength of the material but may decrease the toughness. As seen earlier, the cracks in many PBX materials tend to propagate along the interface, indicating poor adhesion. It is possible that this mode of failure is relatively desirable in explosive materials to avoid cracking the crystals and creating critical hot spots. It may be most useful to increase adhesion enough to increase the strength but without changing the failure mode, if possible.

The adhesion between two materials relies on the properties of the interface [20]. The thermodynamic or true work of adhesion is defined as the increase in free energy of the system caused by the creation of two new surfaces, shown in Equation 1.1,

$$W_a = \gamma_{SV} + \gamma_{LV} - \gamma_{SL} \qquad (1.1)$$

where γ is the surface energy or tension, and the subscripts refer to the solid (S), the liquid (L), and the vapor or atmosphere (V). This expression was originally derived from Young's equation for equilibrium of a droplet on a surface,

$$\gamma_{LV}\cos\theta = \gamma_{SV} - \gamma_{SL} \qquad (1.2)$$

where θ is the angle the liquid droplet makes with the surface [21]. The surface energy is a useful property to measure and depends mainly on the types of chemical bonds and molecules at the surface. However, in most cases applied stresses are dissipated into other mechanisms than fracture, causing the measured adhesion to be many times higher than the true adhesion [22]. For durability purposes, the measured fracture energy, *G*, is the often the most useful property. Equation 1.3 shows the fracture energy as a function of true and practical adhesion,

$$G = W_a + \psi \qquad (1.3)$$

where ψ is the summation of plastic and other energy dissipation, or plastic adhesion [22]. The practical adhesion can be affected by many parameters, but some of the more common ones are addressed here. Using a fracture mechanics approach to define adhesion, the practical adhesion *G* is usually considered an energy release rate or crack extension force and is related to the fracture toughness of the material [20]. In general, any mechanism which slows down or stops crack propagation is considered to increase the fracture toughness of the material. For composite systems, the elastic mismatch between the two (or more) materials is a crucial component [23]. The mismatch affects the phase angle, or ratio of crack opening to crack shearing. A pure shearing mode results in higher toughness in the material.

The specific nature of the interface can also affect the crack propagation. The surface energies can influence the exact nature of the bonding between two materials [24]. The roughness of the adjoining materials also can greatly affect the adhesion by determining the total amount of surface area bonded – higher roughness generally indicates a tougher interface [25]. If the surfaces are very rough, some mechanical interlocking may also occur. One last adhesion concept of particular interest in composites with at least one component being relatively mobile is the interdiffusivity of the interface. The high mobility of many polymers even at room temperature can often result in creation of a new phase at the interface, consisting of a chemical mixture of the polymer and the less mobile material. This interphase region contributes to the fracture toughness. Wang found that the size and strength of this region affected stress transfer in a particle-reinforced polymer composite, and even determined whether the crack would propagate along the interface or through the matrix [26]. A thorough characterization of the explosive crystal – binder interface should provide insight into the measured mechanical properties of the PBX and ideally identify key properties which could be improved with different processing techniques.

A number of characterization techniques have been utilized to study the interface in plastic-bonded explosives. Unfortunately, many traditional methods are not easily applied to very sensitive systems with brittle components. One technique which generally avoids extensive sample preparation is small angle neutron scattering (SANS). It measures the amount of neutron scattering from a neutron source beam interacting with sample nuclei and gives very precise location resolution [27]. One useful aspect of applying this method to polymeric composites is the strong contrast that can be seen between the lighter elements, like nitrogen and hydrogen.

Use of X-rays or electrons instead of neutrons has some advantages, particularly the proportional relationship of scattering length to atomic number. Neutron scattering is ideal for differentiating between isotopes or very similar elements. Koberstein used X-ray scattering to investigate the morphology of a polyurethane block copolymer very similar to Estane, finding that the polymer consisted of hard and soft segments which tended to migrate when heated [28]. At certain temperature ranges the hard segments formed microcrystallites, something which could have implications on the stability of mechanical properties of the polymer during thermal processing. Another study used SANS on PBX 9501 to determine whether the nitroplasticized Estane had any similar phase separation [27]. The result was that the nitroplasticizer tended to associate with the soft segments in the binder instead of having even distribution throughout the polymer.. Additional SANS study on Estane indicated that when the original hard segment concentration was below 30 wt %, the polymer tended to undergo phase separation, with the hard segments migrating into spherical domains with a soft-segment rich shell [29]. The studies indicate that the binder as a whole is not as homogeneous as initially assumed.

A very similar technique with more relevance to the interface specifically is neutron reflectometry. Figure 1.5 illustrates the potential of this technique in identifying chemical structure, bonding and interphase formation. In the figure, a layered polymer structure was created by spin coating polymethylmethacrylate (PMMA) on a quartz substrate, then subsequently spinning layers of polystyrene and deuterated polystyrene. The reflectometry data, the assembled structure, and the profile of the layers is shown in the figure [27].

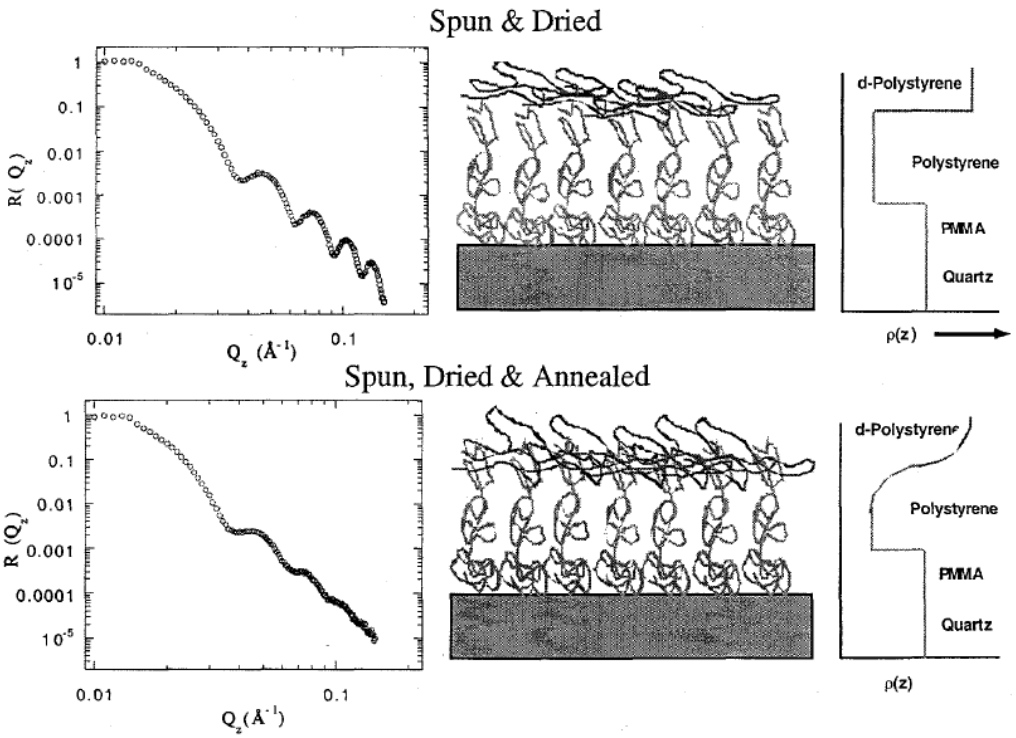

Figure 1.5. Layered composite processed with and without annealing, showing the reflected neutron signal (left), the corresponding polymer chain geometry (middle), and the layer profile (right). Of particular note is the detection of an interphase region forming between the deuterated and non-deuterated polystyrene after an annealing process [27].

1.2.4 Measuring the Interfacial Toughness

Several useful techniques exist for measuring the strength and toughness of the interface in polymer composites. However, the complexity of the plastic-bonded explosive, along with the safety concerns, renders most of the more common testing methods non-ideal. Simplification of the testing parameters would be extremely useful, as long as the simplified scenario adequately represents the true PBX conditions. One such modification could be analyzing the adhesion between only one crystal and the binder. Simple bimaterial interfaces have been studied

classically by many researchers [20, 23, 30-32]. Here attention is focused on interfaces between materials with large differences in elastic properties, such as with the stiff crystal and the compliant binder. This is a common occurrence in thin film systems such as flexible electronic devices. Traditional toughness testing usually relies on forcing a debonding of the film from the substrate. Nanoindentation of the film can induce blister or buckle formation, and combining measurements of the size of the new feature with known mechanical properties (e.g. modulus, residual stress, Poisson's ratio) of both the film and substrate can yield a good estimation of the fracture toughness [20, 33, 34]. Four point bend testing is another possible technique, where a crack propagates straight through the stiff layer and then deflects along the bimaterial interface [32, 35, 36]. This technique is usually used to measure a compliant film on a stiff substrate, but it has been used for the reverse case successfully as well [37]. In general, bimaterial adhesion testing requires either crack propagation or film delamination in order to measure adhesion.

The main problem with applying any of these techniques to the PBX, even to the simplified film system, is that the crystal would be required to withstand applied large stresses without plastic yield or (more likely) fracture. It may be possible to induce buckling or blistering of a binder film on the crystal substrate, and while polymer films do not tend to buckle in response to indentation, nanoindentation could be used to get an estimate of the fracture toughness [38]. A test which applies stress only to the binder but also causes debonding would be ideal, such as the island delamination scenario described by Lu [39]. The methodology and results of nanoindentation and island delamination as applied to simulated PBX materials will be detailed later in this thesis.

1.3 Research Objectives

This study will focus on characterization of plastic-bonded explosive materials both in terms of micro-scale to nano-scale structure and in terms of mechanical properties. Characterization of the plastic-bonded explosives is difficult not only for the reasons described earlier but also because of requisite safety and training for handling the materials. For this reason, simulants will be used for much of the experimentation in this thesis. The molecular crystal acetaminophen (also known as paracetamol) is a polymorph with stable monoclinic (Form I) or orthorhombic (Form II) crystal structure [40]. HMX is also a polymorph, but the stable phase at room temperature is monoclinic [41]. Sugar is another useful explosive crystal simulant for mechanical studies and will be studied also [42]. While much of the data obtained for simulant-binder characterization will be useful primarily for insights into likely PBX behavior, the end product should be a methodology which can then be used to study molecular composites ranging from pharmaceutical tablets to PBX formulations.

Obtaining a complete understanding of the PBX system will require detailed knowledge of the binder, the crystal, and the interface. The explosive crystals (RDX, HMX, and TATB) which will be simulated in this study have largely been characterized previously in terms of bulk thermal, mechanical and chemical properties. However, the surface characteristics have a critical role in determining the nature of the interface. Surface energy and roughness as a function of processing parameters should be investigated to gain some understanding of the crystal-binder interface. The polymer binders will be studied with a variety of thermal and mechanical techniques, including dynamic mechanical analysis (DMA), thermogravimetric analysis (TGA), tensile testing, ellipsometry and synchrotron x-ray or neutron characterization. High fidelity

information regarding the individual materials is critical for understanding the complex behavior of the composite. Composite property measurements will focus on the interface but bulk mechanical behavior data and insights into the formulation process would also be useful.

Initial study of the interface will begin at the thermodynamic level – specifically, the surface energies of the crystals and binders which then give insight into work of adhesion. Neutron scattering and reflectometry will be used to identify the chemical interactions present at the interface. Adhesion testing of these interfaces will be performed with the island delamination test in order to relate material structure to mechanical properties. Indentation testing will also be used to look at bimaterial properties. Initial exploratory nano- and micro-indentation will probe the characteristics of Estane-coated acetaminophen crystals. A variety of tip geometries and loading conditions will be tested in an attempt to induce film delamination. Nanoindentation will also be used to measure the modulus of the PBX as a function of distance from the hard crystals. Similar tests have been used elsewhere to determine the size and properties of an interphase region between a polymer and reinforcing fibers [43, 44].

1.4 Overview of Thesis Organization

This thesis is composed of several chapters which are substantially similar to journal articles in preparation, submission and review processes, or in publication. These chapters are organized in such a way as to lead the reader from fundamental investigations of molecular composite interfacial structure to complex mechanical behavior characterization in the later chapters. Ideally, the chapters will outline a methodology of characterizing molecular composites across time and length scales and in particular relating interfacial structure to critical material properties.

Chapter 2 contains results from synchrotron x-ray imaging of simulated PBX composites, illustrating the advantages and limitations of x-ray study at both static and dynamic (e.g. shock) loading rates. The study was submitted to *Composites Part A: Applied Science and Manufacturing* in May 2011 with the title "High-Speed X-Ray Phase Contrast Imaging for Analysis of Simulated Plastic-Bonded Explosive Microstructure." Chapter 3 presents a study on explosive and binder surface energies, discussing the relevance of each to formulation and performance while also investigating some relevant thermomechanical binder properties. It is taken largely from "Adhesive properties of some fluoropolymer binders with the insensitive explosive 1,3,5-triamino-2,4,6-trinitrobenzene (TATB)" published in the *Journal of Colloid and Interface Science* in 2010 [45]. Chapter 4 summarizes several ellipsometry and neutron reflectometry experiments which characterized the interfacial structure of several composites, including simulated PBXs and pharmaceutical tablets. It is similar to a paper recently accepted for publication in *Polymer* [46]. Chapter 5 is composed of parts from several papers in submission to pharmaceutical journals such as the *International Journal of Pharmaceutics*, and focuses on nanoindentation of Estane / Acetaminophen composites in an effort to mechanically characterize the interface which was observed in Chapter 4. Chapter 5 will also present some preliminary results from the island delamination test, providing insight into interfacial delamination and fracture toughness. Chapter 6 summarizes the thesis and provides a critical reflection on the feasibility and limitations of applying the approaches in this thesis to formulated PBX or pharmaceutical materials as well as application to mechanical deformation and failure models currently employed by the explosives community.

References

[1] E James. The Development of Plastic-Bonded Explosives. UCRL-12439-T. Livermore, CA: Lawrence Radiation Laboratory; 1965. p. 15.

[2] D Dattelbaum. Equations of State of Binders and Related Polymers. In: Peiris SM, Piermarini GJ, editors. Static Compression of Energetic Materials. Berlin: Springer Berlin; 2008.

[3] JT Rogers. Physical and Chemical Properties of RDX and HMX. Kingsport, TN: Holston Defense Corporation; 1962.

[4] B Olinger. Compacting Plastic-Bonded Explosive Molding Powders to Dense Solids Los Alamos, NM: Los Alamos National Laboratory; 2005. p. 43.

[5] JE Field, NK Bourne, SJP Palmer, SM Walley, J Sharma, BC Beard. Hot-Spot Ignition Mechanisms for Explosives and Propellants [and Discussion]. Philosophical Transactions: Physical Sciences and Engineering. 339 (1654), 1992, 269-83.

[6] AM Mellor, DA Wiegand, KB Isom. Hot spot histories in energetic materials. Combust Flame. 101 (1-2), 1995, 26-8.

[7] BA Khasainov, BS Ermolaev, HN Presles, P Vidal. On the effect of grain size on shock sensitivity of heterogeneous high explosives. Shock Waves. 7 (2), 1997, 89-105.

[8] A van der Steen, R Verbeek. Initiation and detonation of RDX and HMX HTPB-Based Plastic-Bonded Explosives. Propellants Explos Pyrotech. 15 (1), 1990, 19-21.

[9] CB Skidmore, DS Phillips, NB Crane. Microscopical Examination of Plastic-Bonded Explosives. Los Alamos National Laboratory, LA-UR-97-2738; 1997.

[10] PJ Rae, HT Goldrein, SJP Palmer, JE Field, AL Lewis. Quasi-Static Studies of the Deformation and Failure of β-HMX Based Polymer Bonded Explosives. Proceedings: Mathematical, Physical and Engineering Sciences. 458 (2019), 2002, 743-62.

[11] JG Bennett, KS Haberman, JN Johnson, BW Asay. A constitutive model for the non-shock ignition and mechanical response of high explosives. Journal of the Mechanics and Physics of Solids. 46 (12), 1998, 2303-22.

[12] GM Swallowe, JE Field. The Ignition of a Thin Layer of Explosive by Impact; the Effect of Polymer Particles. Proceedings of the Royal Society of London A Mathematical and Physical Sciences. 379 (1777), 1982, 389-408.

[13] JK Dienes. Frictional Hot-Spots and Propellant Sensitivity. Materials Research Society. Boston, MA1984. p. 373-81.

[14] FP Bowden, AD Yoffe. Initiation and Growth of Explosion in Liquids and Solids. Cambridge, UK: Cambridge University Press; 1952.

[15] SJP Palmer, JE Field, JM Huntley. Deformation, Strengths and Strains to Failure of Polymer Bonded Explosives. Proc R Soc London, Ser A. 440 (1909), 1993, 399-419.

[16] PJ Rae, SJP Palmer, HT Goldrein, JE Field, AL Lewis. Quasi-static studies of the deformation and failure of PBX 9501. Proc R Soc London, Ser A. 458 (2025), 2002, 2227-42.

[17] HL Berghout, SF Son, CB Skidmore, DJ Idar, BW Asay. Combustion of damaged PBX 9501 explosive. Thermochim Acta. 384 (1-2), 2002, 261-77.

[18] S-Y Fu, X-Q Feng, B Lauke, Y-W Mai. Effects of particle size, particle/matrix interface adhesion and particle loading on mechanical properties of particulate-polymer composites. Composites Part B: Engineering. 39 (6), 2008, 933-61.

[19] D Hull, TW Clyde. An Introduction to Composite Materials. In: D. R. Clarke SS, I. M. Ward, editor. Cambridge Solid State Science Series. 2nd ed. New York, NY: Cambridge University Press; 1996. p. 151-2.

[20] AA Volinsky, NR Moody, WW Gerberich. Interfacial toughness measurements for thin films on substrates. Acta Mater. 50 (3), 2002, 441-66.

[21] T Young. An Essay on the Cohesion of Fluids. Philos Trans R Soc London. 95, 1805, 65-87.

[22] DE Packham. Work of adhesion: contact angles and contact mechanics. Int J Adhes Adhes. 16 (2), 1996, 121-8.

[23] JW Hutchinson, Z Suo, WH John, YW Theodore. Mixed Mode Cracking in Layered Materials. Advances in Applied Mechanics: Elsevier; 1991. p. 63-191.

[24] KL Johnson, K Kendall, AD Roberts. Surface Energy and the Contact of Elastic Solids. Proceedings of the Royal Society of London Series A, Mathematical and Physical Sciences. 324 (1558), 1971, 301-13.

[25] J Comyn, C Philippe. Chapter 1 Theories of adhesion. Handbook of Adhesives and Sealants: Elsevier Science Ltd; 2006. p. 1-50.

[26] W Wang, K Sadeghipour, G Baran. Finite element analysis of the effect of an interphase on toughening of a particle-reinforced polymer composite. Oxford, ROYAUME-UNI: Elsevier; 2008.

[27] RP Hjelm. Neutron Scattering Techniques as Advanced Structural Probes Of Filled And Nanocomopsite Elastomers: A Technique For The 21st Century. American Chemical Society. Dallas, TX2000.

[28] JT Koberstein, TP Russell. Simultaneous SAXS-DSC study of multiple endothermic behavior in polyether-based polyurethane block copolymers. Macromolecules. 19 (3), 1986, 714-20.

[29] JT Mang, RP Hjelm, EB Orler, DA Wrobleski. Small-Angle Neutron Scattering of a Solvent-Swollen Segmented Polyurethane as a Probe of Solvent Distribution and Polymer Domain Composition. Macromolecules. 41 (12), 2008, 4358-70.

[30] Z Suo, JW Hutchinson. Sandwich test specimens for measuring interface crack toughness. Materials Science and Engineering: A. 107, 1989, 135-43.

[31] CF Shih. Cracks on bimaterial interfaces: elasticity and plasticity aspects. Materials Science and Engineering: A. 143 (1-2), 1991, 77-90.

[32] PG Charalambides, HC Cao, J Lund, AG Evans. Development of a test method for measuring the mixed mode fracture resistance of bimaterial interfaces. Mech Mater. 8 (4), 1990, 269-83.

[33] DF Bahr, JW Hoehn, NR Moody, WW Gerberich. Adhesion and acoustic emission analysis of failures in nitride films with a metal interlayer. Acta Mater. 45 (12), 1997, 5163-75.

[34] MJ Cordill, DF Bahr, NR Moody, WW Gerberich. Recent developments in thin film adhesion measurement. Device and Materials Reliability, IEEE Transactions on. 4 (2), 2004, 163-8.

[35] AG Evans, M Rühle, BJ Dalgleish, PG Charalambides. The fracture energy of bimaterial interfaces. Materials Science and Engineering: A. 126 (1-2), 1990, 53-64.

[36] RH Dauskardt, M Lane, Q Ma, N Krishna. Adhesion and debonding of multi-layer thin film structures. Engineering Fracture Mechanics. 61 (1), 1998, 141-62.

[37] JD Yeager, DJ Phillips, DM Rector, DF Bahr. Characterization of flexible ECoG electrode arrays for chronic recording in awake rats. Journal of Neuroscience Methods. 173 (2), 2008, 279-85.

[38] M Li, ML Palacio, C Barry Carter, WW Gerberich. Indentation deformation and fracture of thin polystyrene films. Thin Solid Films. 416 (1-2), 2002, 174-83.

[39] N Lu, J Yoon, Z Suo. Delamination of stiff islands patterned on stretchable substrates. International Journal of Materials Research. 98, 2007, 717-22.

[40] P Di Martino, P Conflant, M Drache, JP Huvenne, AM Guyot-Hermann. Preparation and physical characterization of forms II and III of paracetamol. J Therm Anal Calorim. 48 (3), 1997, 447-58.

[41] RK Weese, JL Maienschein, CT Perrino. Kinetics of the [beta] --> [delta] solid-solid phase transition of HMX, octahydro-1,3,5,7-tetranitro-1,3,5,7-tetrazocine. Thermochim Acta. 401 (1), 2003, 1-7.

[42] KJ Ramos, DF Bahr. Mechanical behavior assessment of sucrose using nanoindentation. Warrendale, PA: Materials Research Society; 2007.

[43] S-H Lee, S Wang, GM Pharr, H Xu. Evaluation of interphase properties in a cellulose fiber-reinforced polypropylene composite by nanoindentation and finite element analysis. Composites Part A: Applied Science and Manufacturing. 38 (6), 2007, 1517-24.

[44] S-L Gao, E Mäder. Characterisation of interphase nanoscale property variations in glass fibre reinforced polypropylene and epoxy resin composites. Composites Part A: Applied Science and Manufacturing. 33 (4), 2002, 559-76.

[45] JD Yeager, AM Dattelbaum, EB Orler, DF Bahr, DM Dattelbaum. Adhesive properties of some fluoropolymer binders with the insensitive explosive 1,3,5-triamino-2,4,6-trinitrobenzene (TATB). J Colloid Interface Sci. 352 (2), 2010, 535-41.

[46] JD Yeager, M Dubey, MJ Wolverton, MS Jablin, J Majewski, D Bahr, F., et al. Examining Chemical Structure at the Interface Between a Polymer Binder and a Pharmaceutical Crystal with Neutron Reflectometry. Accepted to Polymer. 2011.

CHAPTER TWO

HIGH-SPEED X-RAY PHASE CONTRAST IMAGING FOR ANALYSIS OF SIMULATED PLASTIC-BONDED EXPLOSIVE MICROSTRUCTURE

This chapter provides an overview of the possibilities and limitations involved with studying plastic-bonded explosive materials with x-rays. Synchrotron phase contrast imaging was performed at the Advanced Photon Source at Argonne National Laboratory to establish feasibility of studying micron-size features and microsecond duration events in explosives or other low-Z materials. This high-powered technique is compared with a typical laboratory x-ray experiment as well. This chapter provides high-resolution observations of the type of microstructural defects the explosives community wishes to study in detail during dynamic deformation.

2.1. Introduction

Understanding and predicting detonation, failure and general deformation mechanisms in plastic-bonded explosive (PBX) composites is an important goal for the explosives community. PBX materials consist of micron-sized explosive crystals embedded in a polymer matrix. The composites are highly loaded, usually greater than 85% crystals by weight, and both particle size and particle size distribution are known to affect the mechanical properties and detonation behavior [1-3]. The microstructure of PBX 9501, composed of 95% cyclotetramethylene-tetranitramine (HMX) crystals and 5% plasticized Estane 5703 by weight, is shown in Figure 2.1.

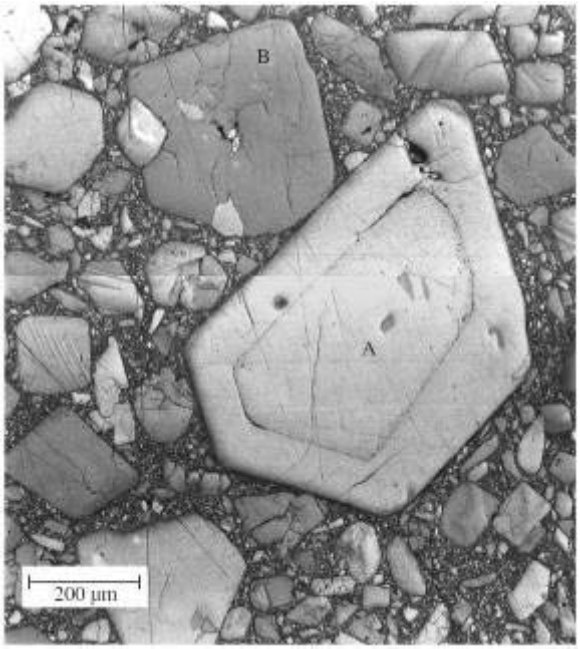

Figure 2.1. Microstructure of PBX 9501, showing a wide distribution of particle sizes and variability in crystal integrity: “A” is relatively defect free, while “B” contains inclusions. From Rae et al., used with permission [3].

The microstructure of the PBX, and in particular the crystal-binder interface, plays an important role in mechanical deformation events, including failure. Defects within crystals, at the crystal-binder interface, in the partially dissolved crystal-binder region (“dirty binder”), or within the binder itself may all contribute to formation of local inhomogeneities (“hot spots”) which initiate deflagration or detonation [4, 5]. Crack propagation between the crystals and the binder has been observed in many systems and is usually the failure mechanism of PBX materials under mechanical strain [6-8]. PBXs are difficult to study at the micro-scale or nano-scale with conventional techniques due to the complexity of the microstructure, the brittle nature of the molecular crystals, the compositional (low-Z) similarities between the crystals and the binder,

and ease of thermal degradation or melting under an electron beam. The use of unique, innovative methods is often necessary to gather structural information for these materials.

X-ray study of composites is gaining in popularity as source and detector technology improves. Three dimensional applications such as tomography have been used recently to identify glass fiber orientation and distribution in sheet molding compounds [9] and reinforced polyamides [10] as well as microsphere and epoxy fracture in syntactic foams [11]. These tomography studies used phase contrast imaging (PCI) which allows greater resolution and contrast than traditional absorption radiography. For an excellent overview of the theoretical aspects of PCI, refer to the review by Wu and Liu [12]. While X-ray tube sources have been successfully used for PCI in structural materials [13], synchrotron sources provide orders of magnitude higher brightness and coherence, allowing for higher resolution and shorter exposure times [14]. The exposure time advantage is particularly useful for samples which suffer localized heat degradation from beam exposure or must be studied on short time scales for other reasons.

Experiments using PCI present exciting possibilities for observing high strain rate deformation (e.g., shock waves) at the microstructural scale in PBX materials. A previous study at the Advanced Photon Source (APS) at Argonne National Laboratory achieved 10 μm spatial resolution of a tungsten – silicon reaction using ultrafast “white” radiation x-ray pulses and microsecond exposure times [15]. The main objective in the current work was to assess the feasibility of performing high-speed PCI measurements on low-Z materials to study microstructure and defects using the synchrotron X-ray beam at APS and available X-ray

detectors. These initial measurements will guide future dynamic loading experiments which will use high-speed PCI to investigate microstructural effects on the dynamic response of PBXs or similar composites. In contrast to quasi-static loading, dynamic loading experiments can readily examine a material's response over a wide range of strain rates (10^2 s^{-1} to 10^7 s^{-1}) and timescales (ns to ms) making it possible to directly examine mechanical deformation in real-time.

Although such dynamic experiments are of great interest to the high-pressure community they pose significant technical challenges related to the use of x-ray detectors and x-ray sources mostly because of the short duration of the dynamic state, which significantly limits the number of photons available for detection. Synchronization of the dynamic event with the incoming photon bunch(s) and the detector is also required. These difficulties coupled with the high costs of dynamic experiments warrant independent feasibility studies as presented here. Key targets of the study included determination of whether we could observe the microstructure at sufficient spatial and temporal resolution to study dynamic response and whether introducing a doping agent was necessary to achieve contrast between crystals and polymers. In addition, observation of cracks, voids, bubbles, or other defects would be particularly interesting. As a side benefit of the PCI feasibility study, we wanted to show that the technique could be useful for other types of low-Z composites, such as pharmaceutical tablets or polymer-matrix composites (PMCs).

2.2. Sample Preparation

In order to demonstrate the usefulness of PCI to studying specific microstructural features, simulated PBX samples with engineered microstructures were fabricated with a variety of

processes. Sucrose (J.T. Baker, Phillipsburg, NJ) and acetaminophen (Acros, Morris Plains, NJ) were grown as single crystals from water or ethanol solutions, following the method of Ramos et al. for the sucrose [16] and the method of Finnie et al. for the acetaminophen [17]. The acetaminophen tends to crystallize from solution by spiral growth, usually resulting in highly defective surfaces [18], while sucrose surfaces can generally be grown with smooth surfaces. Sucrose and acetaminophen were chosen as simulants for the explosive HMX because they have similar crystal structure (monoclinic), solubility in certain solvents, and mechanical properties. Some single crystals were embedded in Angstrom Bond epoxy (Fiber Optic Center, Inc., New Bedford, MA) or the poly(ester urethane) Estane 5703 (B.F. Goodrich, Jacksonville, FL), while others were bonded together with water or epoxy to study crystal-crystal interfaces. Estane was chosen because it used in some explosive formulations and has been well-characterized previously [19]. Certain single crystals were intentionally damaged by creating a 250 μm trench in one surface with a wire saw.

Sucrose powder was also formulated into a plastic-bonded simulant (PBS) pellet using an identical procedure to that for PBX 9501, including using an identical plasticized Estane binder at 5 wt% [6]. The effect of doping was studied by using Bi_2O_3 nanoparticles (90-210 nm in diameter; MTI, Richmond, CA) to enhance contrast in some polymer-embedded samples. PBS pellets were produced with a range of thicknesses and in some cases the PBS molding prills were doped prior to pressing. Additionally, binder cracking was simulated by intentionally cracking a polymethylmethacrylate (PMMA) slab. General sample size along the probing direction was between 0.3 and 3.5 mm. A list of all studied samples is given in Table 2.1.

Table 2.1. List of Formulated Samples for PCI Study

Specimen ID	Description	Bi_2O_3 Used
CRY-1	Single crystal of sugar	No
CRY-2	Single crystal of acetaminophen	No
PMMA	Cracked PMMA slab	No
ENG-1	Two acetaminophen crystals bonded with water	No
ENG-2	Two acetaminophen crystals bonded with epoxy	Yes
ENG-3	Same as ENG-2 but one crystal had a 250 μm trench	Yes
PBS-1	Acetaminophen pressed into Estane pellet	Yes
PBS-2	Plastic-bonded sugar pellet	No
PBS-3	Plastic-bonded sugar pellet	Yes

2.3. X-ray Characterization Experiments

PCI is much more effective for imaging than traditional radiography especially for low-Z materials. The complex index of refraction of a material for x-rays is $n=1-\delta+i\beta$, where β accounts for absorption, and δ contains phase information [12]. Traditional x-ray radiography relies on the spatial variation of β to produce the intensity variation in the image, while PCI relies on the δ-variation. More precisely, the second derivative (or Laplacian) of the phase modulates the intensity after a finite propagation distance, and can be used for imaging the object microstructure. PCI requires a partial degree of spatial coherence for the x-ray beam, but depends weakly on spectral coherence, so there is no requirement for a monochromatic source [20]. Thus, the use of synchrotron radiation without a monochromator is possible for high-speed PCI.

Prior to PCI measurements at the APS, several of the samples were characterized by radiography-based tomography at Los Alamos National Laboratory. Specimens PBS-1 and ENG-3 were scanned with an in-house tungsten anode x-ray source operated at 150 kV. Multiple 2D radiographs could be obtained via rotating the sample, and then converted to a 3D image via reconstruction.

PCI experiments were performed under ambient conditions at 32ID-B beamline of the APS. The experimental configuration is shown in Figure 2.2. The PCI method used a "white" beam which was transmitted through the composite material and single crystal samples and then imaged onto a camera. The storage ring was operating in the standard mode, meaning the beam was chopped into 24 pulses or bunches of 40 ps duration spaced 153 ns apart [21]. The beam intensity and spectra were adjustable by varying the undulator gap with typical operation in the 11-30 mm range. Most of the measurements used an undulator gap of 20 mm. For this gap, the majority of the intensity was located in the first harmonic centered around 9 keV with a bandwidth of 0.4 keV FWHM, and the peak radiance was about 3×10^{14} photons/s/0.1%bw (see Fig. 2.2b) . Two electromechanical shutters (slow and fast) and a slit were placed between the x-ray source and the sample, conditioning the beam temporally and spatially for imaging and controlling the area of illumination on the sample. The slow shutter absorbs more than 99% of the power (to protect samples and diagnostics downstream from beam damage) and the beam goes through for a few milliseconds at a rate of 1 Hz. During this wide time window, the fast shutter produces a narrow time window of 5 μs for imaging. Both shutters were timed against a time-zero reference supplied by the synchrotron storage ring (RF signal), with appropriate delays controlled by a

Stanford Research Systems (SRS) DG535 delay boxes. The illumination area on the sample was controlled with the slit(s). A LAG:Ce scintillator was positioned downstream 120 mm away from the sample. A 45° mirror relayed the optical emission from the scintillator into the recording SensiCam camera (Cooke; 6.3 μm×6.3 μm pixel size, and 1280×1024 pixels), through a 10× microscope objective. The field of view on the sample was approximately 0.85 mm×0.65 mm. The beam was aligned with a foam target and spatial calibration was achieved by use of a 63.5 μm period gold grid. Resolution for the PCI setup was determined to be approximately 2-4 μm. The background intensity was about 80 counts (noise level).

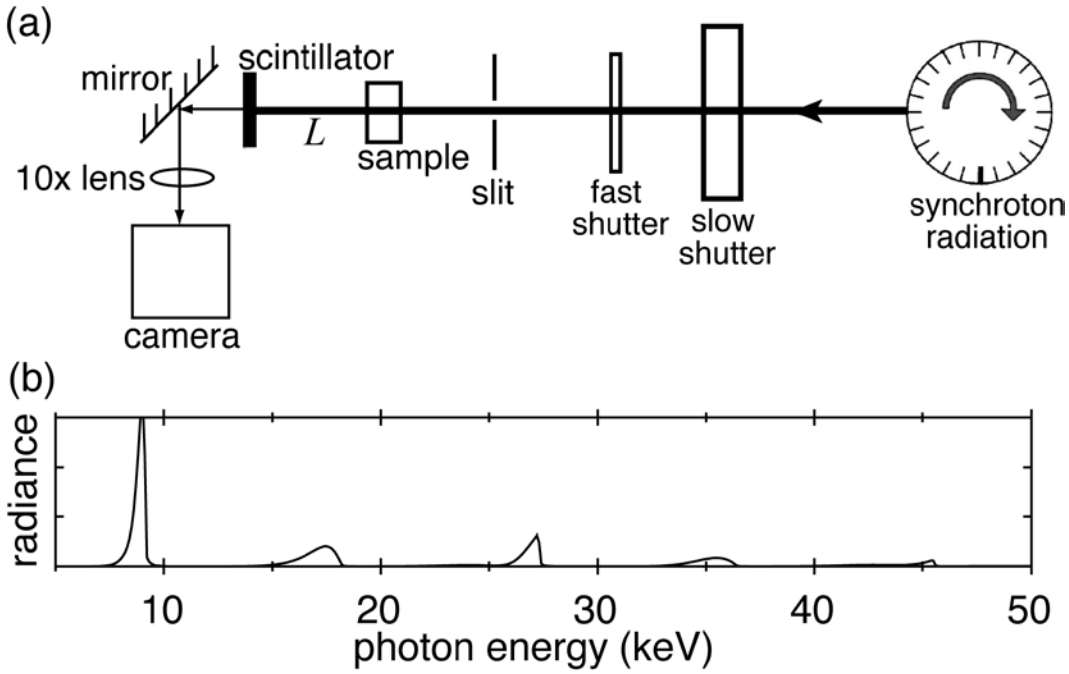

Figure 2.2. (a) Schematic of the experimental setup for PCI at APS 32ID-B. The synchrotron storage ring was operated in the standard mode. The sample-scintillator distance (*L*) was 120

mm. (b) A simulated photon spectrum at 32ID-B for an undulator gap of 20 mm. Each division on the vertical axis represents 10^{14} photons/s/0.1% bandwidth.

2.4. Results

2.4.1 Single Material Characterization

Samples consisting of single crystals or single polymers were characterized in terms of the ability to resolve microstructure and signal to noise ratio (S/N). The strength of the signal is described here by the number of counts the detector records. PCI results are shown in Figure 2.3 for sucrose and acetaminophen single crystals and in Figure 2.4 for bulk PMMA and Estane binders with no stimulant in the field of view (in PBS-1 sample), and S/N is about 25.

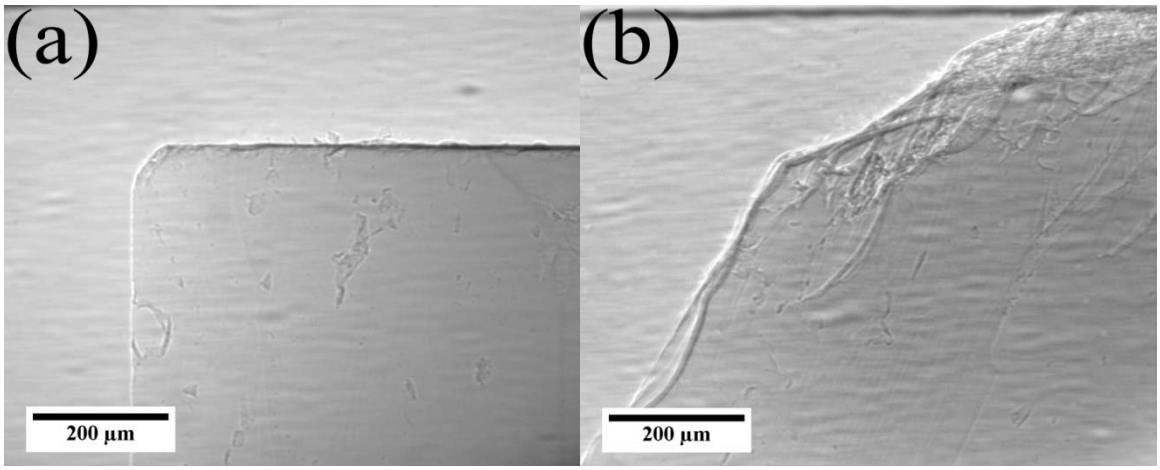

Figure 2.3. PCI at the crystal edge for sucrose (a) and acetaminophen (b), showing clearly observable morphology, surface imperfections, and bulk defects. The intensity is about 2400 counts (a) and 2000 counts (b).

In Figure 2.3, the edges of the crystals are clearly defined and heterogeneities within the crystal are visible as well. For PMMA and Estane (Figure 2.4), suitable intensity was obtained

throughout both specimens, and the images displayed in the figure were chosen to emphasize the ability to observe defects in high resolution. The images are from within the bulk of the polymers, showing internal crack branching and voids. Recall that PCI is a projection technique, so overlapping features are actually at different depths in the sample.

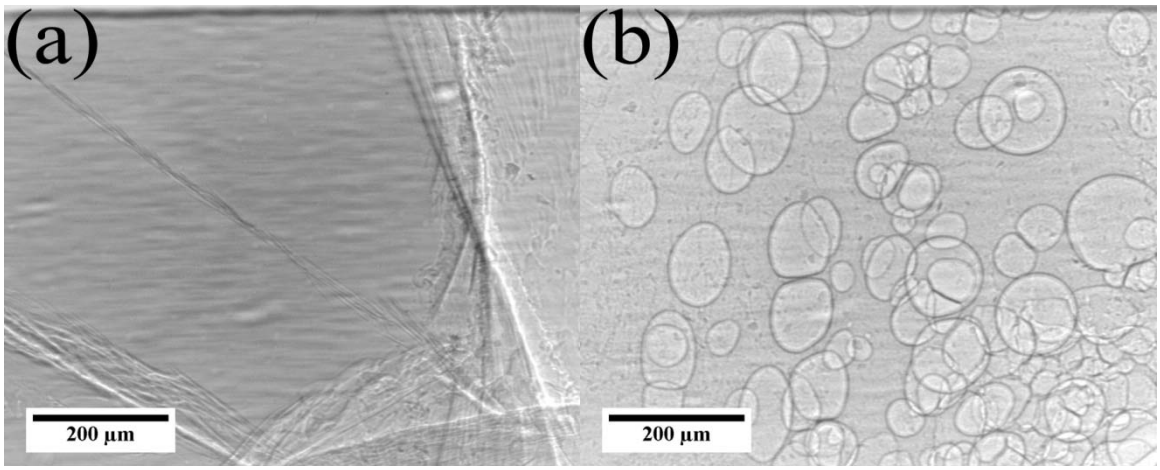

Figure 2.4. PCI within the bulk of PMMA (a) and Estane (b), showing cracking and voids respectively. The intensity is about 2000 counts.

2.4.2 Engineered Sample Characterization

The feasibility of studying interfacial phenomena in detail was assessed with the acetaminophen crystal-crystal samples (or "bicrystals"), ENG-1 and ENG-2. Figure 2.5 focuses on the bicrystal interface in the ENG-1 sample, showing sufficient contrast to resolve the boundaries of each crystal along with various bulk and surface imperfections such as curvature and growth spirals. Both crystals in ENG-1 show high roughness at the surface and noticeable bulk defects. The dark band at the surface of Crystal 2 was probably a result of slight tilting of the sample with respect to the beam axis.

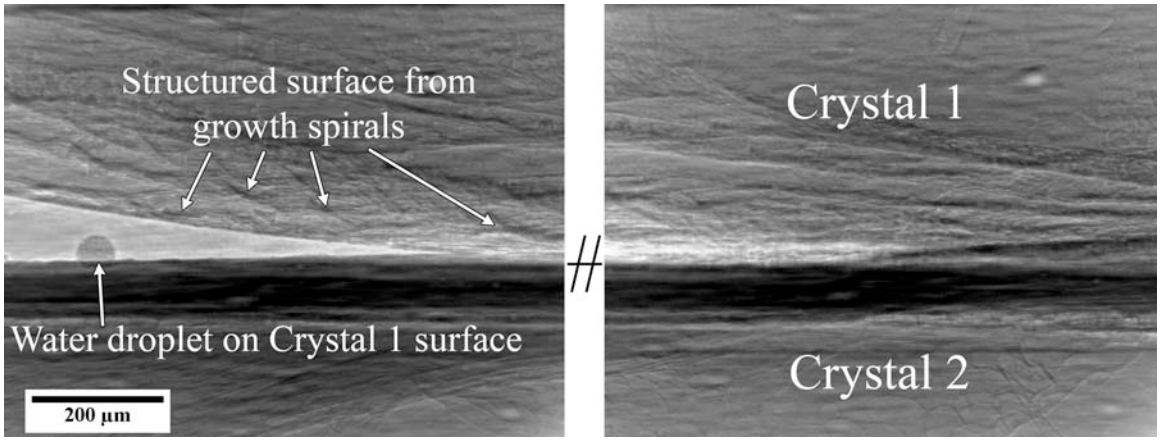

Figure 2.5. Bicrystal interface resulting from bonding with water. The curvature of the surface of Crystal 1 prevented full bonding, but resolution of the two crystals is apparent. Surface defect structure is observed clearly.

The epoxy-bonded bicrystal ENG-2 was characterized with similar resolution to ENG-1 but provided additional insight into polymer-crystal delamination events, Figure 2.6. The large acetaminophen crystals had curved surfaces, and when the surfaces were joined by epoxy they appeared to relax over the duration of the cure time. This resulted in epoxy delamination from the crystal, simulating commonly observed crystal-binder delamination in PBX materials under small tensile loads [2].

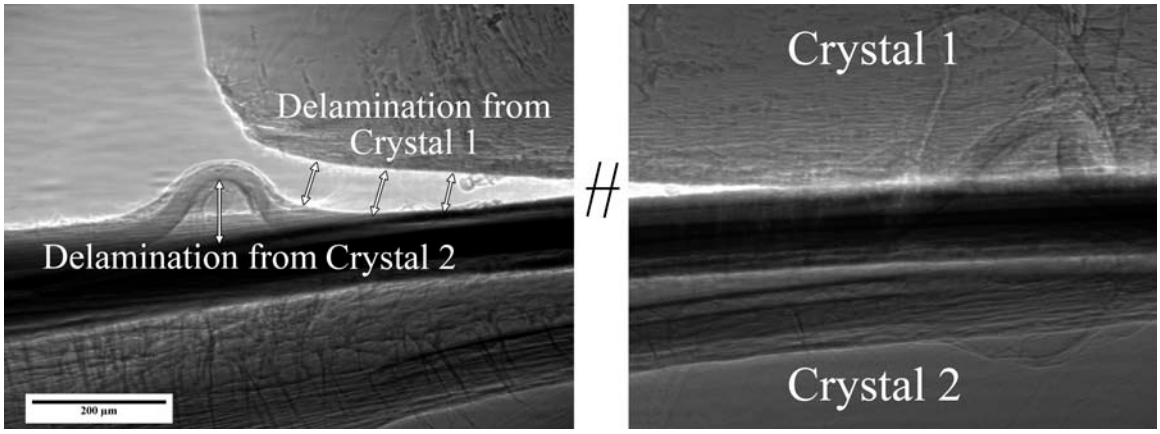

Figure 2.6. Crystal-epoxy-crystal interface observed by PCI in ENG-2. Crystal 1 appeared to delaminate from the epoxy during the 24 hour cure time, possibly pulling the epoxy with it to create delamination from Crystal 2.

Fig. 2.6 appears to show delamination of the epoxy from both crystals. Certainly Crystal 1 has pulled away from the epoxy during the curing stage, but it appears to have initially pulled the epoxy off of Crystal 2 to form a buckle. Another possibility for the buckle formation is that Crystal 2 may have been moved sideways during the cure and caused a pileup of epoxy at the edge of the crystal. Either way, polymer-crystal delamination is well resolved with PCI.

ENG-1 and ENG-2 characterization proved the feasibility of imaging interfaces and small surface defects. However, crystal-crystal regions in typical PBX formulations are rarely as smooth as these engineered samples. ENG-3, the bicrystal with a machined trench, was a step towards real crystal surface imperfections. In order to understand the projection view obtainable with PCI, we first characterized the sample with radiographic microtomography. ENG-3 required doping to obtain contrast for the tomography, but unfortunately the nanoparticles tended to

agglomerate when mixed in the epoxy. The disruption of x-ray signal caused by the large doping particles prevented the software from rendering a complete 3D image. However, we were still able to focus the x-ray signal at a particular depth in the sample, and we chose to focus on the longitudinal center of the trench. Figure 2.7 compares the tomography with PCI, showing the bicrystal interface and the trench in a side-on view. The tomography provided limited resolution of the composite structure and Bi_2O_3 particle distribution, while we were able to well-resolve Bi_2O_3 distribution in the epoxy-filled trench with PCI, as well as surrounding the crystals (not shown).

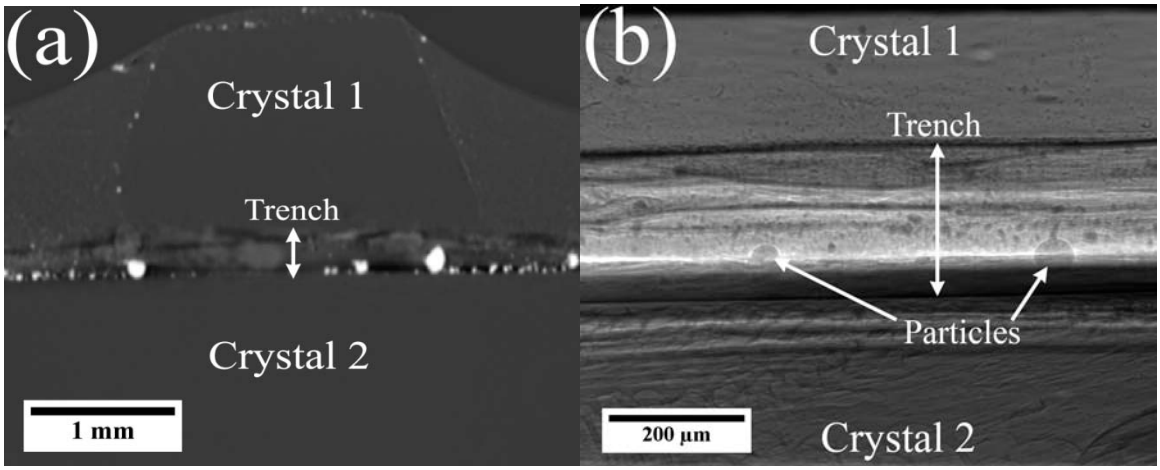

Figure 2.7. ENG-3 sample characterized with absorption microtomography (a) and synchrotron PCI (b). Doping with Bi_2O_3 provided absorption contrast in (a), showing both crystals as well as highlighting the trench effectively. The Bi_2O_3 appears as bright particles in the tomography slice but as dark particles in PCI.

It should be noted that the lateral spatial resolution is much higher for PCI (~2μm) than for tomography (~50μm), though the advantage of tomography clearly lies in the ability to focus on

a depth in the sample rather than averaging signal as a projection. The resolution is a function of effective source size and phase contrast, both of which are superior in synchrotron PCI. In principle, PCI tomography can be done in such a way as to achieve sub-millimeter resolution with only a few seconds of exposure [22]. Alternatively, flash radiography can provide similar resolution at millisecond exposure times [23]. However, no technique currently exists that can provide full 3D phase information with micron spatial resolution and nano-to-microsecond temporal resolution. Within the limitations of current technology, synchrotron PCI appears to be the best option for high-speed study of these low-Z composites.

2.4.3 Plastic-Bonded Simulant Composites

We were able to observe crystals, polymer, voids, and cracks in the pressed Estane pellet, PBS-1. Half of the embedded crystals had been doped with Bi_2O_3 to assess the necessity of using dopant to achieve contrast. This sample had been previously characterized by x-ray tomography at LANL, and the transparency of the Estane allowed for some optical observation as well. Figure 2.8 is a comparison between x-ray tomography, optical microscopy and PCI.

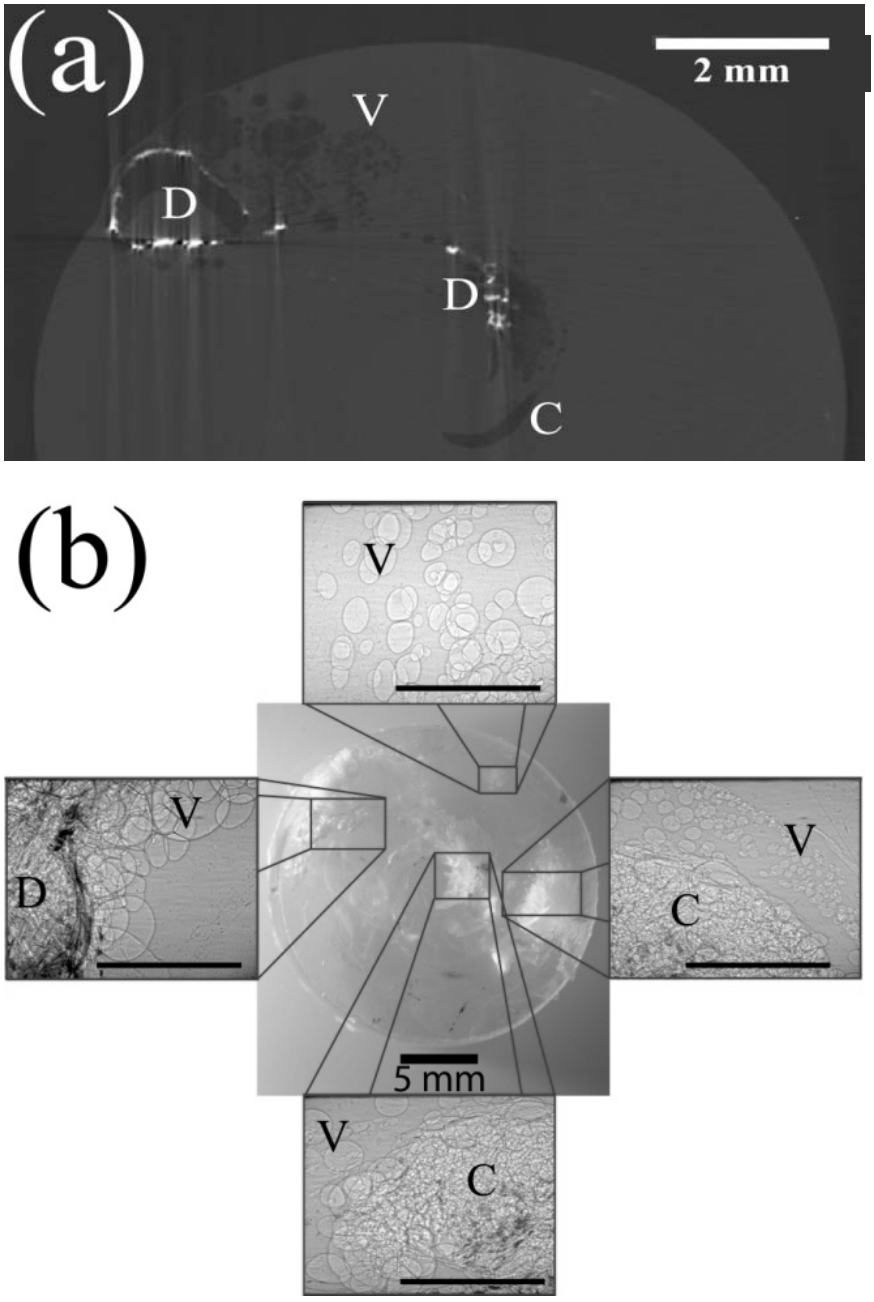

Figure 2.8. X-ray tomography slice (a) compared with optical microscopy and synchrotron PCI (b) from specified locations in specimen PBS-1. “D” refers to doped crystals or interfaces, “C” refers to non-doped crystals or interfaces, and “V” refers to voids. Scale bars in the PCI images are 500 μm.

The dopant appears to be necessary to achieve contrast with the x-ray absorption tomography while it only mildly assists interfacial resolution in the PCI. Despite imaging through the thickness of the sample, PCI reveals fracture within the crystals and extensive void formation around the crystals. Both of these defect structures are likely caused by the high flow stress necessary to shape the original Estane particles into a pellet. PBS-1 was manufactured by pressing millimeter sized Estane particles around several acetaminophen crystals, rather than the wet agglomeration process described earlier, and this change in formulation conditions probably resulted in unusual stress conditions at the crystal-polymer interface. While the processing did not precisely replicate PBX formulation, the observations possible with PCI are both indicative of expected features and likely to be of equivalent utility in future measurements in actual formulations. Further, the excellent resolution observed implies that with proper experimental approach, sample geometry, and fast detector advancements the photon flux is sufficient to perform dynamic observations of failure events with good resolution.

PBS-2 and PBS-3 were made with identical formulation parameters to PBX 9501 but were somewhat difficult to image. The results of both samples, doped and non-doped, are shown in Figure 2.9. It is instructive to compare the microstructure from Fig. 2.9 to the PBX microstructure from Fig. 2.1 in order to understand the imaging concerns.

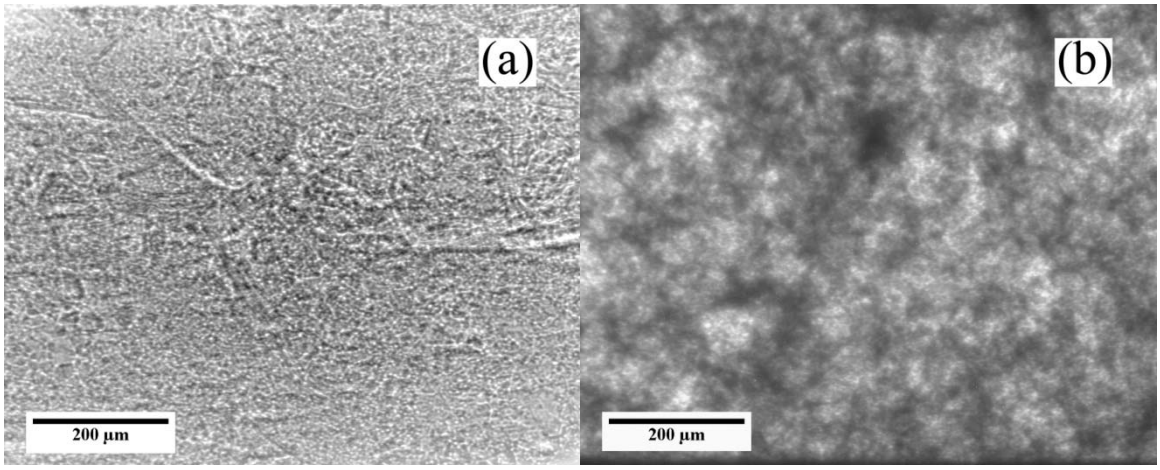

Figure 2.9. Non-doped (a) and doped (b) PBS samples observed by PCI. Some outlines of crystals are visible but resolution of the microstructure is poor. Both samples were approximately 2 mm thick.

The lack of feature resolution in these samples likely has contributions from both x-ray scattering at thousands of interfaces within the sample and absorption of X-rays by the crystals (feature convolution). It was determined that absorption of X-rays was a potential problem by analyzing the number of detector counts for each sample. Counts were as low as 300 per image; 1000-3000 was the targeted intensity. The overall absorption was not likely a function of the polymer since PBS-1 had a much higher weight percentage of polymer and still gave satisfactory intensity. Also, the intensity through the sucrose samples was lower than expected for a low-Z material, so the high concentration of sugar in PBS-2 and PBS-3 probably caused most of the difficulty.

Noting that both the PBS samples were several millimeters thick, the problem was addressed by slicing off thin pieces with a razor. Figure 2.10 shows the same samples as Fig. 2.9 after slicing to a thickness of approximately 400 μm.

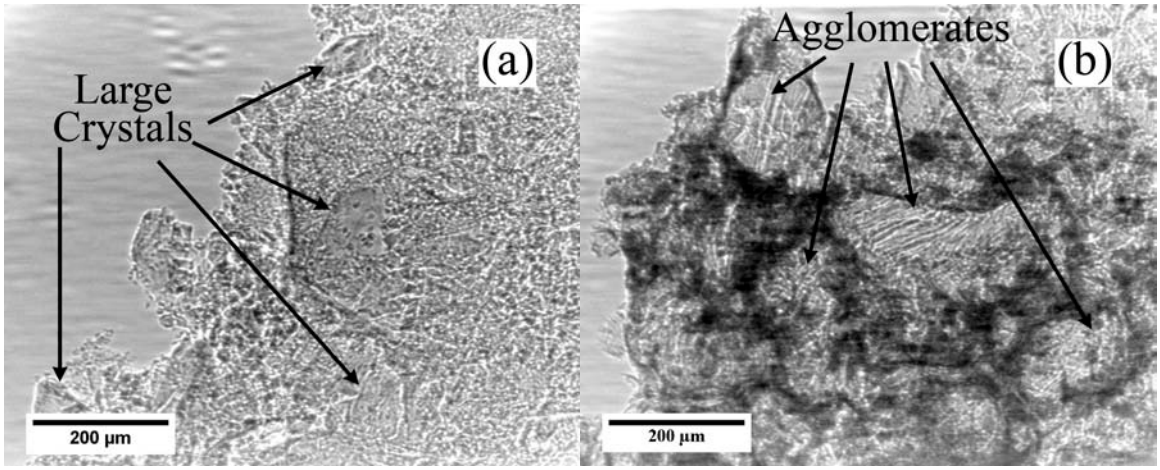

Figure 2.10. Thin PBS samples observed by PCI. Several large facets as well as multiple small crystals are visible in the undoped specimen (a), while the doped specimen (b) appears to show crystal-binder agglomerates rather than individual crystals.

The thinner samples provided much better absolute intensity (~1500 counts). Most of the contrast in the non-doped composite (Fig. 2.10a) arises from the small crystal interfaces but several large crystals are mostly visible. The doped composite reveals a different microstructure previously unobservable. The dopant appeared to surround the molding prills, the crystal-polymer agglomerates, rather than migrate to the crystal-polymer interface. This conclusion was reached by comparing the observed microstructure to the faceted crystal morphology from Fig. 2.1. The dopant also showed a tendency to clump; note that the Bi_2O_3 was a nanopowder before mixing with the PBS molding prills but regions of high concentrations in Fig. 2.10b are hundreds of microns across. This indicates that the presence of the powder may have affected the pressing behavior of the PBS agglomerates, or that the pressing process induces much less polymer flow around crystals than has been previously suspected. Contrasting doped vs. non-doped samples

may be of use to study the effect of changing processing parameters on resulting composite microstructure.

2.5. Implications for dynamic experiments

Single materials and engineered composite samples could be studied in great detail with the current x-ray detector setup at APS. High spatial resolution was achieved even at very fast (5 μs) exposure times. Clear observations were made of defects such as internal cracks, voids, air bubbles, surface imperfections, and polymer delamination.

The high-speed PCI measurements at ambient conditions show promises as well as limitations in resolving *in situ* microstructure in dynamic experiments at APS-type synchrotrons. The key parameter is S/N, determined by the exposure time as required by specific dynamic experiments, beam characteristics (mostly synchrotron operation mode), sample type, and probing thickness, as well as scintillators and x-ray cameras. For the current detector system, a minimum S/N of 3 corresponds to I_{min}=240 counts. This minimum was easily exceeded with 5 μs exposure times for our simulated PBX samples. However, the feasibility of keeping an adequate S/N when trimming the exposure time to capture shock events (~0.5 μs) needs to be discussed.

The nominal intensity in current setup is I_0=2500 counts for 5 μs exposure time in the standard mode (102 mA in 24 bunches during 3.68 μs; the bunch separation is 153 ns). It requires about 3 bunches in the standard mode to obtain I_{min}; 3 bunches in the standard mode correspond to a camera gate width of 207 ns. Thus, for the current detector and the standard mode, the “exposure

time" (image integrated over this period from multiple bunches) will be at least 0.2 μs. The standard mode operation should be sufficient for study of a wide range of dynamic experiments, but APS also offers an alternative operation mode. The hybrid or singlet mode at APS has different time structure of the probing beam. In the hybrid mode, a singlet pulse (16 mA, 65 ps pulse duration) is separated from septuplet pulses (86 mA and 470 ns in total) by 1.594 μs on either side. The singlet is more desirable for time resolution due to the 65 ps duration, but synchronizing the dynamic event with the pulse is likely to be very difficult. Additionally, achieving sufficient S/N requires capturing information from more than one singlet, which will require several μs exposure times. The singlet mode is likely to be most useful for dynamic experiments at medium to low strain rates ($10^2 – 10^4$ s^{-1}). Improving the detector sensitivity or increasing photon fluxes may reduce the exposure time for both standard and hybrid modes at APS to allow for higher strain rate experiments.

One potential concern for dynamic experiments was the difficulty of imaging the simulated PBX composites at thicknesses greater than 1 mm. Sufficient resolution of the microstructure was not reached even with 400 μm thick samples. Adequate sample dimensions are necessary to achieve a sufficiently long, stable state (e.g., supported shock duration) and thus the required exposure time for PCI. However, sample dimensions and exposure times for dynamic study will be tailored to specific loading scenarios, such as drop weight, split Hopkinson pressure bar or Kolsky bar, or gas gun experiments [24-26]. For non-shock strain rate experiments, meaning slower dynamic loading, the exposure time can be correspondingly longer. It is possible that complex microstructures could still be studied with PCI under such conditions. For high

temporal resolution studies, initial efforts on dynamic PCI should be focused on simple microstructures or engineered interfaces with elemental deformation processes.

2.6. Conclusions

PCI has proven to be quite useful for imaging non-transparent simulated plastic-bonded explosives. PCI is superior to absorption radiography in terms of contrast, effective resolution and doping requirements. Doping is not necessary to achieve contrast between similar materials or within composites but can show a different structure (i.e. structure of molding prills rather than crystals). Sufficient contrast and intensity can be achieved for low-Z composites with the APS X-ray source in the standard operation mode and that dynamic study at high strain rates is feasible. Synchrotron PCI should be able to reveal the response of preexisting microstructure to shock loading. Specifically, void nucleation and collapse, fracture delamination, grain boundary/interface deformation, and hot spot formation may be studied with high temporal and spatial resolution. In addition, PCI may be useful for imaging mechanical or chemical behavior of other low-Z composites, statically or dynamically, even at microsecond time scales.

References

[1] BA Khasainov, BS Ermolaev, HN Presles, P Vidal. On the effect of grain size on shock sensitivity of heterogeneous high explosives. Shock Waves. 7 (2), 1997, 89-105.

[2] SJP Palmer, JE Field, JM Huntley. Deformation, Strengths and Strains to Failure of Polymer Bonded Explosives. Proc R Soc London, Ser A. 440 (1909), 1993, 399-419.

[3] PJ Rae, SJP Palmer, HT Goldrein, JE Field, AL Lewis. Quasi-static studies of the deformation and failure of PBX 9501. Proc R Soc London, Ser A. 458 (2025), 2002, 2227-42.

[4] JE Field, NK Bourne, SJP Palmer, SM Walley, J Sharma, BC Beard. Hot-Spot Ignition Mechanisms for Explosives and Propellants [and Discussion]. Philosophical Transactions: Physical Sciences and Engineering. 339 (1654), 1992, 269-83.

[5] HL Berghout, SF Son, CB Skidmore, DJ Idar, BW Asay. Combustion of damaged PBX 9501 explosive. Thermochim Acta. 384 (1-2), 2002, 261-77.

[6] PJ Rae, HT Goldrein, SJP Palmer, JE Field, AL Lewis. Quasi-Static Studies of the Deformation and Failure of β-HMX Based Polymer Bonded Explosives. Proceedings: Mathematical, Physical and Engineering Sciences. 458 (2019), 2002, 743-62.

[7] P Chen, H Xie, F Huang, T Huang, Y Ding. Deformation and failure of polymer bonded explosives under diametric compression test. Polym Test. 25 (3), 2006, 333-41.

[8] ZW Liu, HM Xie, KX Li, PW Chen, FL Huang. Fracture behavior of PBX simulation subject to combined thermal and mechanical loads. Polym Test. 28 (6), 2009, 627-35.

[9] TH Le, PJJ Dumont, L Orgéas, D Favier, L Salvo, E Boller. X-ray phase contrast microtomography for the analysis of the fibrous microstructure of SMC composites. Composites Part A: Applied Science and Manufacturing. 39 (1), 2008, 91-103.

[10] A Bernasconi, F Cosmi, D Dreossi. Local anisotropy analysis of injection moulded fibre reinforced polymer composites. Compos Sci Technol. 68 (12), 2008, 2574-81.

[11] F Awaja, BD Arhatari. X-ray Micro Computed Tomography investigation of accelerated thermal degradation of epoxy resin/glass microsphere syntactic foam. Composites Part A: Applied Science and Manufacturing. 40 (8), 2009, 1217-22.

[12] X Wu, H Liu. Clinical implementation of x-ray phase-contrast imaging: Theoretical foundations and design considerations. Medical Physics. 30 (8), 2003, 2169-79.

[13] B Zoofan, JY Kim, SI Rokhlin, GS Frankel. Phase-contrast x-ray imaging for nondestructive evaluation of materials. J Appl Phys. 100 (1), 2006, 014502-7.

[14] Y Wang, X Liu, K-S Im, W-K Lee, J Wang, K Fezzaa, et al. Ultrafast X-ray study of dense-liquid-jet flow dynamics using structure-tracking velocimetry. Nat Phys. 4 (4), 2008, 305-9.

[15] RV Reeves, JDE White, EM Dufresne, K Fezzaa, SF Son, A Varma, et al. Microstructural transformations and kinetics of high-temperature heterogeneous gasless reactions by high-speed x-ray phase-contrast imaging. Physical Review B. 80 (22), 2009, 224103.

[16] KJ Ramos, DF Bahr. Mechanical behavior assessment of sucrose using nanoindentation. J Mater Res. 22 (7), 2007, 9.

[17] S Finnie, K Prasad, D Sheen, J Sherwood. Microhardness and Dislocation Identification Studies on Paracetamol Single Crystals. Pharm Res. 18 (5), 2001, 674-81.

[18] RI Ristic, S Finnie, DB Sheen, JN Sherwood. Macro- and Micromorphology of Monoclinic Paracetamol Grown from Pure Aqueous Solution. The Journal of Physical Chemistry B. 105 (38), 2001, 9057-66.

[19] JT Mang, RP Hjelm, EB Orler, DA Wrobleski. Small-Angle Neutron Scattering of a Solvent-Swollen Segmented Polyurethane as a Probe of Solvent Distribution and Polymer Domain Composition. Macromolecules. 41 (12), 2008, 4358-70.

[20] SW Wilkins, TE Gureyev, D Gao, A Pogany, AW Stevenson. Phase-contrast imaging using polychromatic hard X-rays. Nature. 384 (6607), 1996, 335-8.

[21] VV Sajaev. Storage Ring Operation Modes. http://aps.anl.gov/Facility/Storage_Ring_Parameters/node5.html. Accessed 05/09/2011 2011.

[22] AK Willi. X-ray computed tomography. Physics in Medicine and Biology. 51 (13), 2006, R29.

[23] S-A Zhou, A Brahme. Development of phase-contrast X-ray imaging techniques and potential medical applications. Physica Medica. 24 (3), 2008, 129-48.

[24] MA Meyers. Dynamic behavior of materials. Wiley; 1994. p. 271-95.

[25] W Goldsmith. Impact: the theory and physical behaviour of colliding solids. Dover Publications; 2001. p. 145-242.

[26] H Kolsky. An Investigation of the Mechanical Properties of Materials at very High Rates of Loading. Proceedings of the Physical Society Section B. 62 (11), 1949, 676.

CHAPTER THREE

SURFACE ENERGY, CALCULATED WORK OF ADHESION, AND THERMAL PROPERTIES FOR SEVERAL BINDERS AND CRYSTALS

This chapter presents a study on surface properties and thermomechanical behavior of several plastic-bonded explosive binder candidates. It includes a detailed discussion of the insensitive high explosive TATB, and compares new fluoropolymer binders to existing explosive materials. In contrast to Chapter Two, in which micron-sized features of the microstructure are characterized, this chapter focuses on nano-scale structure and chemistry in an effort to understand crystal-binder delamination and deformation.

3.1 Introduction

The use of polymers to "bind" high explosive crystals is paramount to the widespread, safe use of plastic-bonded explosives (PBX). PBXs are a unique type of composite containing explosive crystals at high loading percentages (typically exceeding 85 wt%) with the polymeric binder coating the individual explosive grains. Polymeric binders reduce the sensitivity of explosive charges to insults such as impact or friction, as well as provide enhanced mechanical stability. Selection of binders in PBX formulations, however, remains largely an iterative, trial-and-error process based on a handful of guiding principles, and constraints dictated by the physical properties of the explosive being formulated (such as solubility, decomposition temperature, etc.). While the thermomechanical properties of the binder have been shown to be important for manufacturing PBXs [1], binder-explosive adhesive properties have been linked to an ability to fabricate (machine) parts, maintain long-term durability, and inhibit failure. Bower *et al.* showed

that thermomechanical properties such as glass transition temperature (Tg) and extensibility, as well as surface wettability of the binder, are critical for explosive performance and safety [2]. The most common and limiting mode of failure in plastic-bonded explosives under thermal or mechanical loads is crack formation and subsequent propagation along explosive crystal-binder interfaces [3-6]. For example, the mechanical properties of several PBXs were investigated by Palmer et al., revealing that even the most robust material failed by interfacial cracking at tensile stresses as low as 6.8 MPa [6]. Understanding and exploiting surface interactions between explosive crystals and the polymeric binder are therefore of great interest for potentially improving the failure limits of PBXs.

3.1.1 Insensitive Explosives and Binders

Here, the results of an experimental investigation of the adhesive properties of a number of fluoropolymer binders with the insensitive high explosive TATB are reported. The TATB crystal is inherently anisotropic, with molecules adopting a $P_{\bar{1}}$ (triclinic) crystal structure in which the molecules are arranged in graphite-like sheets in the a-b plane, Figure 2.1. The edges of the crystal arrangement of TATB are highly oxygen rich with strong intra- and intermolecular hydrogen bonding, whereas the planar a-b surface is dominated by π interactions associated with the benzene rings. As a result of this structural anisotropy, the thermal and mechanical properties of TATB are likewise highly anisotropic, and a phenomenon of irreversible growth and dimensional changes, known as ratchet growth, occurs in temperature-cycled TATB formulations [7].

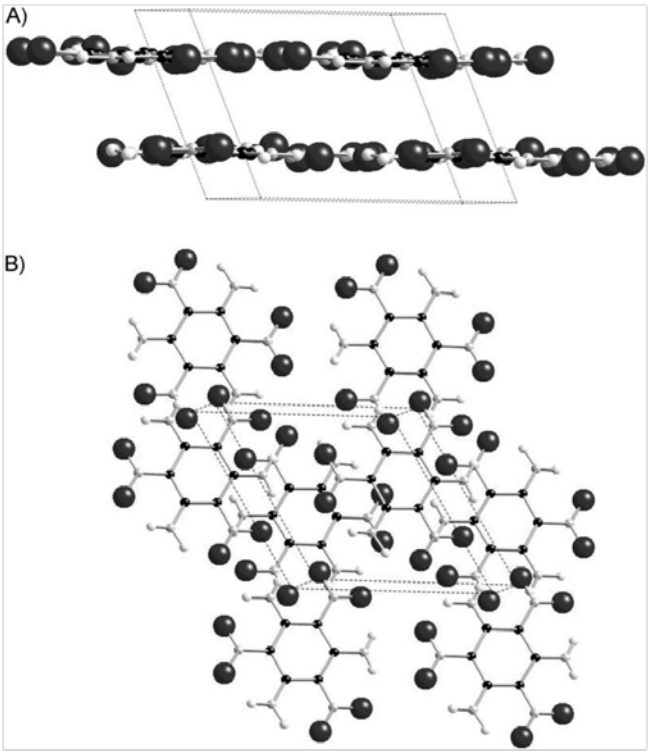

Figure 3.1. Crystal structure of TATB shown parallel to the *ab*-plane (a), and perpendicular to the *ab*-plane [7].

Fluoropolymers are attractive as binders in PBX formulations due to their high densities, high temperature and chemical stabilities, and history of favorable performance [8]. Kel-F 800, a copolymer of chlorotrifluoroethylene and vinylidene fluoride (75:25 ratio by weight), is currently used in two PBX formulations with TATB. Here, we compare the surface properties of Kel-F 800 with related fluoropolymers that differ by their monomer chemistry, using contact angle measurements to measure the surface energies or surface tensions of polymer films. Furthermore, this information is used to make evaluations of the polymers as potential binders for TATB. For comparison, some study was also performed on a binder for another PBX

formulation, Estane 5703 with a nitroplasticizer, and all binders were evaluated for adhesion to the explosive 1,3,5,7-tetranitro-1,3,5,7-tetrazocane (HMX), 1,3,5-trinitroperhydro-1,3,5-triazine (RDX), and acetaminophen.

3.1.2 Surface Energy Determination

The usefulness of the plastic-bonded explosive depends on the individual and combined properties of the binder and explosive crystal. Surface properties, including the dispersive and polar components of the surface energy, are particularly relevant for evaluating adhesion between the explosive crystal and polymeric binder. Thermodynamically, the work of adhesion is defined as the increase in free energy from creating two surfaces, and can be defined for liquid-solid interfaces by

$$W_a = \gamma_{SV} + \gamma_{LV} - \gamma_{SL} \qquad (3.1)$$

where γ is the surface energy or tension, and the subscripts refer to the solid (S), the liquid (L), and the vapor or atmosphere (V) [9]. This expression was originally derived from Young's equation for equilibrium of a droplet on a surface,

$$\gamma_{LV} \cos\theta = \gamma_{SV} - \gamma_{SL} \qquad (3.2)$$

where θ is the angle the droplet makes with the surface [10]. Zisman discovered that a reasonable value for the critical wetting surface energy of a solid could be found by plotting liquids of

known surface tensions against the cosine of their contact angle, then linearly extrapolating back to the "perfect wetting" value of cos θ = 0. However, the critical surface energy was pointed out by subsequent researchers, and Zisman himself, to be different than the thermodynamic quantity of surface energy [11]. Indeed, researchers have found that the Zisman method consistently underestimates the true surface energy [12]. To correctly measure the surface energy, both polar and dispersive contributions are important, and any determination of surface energy must use liquids with a large range of these components [11-15]. For simplicity, the geometric mean method will be used in this thesis. The geometric mean calculation, which uses the polar and dispersive components of the liquid and solid to determine the liquid-solid surface energies is

$$\gamma_{LV}(\cos\theta + 1) = 2(\gamma_L^d \gamma_S^d)^{1/2} + 2(\gamma_L^p \gamma_S^p)^{1/2} \quad (3.3)$$

where the superscript "d" stands for dispersive, and "p" stands for polar. The notation for vapor "V" has been removed here for brevity. Using the approaches in Eq. 3 to solve for the surface energies, the polar and dispersive components for the solid surface can be determined by measuring contact angles using two liquids with well-defined surface properties. However, it is common for three or more liquids to be used in order to ensure accuracy [15-17].

3.2 Material and Methods

3.2.1 Fluoropolymers

The polymers investigated contain common fluorinated monomers that make up the broad class of industrial fluoroelastomers. These include chlorotrifluoroethylene (CTFE), vinylidene

fluoride (VDF), hexafluoropropylene (HFP), and tetrafluoroethylene (TFE). Copolymerization improves the solubilities of the fluoropolymers in organic solvents as well as the enables a tunability of their thermal and mechanical properties while maintaining high densities and other advantageous properties such as low coefficients of friction and chemical stabilities. Table 3.1 details the chemical structures of the fluoropolymers investigated, as well as their as-received form and source. The fluoropolymers in Table 3.1 are soluble in common organic solvents, such as methyl ethyl ketone (MEK), ethyl acetate (EtOAc), tetrahydrofuran (THF), and toluene.

Table 3.1. Chemical structures and as-received form of fluoropolymers investigated.

Polymer Name	**Chemical Structure**	**As-received form**
THV 220	Poly(tetrafluoroethylene-co-hexafluoropropylene-co-vinylidene fluoride) (40:40:20 TFE:HFP:VDF by weight)	Off-white granules from 3M, Inc.
FC-2175/LFC-1 (mixed in both 50:50 and 75:25 ratios by weight)	Poly(hexafluoropropylene-co-vinylidene fluoride) in high/low MW forms (monomer ratios proprietary)	white gum/Amber viscous liquid from 3M, Inc.
Kel-F 800	Poly(chlorotrifluoroethylene-co-vinylidene fluoride) (75:25 CTFE:VDF by weight)	White granules from 3M, Inc.
Oxy 461 (Exon 461)	Poly(chlorotrifluoroethylene-co-tetrafluoroethylene-co-vinylidene fluoride) (monomer ratios unknown)	White granules from DOE storage (not commercially available)
Kel-F 3700	Poly(chlorotrifluoroethylene-co-vinylidene fluoride) (31:69 CTFE:VDF) by weight)	White granules from 3M, Inc.
Viton A	Poly(hexafluoropropylene-co-vinylidene fluoride) (20-23 mol HFP:77-80 mol VDF)	White pellets from DuPont

Some of the binders listed in Table 3.1 are not commercially available but have been used in historical PBX formulations. An example is Oxy (or Exon) 461, which has been previously used

in PBX 9407, which consists of 94% cyclotrimethylenetrinitramine (RDX) and 6% binder. Of historical note is that production of Kel-F 800 was paused from 2002-2007 and resumed using a different process that avoided the use of perfluorinated surfactant. Consequently, the new production material studied here has fewer impurities (undetectable vs. 2% in old production material) and a smaller granule size than some older material studied in the literature [18].

Differential scanning calorimetry (DSC) was used to measure the thermal properties of all fluoropolymers used in this study. These results provide an initial assessment of the thermal transitions, which bound the processing and use temperatures for binder candidates. DSC measurements were performed on a TA Instruments Q2000 Modulated Differential Scanning Calorimeter. The temperature was controlled using a refrigerated cooling accessory (RCA90). The samples were encapsulated in aluminum Tzero$^{@}$ pans. The instrument was calibrated with indium and sapphire standards. Unless otherwise noted, the DSC scans were run at 10 ^{o}C/min heating rate from -90 to 250 ^{o}C. The Tg was defined as temperature at the midpoint in heat flow step transition. The melting temperature was defined as the peak in the melting endotherm and the ΔH_f was defined as the area under the melting endotherm.

3.2.2 Contact Angle Measurements

A half-angle contact angle meter (ChemInstruments, Mentor, OH) was used to measure the static advancing contact angle of several liquids on the polymer films. All polymer films studied here were originally formulated for bulk specimens. Solutions of 3 wt% polymer were prepared by placing bulk specimens in either EtOAc or MEK, followed by ultrasonic vibration for at least 15 minutes to ensure dissolution. Glass microscope slides (Fisher Scientific, Pittsburgh, PA) were

used as film substrates, and were cleaned prior to coating by sequential acetone, ethanol and water washes, and atmospheric plasma etching for 5 min. The films were formed by dip coating the slides at a rate of 25 mm/min in a humidity-controlled glove box (% humidity = 25-30%).

The films were dried in air for at least 2 days prior to making contact angle measurements using water (18MΩ/cm), glycerol (Invitrogen, ultrapure), and diethylene glycol. Figure 3.2 shows a droplet of a measuring liquid on a binder to illustrate the surface energy equations mentioned previously.

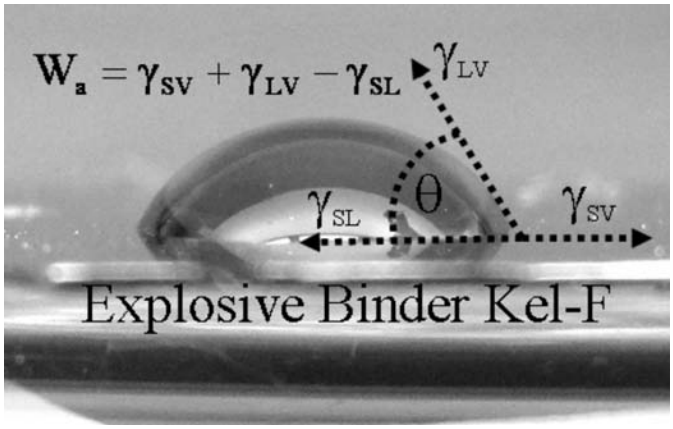

Figure 3.2. A typical deionized water droplet on Kel-F 3700 film, illustrating the surface energies and work of adhesion from Eq. (3.1).

A fourth liquid, either hexadecane (Acros, 99+%) or dimethyl sulfoxide, was also measured in order to give a larger range of polar and dispersive liquids, as shown in Table 3.2. Hexadecane was used in situations where the dimethyl sulfoxide showed evidence of dissolving the film.

Contact angles were measured again after one week to ensure the accuracy of the original measurements.

Table 3.2. Summary of test liquids & reference solids, energies in dyn/cm.

Test Liquid	γ_{LV}	γ^p	γ^d	Ref.
Water	72.8	51	21.8	[19]
Glycerol	63.1	26.1	37	[12]
Diethylene Glycol (DEG)	44.4	12.7	31.7	[19]
Dimethyl sulfoxide (DMSO)	44	8	36	[19]
Hexadecane	27.6	0	27.6	[16]
Reference Solid	γ_{SV}	γ^p	γ^d	Ref.
Poly(tetrafluoroethylene) (PTFE)	19.1	0.5	18.6	[11]
Triaminotrinitrobenzene (TATB)	36.5	24.7	11.8	[16]
Calculated TATB [001]	66			[8]
Calculated TATB [100]	208			[8]
HMX [011]	45	11.2	33.8	[20]
HMX [010]	46	15.6	30.4	[20]
HMX [110]	48	17.3	30.7	[20]

There is some discrepancy in the values of γ_{SV} for TATB. Rivera used an advancing dynamic contact angle method to measure the energies of several polymers and TATB [16]. However, Rivera did not specify any particular crystallographic face for the TATB measurement. Gee et al. reported substantially dissimilar values for the two crystallographic surfaces of [001] and [100] in addition to calculations of amorphous fluoropolymer surface energies [8]. By comparison, the [110], [010] and [011] faces of HMX differ by only ~ 3 dyn/cm [20]. It is beyond the scope of this thesis to reconcile the differences in the two studies, though it should be noted that Gee used simulations on isolated planes while Rivera measured grown TATB crystals.

In addition to the surface energies reported here, work of adhesion calculations using Rivera's TATB values are compared to Gee's simulations.

3.3 Results

3.3.1 Differential Scanning Calorimetry

The mechanical properties of polymeric binders are dominated by their thermal transitions. Below the glass transition temperature (Tg), the polymer is glassy and has a modulus on the order of 10^{10} dyn/cm^2. For an amorphous polymer, the elastic modulus can decrease by three orders of magnitude as the polymer is heated above Tg and the polymer begins to flow above Tg. For semicrystalline polymers, the crystalline structure acts as intermolecular cross-links that increase the modulus between Tg and Tm. Above Tg, the modulus is proportional to the level of crystallinity and small levels of crystallinity can increase the elastic moduli by more than an order of magnitude [21, 22]. Above Tm, the polymer flows and can be easily processed. Table 2.3 summarizes the thermodynamic properties associated with constituent homopolymers. With exception of HFP, all monomeric constituents can crystallize upon polymerization. In addition to Tg, Table 3 shows the equilibrium melting temperature (Tm^0) and the heat of fusion for a 100% crystalline polymer ($\Delta H_f{}^0$).

A fundamental understanding of thermodynamic transitions of the homopolymer components is necessary for understanding the effects of copolymerization of various monomers. This understanding is particularly important if future work requires tailoring a specific property (e.g. Tg or Tm) for the HE binder. Changes in the copolymer composition can dramatically affect the

thermal and associated mechanical properties of the copolymer. For example, the Tg of copolymers can often be predicted using the generalized Fox Eq.:

$$\frac{1}{Tg} = \sum_i \frac{w_i}{Tg_i} \qquad (3.4)$$

where Tg_i (in K) is the glass transition temperature and w_i is the weight fraction of component i [23]. DSC endotherms for the "as received" fluoropolymers binders are shown in Figure 3.3.

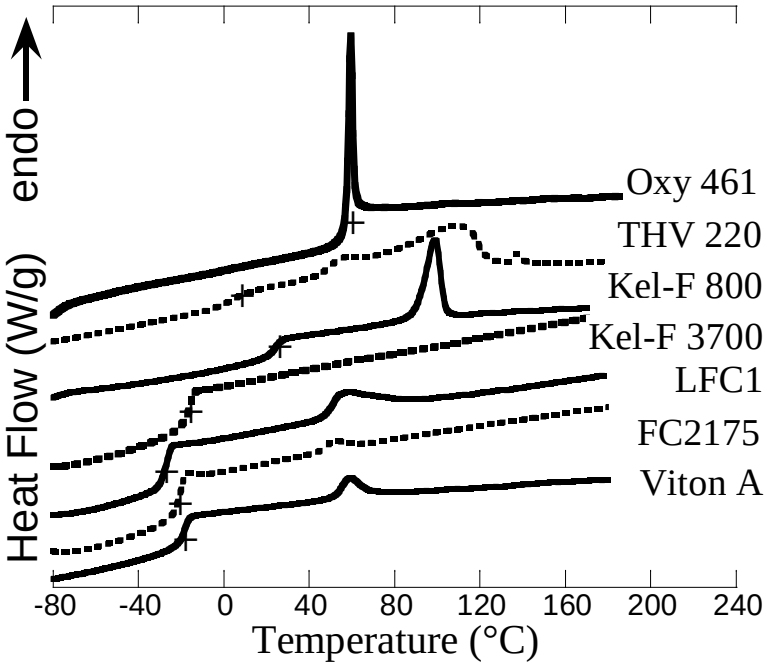

Figure 3.3. DSC data of ''as-received" binder samples. The ''+" indicates Tg.

Comparison of the copolymer DSC data with the homopolymer transitions in Table 3.3 reveals how variation of the monomer content in the polymer allows the glass transition to be tuned between that of the homopolymers. Generally, copolymerization also reduces the melting point and level of crystallinity in semicrystalline copolymers [18].

Table 3.3. Thermodynamic properties of fluorinated homopolymers [24].

Polymer	Tg (^{o}C)	Tm^{o} (^{o}C)	ΔH_f ^{o}(J/g)
PTFE	-73	332	82
PHFP	162	NA	NA
PVDF	-61	210	104
PCTFE	52	220	43

DSC results for the "as received" fluoropolymers binders are summarized in Table 3.4. The data reveal how variation of the monomer content in the polymer allows the glass transition to be tuned between that of the homopolymers. For example, for Kel-F 800, the homopolymers of PCTFE and PVDF have glass transition temperatures (Tg) of +52 and -61^{o}C respectively. The Tg of Kel-F 800 is closer to that of PCTFE, due to its 75 wt% content in the copolymer. Likewise, the Tg of Kel-F 3700 is significantly lower than Kel-F 800, -16^{o}C, due to the greater VDF content[25, 26]. While Eq. 3.5 works well for Kel-F 800 and most hydrocarbon polymers, it does not work well for some fluoropolymers such as VDF/HFP copolymers [27]. More advanced models have been developed for prediction of Tg of fluoropolymers, however, information on the sequence distribution of the monomers units is required [28]. The sequence information can be determined using nuclear magnetic resonance (NMR) but is beyond the scope of this project.

Table 3.4. Summary of DSC results of the binders.

Sample	Tg obs (^{o}C)	Tg Fox (^{o}C)	Tm Max^{+} (^{o}C)	~ΔH_f (J/g)
Kel-F 800	27	27	110	6
Kel-F 3700	-17	-22	N/A	N/A
Viton A	-19	-11	83	1.8
FC-2175	-21	35	65	0.8
LFC-1	-27	35	91	3.4
THV220	4	-27	140	14
Oxy-461	~50	N/A	N/A	N/A
Estane 5703	-31 [29]	N/A	105 [29]	N/A

3.3.2 Contact Angle Measurements

At least 10 measurements were taken of each polymer film with each solvent, and the results are summarized in Table 3.5. The error on each measurement is ~2 degrees.

Table 3.5. Advancing contact angles of test liquids on the binder films (in degrees)

Polymer	Water	Glycerol	DEG	DMSO	Hexadecane
50 FC-2175 / 50 LFC-1	101	96	79	-	45
75 FC-2175 / 25 LFC-1	102	93	75	24	-
Kel-F 800	97	88	62	59	-
Kel-F 3700	98	87	61	-	14
Oxy-461	87	77	51	45	-
PTFE	111	94	79	67	-
THV	101	93	72	69	-
Viton A	97	101	77	48	-
NP/Estane	85	-	25	18	-

"-" *indicates the measured angle was not used due to observed dissolution of the film*

The static advancing contact angle of water on polytetrafluoroethylene (PTFE) was used to verify the method, agreeing well with literature values of between 108° and 119° [11, 30, 31]. All of the binders showed low water wettability; an unsurprising consequence of the inclusion of fluorine in the polymer backbone.

3.4 Discussion

Polar and dispersive contributions to the binder surface energy were calculated using both the geometric and harmonic mean approaches. Dalal found that judicious choice of dissimilar liquids for calculating the solid surface energy resulted in smaller standard deviations than averaging results from a large number of liquids [15]. Table 3.6 shows the results of geometric

mean calculations for all liquids and for selected dissimilar pairs, as well as the thermodynamic work of adhesion to TATB. In this case, the dissimilar pairs were H_2O / DEG and H_2O / DMSO or hexadecane.

Table 3.6. Surface energy of the polymer binders and work of adhesion to explosives (dyn/cm, ± standard deviation)

Polymer	*Dissimilar liquids*			*All*	*Dissimilar*	*Dissimilar*
	γ^d	γ^p	γ_s	γ_s	**W_a to TATB**	**W_a to HMX**
50 FC/ 50 LFC	16.5 ± 5.1	2.2 ± 1.2	18.8 ± 3.9	16.7 ± 4.5	40.2	57.2
75 FC/ 25 LFC	15.1 ± 6.0	5.6 ± 2.4	20.7 ± 3.6	19.4 ± 3.4	48.1	61.8
Kel-F 800	26.4 ± 0.5	1.2 ± 0.1	27.6 ± 0.4	24.5 ± 5.4	42.7	66.2
Kel-F 3700	27.1 ± 0.4	0.9 ± 0.0	28.0 ± 0.4	25.0 ± 5.3	41.7	65.9
Oxy-461	29.1 ± 3.2	3.3 ± 0.7	32.4 ± 2.5	29.7 ± 5.0	51.6	74.5
PTFE	22.2 ± 2.9	0.0 ± 0.1	22.2 ± 2.9	22.9 ± 2.3	28.0	53.4
THV 220	19.9 ± 0.9	1.4 ± 0.2	21.3 ± 0.7	19.1 ± 4.0	39.5	59.3
Viton A	15.2 ± 5.3	4.0 ± 1.8	19.0 ± 3.6	18.3 ± 3.0	44.4	57.2
NP/Estane	26.3 ± 0.1	6.8 ± 3.1	33.1 ± 3.2	39.2 ± 7.8	61.1	77.7

Calculation of surface energies using the H_2O / glycerol combination consistently resulted in large outliers, as seen in the higher standard deviation for “all test liquids” reported. The only exceptions were PTFE, Viton A and 75FC/25LFC, which had approximately the same uncertainty using all solvent pairs. As a verification of the geometric mean calculations, the PTFE surface energy of 22.2 dyn / cm is in the range of 18 – 23.9 dyn / cm reported by Wu for various energy determination methods [14]. Table 3.7 compares the results for PTFE from this work with those in the literature.

Table 3.7. Experimentally determined surface energies from this study compared with literature values. Also cited is the method used previously for determining the surface energy.

Polymer	γ_S **(this study)**	γ_S **Ref.**	**Method**
PTFE	22.2	18 [14]	Critical surface tension
		18.8 [14]	Geometric mean
		22.6 [14]	Harmonic mean
		23.9 [14]	Liquid homologue
		32 [16]	Geometric mean
Kel-F 800	27.6	27 [8]	Molar parachor
		28 ± 1 [32]	Molecular dynamics sim.
Viton A	26.3	29.7[16]	Geometric mean

Kel F 800 and Viton A are the only investigated materials for which the surface free energies have been previously reported. Small differences were observed between our calculated values for γ_s and those of Rivera for Kel-F 800. However, the surface energy of Kel-F 800 determined from the contact angle measurements is in remarkable agreement with recently calculated values using a molar paranchors group additive method (27 dyn/cm) [8], and molecular dynamics simulations (28 ± 1 dyn/cm) [32]. In general, the alignment of the values in this study with these calculated values, along with the earlier literature value for Viton A, lends confidence to the methods and solvent combinations chosen here.

Inspection of Table 3.6 shows that overall the surface energies for the fluoropolymers studied do not differ by more than 15 dyn/cm across the series. The values for the range of fluoropolymers reported here are in line with the values reported for the related fluoropolymers PTFE, PVDF, PCTFE, and polytrifluoroethylene by Owens [11] and Kaelble [13]. Kaelble and Owens have both reported correlations between the polar and dispersive components of the surface energy

and degree of substitution of the backbone H atoms with Cl- or Fl-. Here, all of the binders contain over 50% F-for-H substitutions, and the complexity of the monomer compositions and weight or mole percentages makes correlations of the subtleties of the backbone structures with surface energies difficult. For binder evaluation purposes, however, the total surface energies of the other binders are similar to Kel-F 800 with the greatest difference observed for the FC-2175/LFC-1 mixtures. These mixtures are medium and low molecular weight analogues (~85 kD and ~10 kD respectively) of the HFP-VDF class of copolymers that includes Viton A [33]. In addition to containing bulky HFP side groups, the two FC-2175/LFC-1 copolymers had the most different starting forms, as high viscosity gums and liquids compared with brittle granules or agglomerates of the other binders. The starting forms may influence thin film formation and surface morphology. Interestingly, the surface energies of the two CTFE-VDF copolymers, Kel-F 800 and Kel-F 3700, are quite similar, despite known differences in chain length and chemistry. The two polymers differ by the monomer ratios and molecular weight, with Kel-F 3700 having substantially (by an order of magnitude) longer chains, and greater (by over 2×) VDF content.

Gee *et al*. calculated the surface energies and work of adhesion to TATB for 4 binders including Kel-F 800 and three high-Tg, amorphous fluoropolymers using molecular dynamics (MD) simulations [8]. The MD simulations were validated by computation of the polymers' glass transition temperatures. The works of adhesion of Kel-F 800 were 76 dyn / cm for the [001] surface and 271 dyn / cm for the [100] surface of TATB, again illustrating the anisotropy of TATB crystals. Here, the calculated work of adhesion using Rivera's TATB surface energies was 43 dyn / cm, a significant difference. It is possible that the difference between Gee's

simulations and Rivera's measurements is derived from surface defects, or other experimental variables (such as the crystallographic direction tested in the experiments which was not specified). In Gee's study, the fluoropolymer binders showed a greater Wa, or more favorable interaction, with the [100] surface compared to the [001] surface. The [100] interface was found computationally to be a rough surface, with exposed nitro- and amino- groups, and increased surface area, promoting binder-crystal adhesion and dipole-dipole interactions between the polar moieties and fluorine in the polymers' backbones. Similarly the spreading coefficients were also found to be greater for [100] vs. [001], indicating that the binders better wet the [100] surface as well.

Of the fluoropolymer binders studied here, Oxy 461, the CTFE-TFE-VDF copolymer, may exhibit slightly improved adhesion to TATB over the other binders, with PTFE expected to be the worst, if it were processable with TATB. Kel-F 800 is in the middle of the range of values. Overall, the difference in the work of adhesion across the series (in the absence of PTFE, which is not soluble) is not large (~15 dyn/cm), as may be expected due to the similarities in copolymer compositions. There appears to be little interpretable correlation between F- substitution or side group (HFP) content on the copolymers' surface properties, due to the complexity of the copolymer compositions across the series. Since the adhesion to TATB is expected to be similar across the series, it is expected that the polymers' physical properties (thermal expansion coefficient, crystallization/melting, elastic modulus) would have more of a dominant effect on TATB-based PBX mechanical properties. For example, Rizzo *et al.* have previously reported that TATB formulated with high-Tg binders can reduce the bulk linear coefficient of thermal

expansion (by up to 25%), and ratchet growth phenomena (by up to fivefold), particularly between 40-70^{o}C [7].

Though not the original goal of the study, it is worthwhile to compare the work of adhesion between the various binders to several molecular crystals of interest in this thesis. Figure 3.4 illustrates the calculated work of adhesion between the binders to TATB, HMX, 1,3,5-trinitroperhydro-1,3,5-triazine (RDX), and acetaminophen. Surface energies used in the calculation are as stated earlier for TATB and HMX and are taken from the literature for RDX [34] and acetaminophen [35].

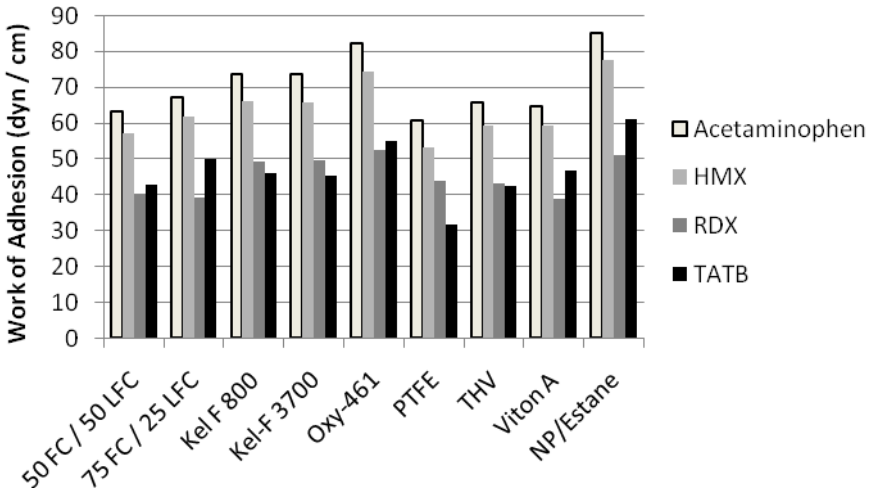

Figure 3.4. Work of adhesion between the studied binders and four molecular crystals

NP/Estane generally shows the highest thermodynamic adhesion to each of the crystals, though Oxy-461 is very close. Either of these binders are preferable to the others studied. In cases where compliant polymers are needed, the NP/Estane should probably be the binder of choice.

However, if chemical resistance or specific processing is desired, the fluropolymer Oxy-461 is likely to be more suitable.

3.5 Conclusions

A series of fluoroelastomer binder candidates have been evaluated for their adhesive interactions with the high explosive crystal TATB by measuring their respective surface energies using contact angle methods. Additional formulations were evaluated by considering the PBX 9501 binder and several other molecular crystals. The copolymer compositions of the binders are varied, and no strong correlations of the surface energies with backbone structure were found to exist across the series. By using the measured values of the surface energy of acetaminophen, HMX, RDX and TATB, the work of adhesion of the binders was determined for a variety of scenarios. While the adhesion of the binder to the crystal is not the only factor for determining the best possible binder in a plastic-bonded explosive, the common failure mode of a crack propagating along crystal-binder boundaries indicates that adhesion is critical for composite durability. Based on these results, Oxy 461 and NP/Estane might be expected to show slightly improved adhesive strength to the molecular crystals of interest. The remaining binders in the series are expected to have similar adhesion compared with Kel-F 800, and may be sensible choices for substitution in PBX formulations. Due to the similar adhesive properties of the binders, the thermal and mechanical properties of the binders are expected to be a more dominant factor in overall PBX mechanical performance.

References

[1] E James. The Development of Plastic-Bonded Explosives. UCRL-12439-T. Livermore, CA: Lawrence Radiation Laboratory; 1965. p. 15.

[2] JK Bower, JR Kolb, CO Pruneda. Polymeric Coatings Effect on Surface Activity and Mechanical Behavior of High Explosives. Industrial & Engineering Chemistry Product Research and Development. 19 (3), 1980, 326-9.

[3] ZW Liu, HM Xie, KX Li, PW Chen, FL Huang. Fracture behavior of PBX simulation subject to combined thermal and mechanical loads. Polym Test. 28 (6), 2009, 627-35.

[4] P Chen, H Xie, F Huang, T Huang, Y Ding. Deformation and failure of polymer bonded explosives under diametric compression test. Polym Test. 25 (3), 2006, 333-41.

[5] PJ Rae, SJP Palmer, HT Goldrein, JE Field, AL Lewis. Quasi-static studies of the deformation and failure of PBX 9501. Proc R Soc London, Ser A. 458 (2025), 2002, 2227-42.

[6] SJP Palmer, JE Field, JM Huntley. Deformation, Strengths and Strains to Failure of Polymer Bonded Explosives. Proc R Soc London, Ser A. 440 (1909), 1993, 399-419.

[7] HF Rizzo, JR Humphrey, JR Kolb. Growth of 1,3,5-Triamino-2,4,6,-Trinitrobenzene (TATB). II. Control of growth by use of high Tg polymeric binders. Propellants Explos Pyrotech. 6 (2), 1981, 27-36.

[8] RH Gee, A Maiti, S Bastea, LE Fried. Molecular Dynamics Investigation of Adhesion between TATB Surfaces and Amorphous Fluoropolymers. Macromolecules. 40 (9), 2007, 3422-8.

[9] A Dupré. Théorie Méchanique de la Chaleur. Paris: Gauthier-Villars; 1869.

[10] T Young. An Essay on the Cohesion of Fluids. Philos Trans R Soc London. 95, 1805, 65-87.

[11] DK Owens, RC Wendt. Estimation of the surface free energy of polymers. J Appl Polym Sci. 13 (8), 1969, 1741-7.

[12] T Nguyen, WE Johns. The effects of aging and extraction on the surface free energy of Douglas fir and redwood. Wood Sci and Technol. 13 (1), 1979, 29-40.

[13] DH Kaelble. Dispersion-Polar Surface Tension Properties of Organic Solids. J Adhes. 2 (2), 1970, 66 - 81.

[14] S Wu. Polymer Interface and Adhesion. New York: Marcel Dekker, Inc.; 1982.

[15] EN Dalal. Calculation of solid surface tensions. Langmuir. 3 (6), 1987, 1009-15.

[16] T Rivera, ML Matuszak. Surface properties of potential plastic-bonded explosives (PBX). J Colloid Interface Sci. 93 (1), 1983, 105-8.

[17] PK Sharma, KH Rao. Analysis of different approaches for evaluation of surface energy of microbial cells by contact angle goniometry. Adv Colloid Interface Sci. 98 (3), 2002, 341-463.

[18] WE Cady, LE Caley. Properties of Kel F-800 Polymer. Livermore, CA: Lawrence Livermore National Laboratory; 1977.

[19] TA Mykhaylyk, SD Evans, CM Fernyhough, IW Hamley, JR Henderson. Surface energy of ethylene-co-1-butene copolymers determined by contact angle methods. J Colloid Interface Sci. 260 (1), 2003, 234-9.

[20] RY Yee, A Adicoff, EJ Dibble. Surface Properties of HMX Crystal. China Lake, CA: Naval Weapons Center; 1981.

[21] DM Hoffman, FM Matthews, CO Pruneda. Dynamic mechanical and thermal analysis of crystallinity development in Kel-F 800 and TATB/Kel-F 800 plastic bonded explosives : Part I. Kel-F 800. Thermochim Acta. 156 (2), 1989, 365-72.

[22] A Siegmann, G Cohen, Z Baraam. The crystallization and transition behavior of poly(vinylidene fluoride)/copoly(chlorotriofluorethylene-vinylidene fluoride) blends. J Appl Polym Sci. 37 (6), 1989, 1481-9.

[23] TG Fox. Bull Amer Phys Soc. 1 (2), 1956, 123.

[24] B Wunderlich. Thermal Analysis of Polymeric Materials. New York: Springer-Verlag; 2005.

[25] LH Sperling. Introduction to Physical Polymer Science. 3rd ed. New York: Wiley; 2001.

[26] S Polowinski. Properties of copolymers: Estimation and prediction. J Appl Polym Sci. 79 (10), 2001, 1924-7.

[27] P Bonardelli, G Moggi, A Turturro. Glass transition temperatures of copolymer and terpolymer fluoroelastomers. Polymer. 27 (6), 1986, 905-9.

[28] NW Johnston. Sequence Distribution-Glass Transition Effects. Macromolecules. 14 (2), 1976, 215 - 50.

[29] NK Bourne, GT Gray, Iii. Dynamic response of binders; teflon, estane[trademark sign] and Kel-F-800[trademark sign]. J Appl Phys. 98 (12), 2005, 123503.

[30] DH Kaelble. Peel Adhesion: Influence of Surface Energies and Adhesive Rheology. J Adhes. 1 (2), 1969, 102 - 23.

[31] H Kamusewitz, W Possart. The static contact angle hysteresis obtained by different experiments for the system PTFE/water. Int J Adhes Adhes. 5 (4), 1985, 211-5.

[32] J Bicerano. Prediction of Polymer Properties. 3rd ed. New York: Marcel Dekker, Inc.; 2002.

[33] 3M. Technical Data Sheets. Minneapolis, MN2009.

[34] L Yunjun, D Meina. The Use of Inverse Gas Chromatography (IGC) to Determine the Surface Energy of RDX. Propellants Explos Pyrotech. 32 (6), 2007, 496-501.

[35] E Ålander, M. , Å Rasmuson, C. . Agglomeration and adhesion free energy of paracetamol crystals in organic solvents. AlChE J. 53 (10), 2007, 2590-605.

CHAPTER FOUR

EXAMINING CHEMICAL STRUCTURE AT THE INTERFACE BETWEEN POLYMER BINDERS AND PHARMACEUTICAL CRYSTALS

This chapter presents the results of neutron reflectometry, infrared spectroscopy and ellipsometry of several idealized plastic-bonded explosives. It expands upon the microstructural characterization done with synchrotron x-rays and the interfacial chemistry characterization done with contact angle measurements, which were both presented previously in this dissertation. Neutrons interact with the lighter elements found in polymers much more strongly than x-rays, allowing for improved spatial resolution at the interface of polymer-crystal composites. While infrared spectroscopy and ellipsometry do not give higher spatial resolution data than shown in the x-ray study, they provide an insight into chemical bonding and intermixing to complement the neutron reflectometry results.

4.1 Introduction

The mechanical behavior of compacted granules is of importance for both pharmaceutical compacts and plastic-bonded explosives (PBX). Many pharmaceutical powders used in medicine display poor compaction behavior and consequently are coated with a binder to improve tablet-formation properties [1-4]. The powders are coated in a process called granulation, which can be performed with liquid (“wet”) or solid (“dry”) binding material. Dry granulation involves mixing the solid binder with the powder and pressing or rolling into a compacted solid. In wet granulation, a liquid binder is mixed with the powder by spraying, dissolving, or physical mixing. Typical binders are natural or synthetic organics such as acacia, starch, gum, gelatin, and

various polymers [5-7]. The resulting granule typically is powder coated with a binder layer of some thickness. Initial powder size and shape, agglomerate size and shape, surface area, moisture content, and various processing parameters all affect the resulting tablet mechanical and chemical properties [8]. Tablet durability and mechanical failure is a serious problem with many pharmaceutical drugs, and determining the processing-structure-properties relationship for these powders is an active area of research [9].

Plastic-bonded explosives (PBX) are analogous to compacted pharmaceutical tablets as composites. A typical PBX consists of an explosive molecular organic crystal coated with a polymer binder [10]. Material formulation is similar to wet granulation for pharmaceuticals – the micron-sized explosive crystals are suspended in water and subsequently mixed with a polymer in a solvent. The polymer coats the particle by preferential wetting, displacing the water. For example, the Los Alamos National Laboratory material designated PBX 9501 is formulated by mixing cyclotetramethylene-tetranitramine (HMX) powder with a nitroplasticized statistical copolymer in methyl ethyl ketone (MEK) [11]. The agglomerates, referred to as “molding prills”, can then be pressed into billets suitable for machining. The plasticized binder provides mechanical stability and decreased sensitivity while retaining the detonative properties of HMX [12].

The mechanical properties of PBX and pharmaceutical compacts are defined similarly and display similar failure pathways. Cracking and debonding of the crystals from the binder results in anisotropy within the composite. Such brittle failure, sometimes termed “capping” in pharmaceutical tablet compaction, can cause processing and stability problems in these

materials. In explosives, such cracks can have serious implications for safety and sensitivity, or the ease of accidental burning or detonation of the explosive [11-14]. Detonative properties in intentional use might also be affected; the affect of such cracks is poorly understood in this regime [15]. Observations of microstructures in these composites that have undergone mechanical failure reveal crack paths that primarily follow the interface between crystals and the binder matrix [11]. Therefore, characterization of the interface between the binder and the crystal is of interest. The properties of the interface depend on surface chemistry and structure [16-18]. Surface energies have been measured for several binders and active ingredients [19], but interfacial structure and chemistry and the effects of the formulation process in this interface have not been studied in detail. Current mechanical and failure models often assume that the interface is sharp, with no intermixing, and that the chemical composition of the polymer at the interface is the same as in the bulk [20, 21]. This may be the case for certain formulations but has not been demonstrated previously, and that assumption is of particular importance for composites in which the crystals could be soluble in the polymer solution.

Mechanical properties and failure of both classes of materials have important consequences in terms of product development, durability, and safety. Here, the interfacial properties of a few model systems are studied systematically with a variety of complementary techniques. The systems are various crystal-polymer combinations of the pharmaceutical crystals acetaminophen (paracetamol) and sulfamerazine with the polymers Estane, a 50:50 mix of nitroplasticizer and Estane (the PBX 9501 binder), and hydroxypropyl cellulose (HPC). Acetaminophen is chosen due to its poor compaction properties even in the presence of a binder [1] and is a suitable simulant for HMX. Acetaminophen is similar in crystal structure to HMX, being stable in the

monoclinic space group $P2_1/c$ while HMX is referenced to $P2_1/n$, and both materials exhibit polymorphism [22]. Additionally, both crystals are known to be soluble in polar solvents, such as MEK [23], which may lead to diffusion of the crystals into the binder during formulation. Similarly, sulfamerazine is a polymorphic crystal with interesting compaction properties, but the solubility in many common polymer solvents is much lower than acetaminophen [24-26]. The polymers were chosen to study both chain complexity and monomer volume; Estane is a small statistical copolymer while the cellulose monomer is relatively large but simple in chemistry as shown in Figure 4.1. The model chosen to directly simulate PBXs is acetaminophen coated with PBX 9501 binder. The PBX 9501 binder is a 1:1 mixture of Estane 5703 and a nitroplasticizer. Estane segregates into hard and soft domains, causing mechanical heterogeneity throughout the polymer [17, 27, 28]. In the figure, the hard domains are repeated "m" units, while the soft domains are repeated "n" units.

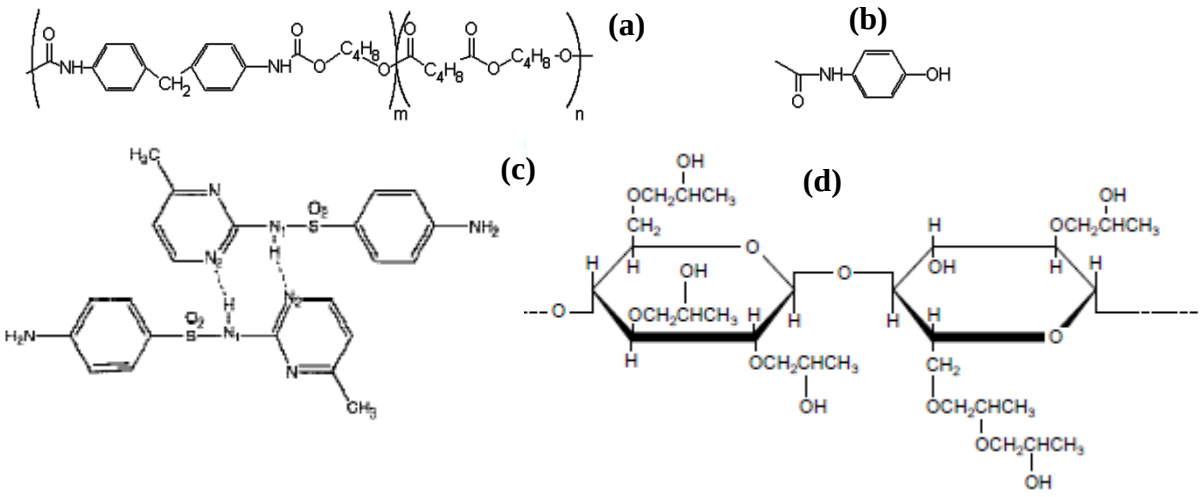

Figure 4.1. The chemical structures of Estane (a), acetaminophen (b), a dimer of sulfamerazine showing hydrogen bonding (c), and hydroxypropylcellulose (d). For Estane 5703, m and n represent typically 20 and 80 percent of the polymer by volume, respectively [17].

This chapter presents an ellipsometry, transmission infrared spectroscopy and neutron reflectometry investigation of the chemistry and structure of the simulated wet-agglomeration materials. Ellipsometry was used to determine the optical properties of the samples and film thicknesses. In addition, by scanning at multiple angles and with multiple wavelengths, complex analysis of intermixing of films was performed. Because acetaminophen is soluble in the MEK-polymer mixture and could wash off during the coating process, infrared spectroscopy was used to verify the presence of acetaminophen in the coated samples. Infrared spectroscopy was not needed for the sulfamerazine samples. Neutron reflectometry (NR) has been used to study the interfaces and inter-mixing of polymeric systems [29-31]. Incident neutrons are scattered from polymer nuclei, and therefore their scattering intensity is a function of the nuclear constituents. Since neutrons are weakly scattered by nuclei, they can probe buried interfaces [32]. Neutron reflectometry has been used previously by Smith et al. to investigate the migration of the nitroplasticizer within Estane 5703 [33]. Smith et al. examined samples of PBX 9501 binder spin-coated onto silicon wafers and found that the nitroplasticizer tended to concentrate at the Si-polymer and polymer-air interfaces. However, the effect of such phase segregation has not previously been experimentally determined at crystal/binder interfaces.

4.2. Experimental Methods

4.2.1 Sample Preparation

One of the historical difficulties in studying compressed agglomerates is the complex microstructure of the composite created in the formulation and pressing process. In order to focus only on the interfacial structure, composite interfaces were simulated with layers of thin films prepared with actual formulation materials. Two materials were used as film substrates,

depending on the experiment technique employed. Silicon wafers (Silicon Sense, Inc., Neshua, NH) were used as the substrate for ellipsometry and neutron reflectometry. The Si wafers were cleaned with an acetone wash and atmospheric plasma etching prior to film deposition. For infrared spectroscopy IR-grade potassium bromide (KBr) powder (Acros, Morris Plains, NJ) was pressed into disks and used as an alternative substrate.

Acetaminophen powder (Acros, Morris Plains, NJ) was dissolved in ethanol (Pharmco-AAPER, Brookfield, CT) to form a 7.5 wt% solution. Acetaminophen films were formed by dip-coating the substrates in the solution at 50 mm / min in a humidity-stabilized environment (~25%). Sulfamerazine (provided by the University of Minnesota) was also dissolved in ethanol to form 1.5 wt% solutions and an identical dip-coating procedure was used to produce films. Estane 5703 (B. F. Goodrich, Jacksonville, FL) pellets were dissolved in MEK (Fisher Chemical, Pittsburgh, PA) along with the nitroplasticizer to make PBX 9501 binder. The nitroplasticizer (NP) is a eutectic mixture of bis-2,2-dinitropropyl-acetal (BDNPA) and bis-2,2-dinitropropyl-formal (BDNPF), often referred to as BDNPA/F. The plasticizer was manufactured in-house. Estane pellets were also dissolved in MEK without the plasticizer for comparison. The PBX 9501 solution was 1.5% Estane and 1.5% plasticizer by weight, while the Estane comparison solution was 3.0 wt%. Klucel HPC (Ashland Inc., Covington, KY) was dissolved in ethanol to create 5 wt% solutions. Polymer films were dip-coated in a similar manner to the acetaminophen films. All films were allowed to dry at room temperature for at least 48 hours prior to any measurements.

Several acetaminophen and sulfamerazine films were then coated with the various polymers from solution for the representative composite interface samples. Polarized-light optical micrographs of a layered acetaminophen-NP/Estane film on Si are shown in Figure 4.2. The figure shows a top-down view of the surfaces of the two films, with the polymer partially coating the acetaminophen film on the right in Fig. 4.2(a) and uncoated acetaminophen visible on the left. Fig. 4.2(a) highlights the boundary or interface of the two films, and shows the dissolution of the acetaminophen structure forming a gradient of composition at the interface. In Fig. 4.2(b) the rough polycrystalline surface of the uncoated acetaminophen film is shown in more detail.

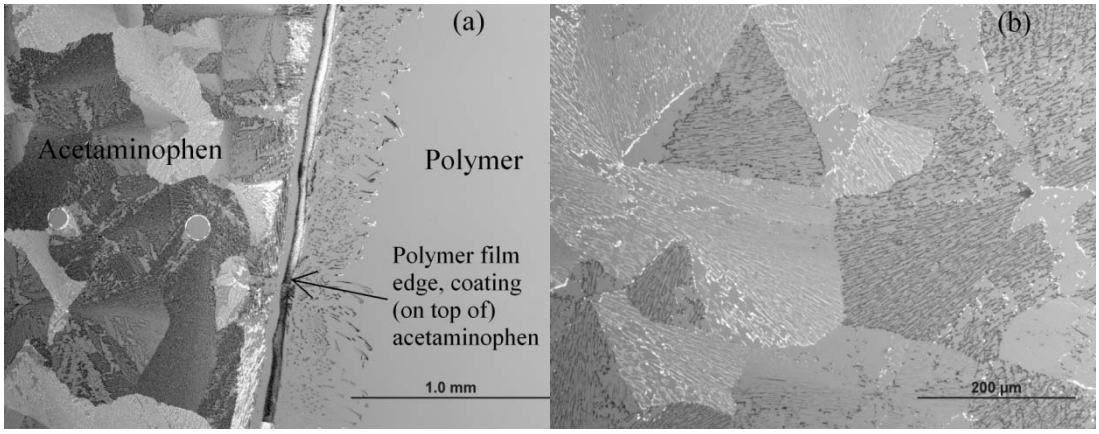

Figure 4.2. (a) Polarized light micrograph of the Estane film coating polycrystalline acetaminophen. (b) Higher magnification of acetaminophen film, showing distinct surface features.

4.2.2 Ellipsometry

Ellipsometry was performed with a variable angle spectroscopic ellipsometer (VASE) (J.A. Woolam Co., Inc, Lincoln, NE). The software was calibrated using a Si wafer with 137 Å of surface oxide. Each sample was scanned in the wavelength range of 3000 to 10000 Å, recording

data every 100 Å. The samples were aligned at 70° and measured at 65, 70, and 75°. Optical constants and film thicknesses were determined by fitting the data with a Cauchy approximation model, as in [34], and the accuracy of the fit was verified by a mean square error (MSE) calculation.

The samples were all assumed to be optically isotropic. Acetaminophen has three refractive indices [35], but since the films were polycrystalline they were modeled as isotropic. Sulfamerazine presented similar difficulties in modeling. Indeed, attempts to model the pharmaceutical ellipsometry data using multiple refractive indices were unsuccessful. In all cases, the MSE was high for the polycrystalline films. Layered samples were modeled both as a single film and as a composite structure for comparison. The VASE software includes several analysis packages for graded or intermixing films, and these were employed with varying success. The optical constants measured for these samples were the real (n) and imaginary (ik) components of the complex index of refraction ($\tilde{n}$). In polymers, k depends upon molecular conformation and orientation [36].

4.2.3 Infrared Spectroscopy

Composite film samples were compared to reference films and acetaminophen powder. Fourier transform infrared (FTIR) spectra were collected with a commercial bench-top spectrometer (Thermo-Nicolet Nexus 670 FTIR). Reference spectra of bulk powder and solvents were measured with the use of an attenuated total internal reflection (ATR) module. Spectra of films were measured by IR transmission through films deposited on KBr and Si wafers subtracting the transmission of the plain wafer as background.

4.2.4 Neutron Reflectometry (NR)

NR experiments were performed on the Surface Profile Analysis Reflectometer (SPEAR), a time-of-flight reflectometer at the Los Alamos National Laboratory Lujan Neutron Scattering Center. SPEAR receives neutrons from a polychromatic, pulsed (20 Hz) source that pass through a partially coupled liquid hydrogen moderator at 20 K and a beryllium filter to shift their energy spectrum. Choppers and frame-overlap mirrors reduce the wavelength (λ) range of the neutrons to 4-16 Å. By measuring the time it takes a neutron to travel the length of the instrument, the neutron's momentum, and therefore its wavelength, can be determined by the de Broglie relation. During a NR experiment, neutrons impinge on a sample at a small angle, θ, and the ratio of elastically scattered to incident neutrons is measured. This ratio is defined as the reflectivity, R, and is measured as a function of the momentum transfer vector, Q_z, where $Q_z = 4\pi\sin(\theta)\lambda^{-1}$. Because the average intensity over a large area is measured, reflectivity is sensitive to the surface coverage of the film.

Analysis of specular reflectometry data provides information regarding the coherent scattering length density (SLD) distribution normal to a sample's surface, SLD(z) where z denotes distance from the substrate. SLD is a value unique to a particular chemical composition and is the sum of the coherent scattering lengths of the constituent elements divided by the volume they occupy. It is important to note that the measured SLD values are absolute because NR data is normalized to the incident neutron intensity. To obtain a real-space interpretation of the scattering data, SLD(z), a Fourier transform can be applied. Because only intensity and no phase information is collected, a unique Fourier transform between a single NR profile and its real-space interpretation does not exist. Therefore, modeling was employed to interpret the NR data, following the general

technique described by Nelson [37]. Briefly, the continuous function SLD(z) is often well-approximated by a number of layers, referred to as boxes, each with a constant SLD. Interlayer roughness is taken into account by using an error function centered at each interface. The incident neutron beam is refracted at each interface, and a theoretical NR curve can be calculated using the Abeles matrix formalism, as in [38]. The measured and theoretical NR curves are compared, and using genetic optimization and the Levenburg-Marquardt nonlinear least-squares method, the best least-squares fit, corresponding to the lowest χ^2 value, is obtained. The simplest SLD model (least number of boxes) of physical relevance was used to interpret the NR data.

4.3. Results

4.3.1 Ellipsometry

Optical observations clearly indicate that the acetaminophen dissolves into the polymer film as a result of the coating process, as shown in Figure 4.2. Sulfamerazine showed similar dissolution behavior. By comparing the ellipsometry data from standalone films with the layered structure, an estimate of the remaining acetaminophen layer, if any, could be obtained. Figure 4.3 shows a typical data set from ellipsometry, including the Cauchy fit.

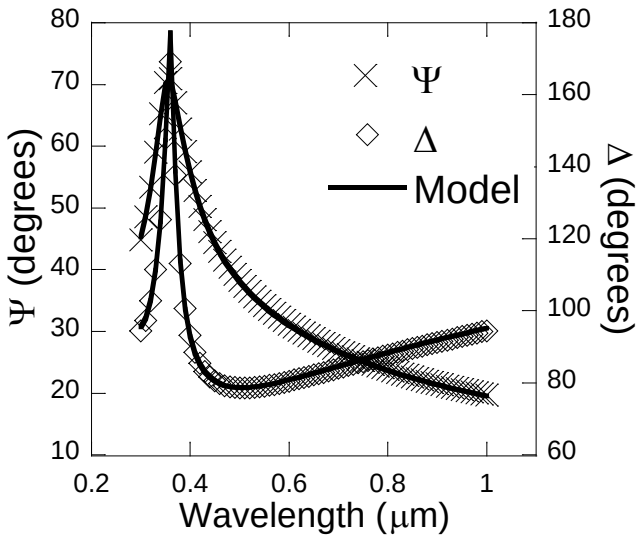

Figure 4.3. Change in amplitude (Ψ) and phase (Δ) of polarized light reflected from the Estane 5703 sample at 70°, along with the model fit.

The quality of the fit was assessed by the MSE. Any fit with error below 25 was deemed acceptable. Table 4.1 is a summary of the optical constants and thicknesses of the dip-coated films. The values in Table 4.1 are obtained using the Cauchy approximation model for a single layer only. In the case of layered samples, very good model fits were obtained using the single layer approximation.

Table 4.1. Dip-coating parameters and optical constants determined by ellipsometry

Sample	Coating Speed (mm / min)	Thickness (nm)	Variation (%)	*n*	*k*	MSE fit
BDNPA/F (NP)	50	523±2.0	9.55±0.20	1.472	0.002	24.8
Estane 5703	50	67.0±0.01	2.93±0.17	1.489	0.000	2.55
Acetaminophen	50	136 ± 0.29	19.6±0.69	1.568	0.005	20.6
Sulfamerazine	50	38.4 ± 0.13	negligible	1.634	0.15	8.72
HPC	50	41.7 ± 0.15	33.2 ± 20.1	1.478	0.001	0.985
NP/Estane	100	72.6 ± 0.10	3.09±0.05	1.486	0.006	8.35
NP/Estane on Aceta.	100	70.4 ± 0.07	8.89±0.25	1.475	0.005	6.22
Estane on Aceta.	100	114 ± 0.11	18.7±0.18	1.508	0.001	14.2
HPC on Aceta.	50	62.6 ± 0.4	65.1 ± 5.8	1.449	0.000	15.6
HPC on Sulfa.	50	41.1 ± 0.12	27.0±19.5	1.492	0.000	0.797

The models employed to produce Table 4.1 allowed all variables to float, yielding the best possible fit. One possible drawback of this approach is that model outputs can become physically unreasonable. This possibility was not observed; fit parameters obtained by utilizing realistic initial guesses for the model compare favorably with values available in the literature for similar materials [35, 39]. Variation in *n* between samples is explainable by the rule-of-mixtures approach. For example, the NP/Estane sample has a value of *n* between that of the pure Estane and the plasticizer, and the Estane – acetaminophen composite sample has *n* between that of the Estane and the acetaminophen individually. However, an explanation for the absorbance behavior of the samples is less obvious. It is likely that mixing the plasticizer and / or

acetaminophen in the polymer not only introduced absorbing material but also changed the polymer structure. Indeed, such a result is often the goal of plasticizing a polymer.

Fitting the data for the acetaminophen layer to a model was not as successful as for the polymers, likely due to the polycrystalline texture and high surface roughness of the film. However, the optical constants do agree with literature values [35]. For the NP/Estane – acetaminophen system, the accuracy of the fit was not changed significantly by a model wherein a very thin acetaminophen layer is beneath the polymer film. Therefore, the existence of such a layer is consistent with the ellipsometry data but is not required for the model. Similarly, the HPC-Sulfamerazine system only implicity showed an effect on the polymer from the crystal. Only the index of refraction was noticeably different when comparing HPC-Sulfamerazine composite film to the regular HPC film.

In contrast, the other two composite systems showed evidence of multiple layers. Table 4.2 summarizes the results of various models employed to fit the data for the Estane-acetaminophen and the HPC-acetaminophen ssamples. Thickness variation and measurement error in thickness are not included in Table 2 because they were all similar to the one-layer model from Table 4.1.

Table 4.2. Model parameters used for Estane – Acetaminophen samples. Italics indicate fixed inputs.

Sample	Model	Thickness (nm)	n	k	MSE fit
Estane-acetaminophen	Estane (top) coating Acetaminophen (bottom)	99.8 15.1	1.483 1.529	*0* *0.005*	24.0
	3 vol% Acetaminophen dispersed in Estane*	113	*1.489* *1.568*	*0* *0.005*	15.8
	Estane (top) coating Acetaminophen (bottom)	108 5.9	*1.489* *1.568*	*0* *0.005*	15.4
	One homogeneous layer	114	1.508	0.001	14.2
HPC-acetaminophen	One homogeneous layer	62.6	1.449	0.000	15.6
	HPC (top) coating Acetaminophen (bottom)	45.3 15.8	*1.478* *1.568*	*0.001* *0.005*	7.1
	HPC (top) Intermixed region† Acetaminophen (bottom)	45.3 2.2 15.8	*1.478* 1.523 *1.568*	*0.001* 0.003 *0.005*	7.1
	HPC (top) coating Acetaminophen (bottom)	57.7 3.9	1.485 *1.568*	*0.032* *0.005*	5.1

* An Effective Medium Approximation (EMA) was used: the two materials with fixed optical constants were modeled as a homogeneous distribution of one material through the other

† An "Intermixed" layer was used: the intermixed region had an evenly weighted mixtures of optical properties

The various modeling approaches in Table 4.2 provide some insight into the Estane-Acetaminophen sample. The effective medium approximation (EMA) is an analysis package included with the VASE software wherein two or more materials are considered intermixed. Here, the EMA assumed the film was a disordered medium and found a good fit for 3 vol% acetaminophen being dispersed throughout the Estane. A slightly better fit resulted from forcing the film to have previously determined (Table 1) optical constants and modeling them with a non-diffuse interface. The best fit assumed that the composite was one homogeneous film by allowing all the variables to float. However, the difference in error among the last three fits is not large. While Table 4.2 shows evidence of species mixing or diluting of the Estane layer, use of this technique alone to determine the film structure for these samples should be considered inconclusive.

Similarly, the HPC-acetaminophen sample showed evidence of some sort of intermixing. Adding a simple intermixing layer did improve the model from just using two standard films with properties from Table 4.1, but allowing the optical constants of the polymer to float did result in a better fit. In particular, the increase in *k* revealed serious disruptions in absorption behavior within the polymer, probably resulting from incorporated acetaminophen. The difference in model fits is shown in Figure 4.4, in which the dashed lines represent the two-standard-films model and the solid line represents the acetaminophen-modified HPC model. The dashed line does not appear to capture the experimental data quite as well as the solid line, particularly for the lower wavelengths.

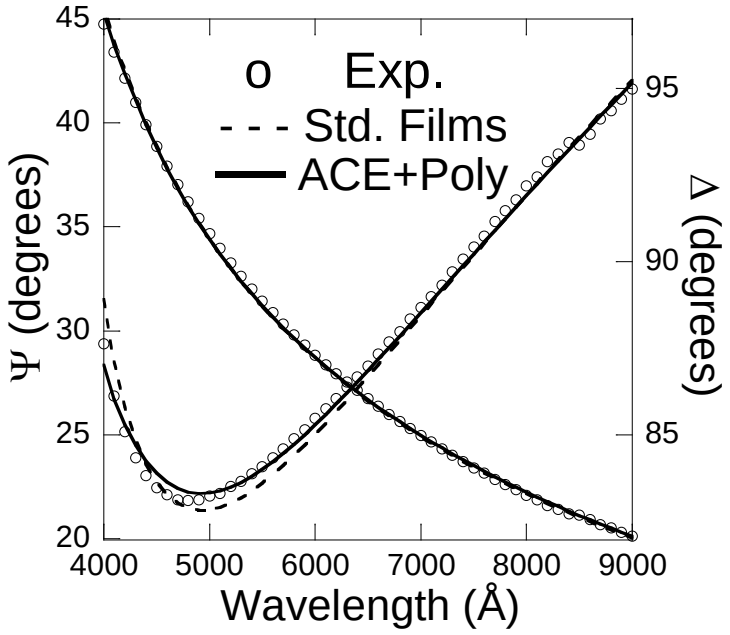

Figure 4.4. Change in amplitude (Ψ) and phase (Δ) of polarized light reflected at 70° from the acetaminophen-cellulose system, along with two models. Experimental data is shown in circles, the standard model fit as a dashed line, and the modified model fit as a solid line.

The acetaminophen which is responsible for the disrupted structure is not likely to be entirely at the interface, evidenced by the weaker model fit for an intermixing layer. One possible explanation is that acetaminophen from the underlying film was "washed off" during coating the HPC from ethanol, and molecules of acetaminophen became physically entrapped in the polymer matrix as it dried. However, ellipsometry is not powerful enough to positively identify an explanation.

4.3.2 Infrared Spectroscopy

Transmission measurement of the IR spectra was complicated slightly by the high attenuation of the Si wafers. Wafers coated with the polymer were too opaque to obtain a quality spectrum.

Therefore, an identical dip coating procedure was repeated with potassium bromide wafers which have much higher transparency at infrared wavelengths. NP/Estane was the only composite studied in this case because ellipsometry could not prove the existence of an acetaminophen layer beneath the polymer, whereas ellipsometry did give indications of crystalline layers in the other composites.

Figure 4.5 shows a comparison of the spectra of an acetaminophen film on KBr, an Estane film on KBr, and layered acetaminophen - Estane films on KBr. The spectrum of acetaminophen on KBr showed no significant differences from spectrum of bulk acetaminophen powder. The spectrum of the layered film on KBr sample clearly possesses peaks not present in the polymer film alone, and which correspond exactly to the prominent features in the acetaminophen film sample. The location of three such features are annotated by dotted lines in Fig. 4.5.

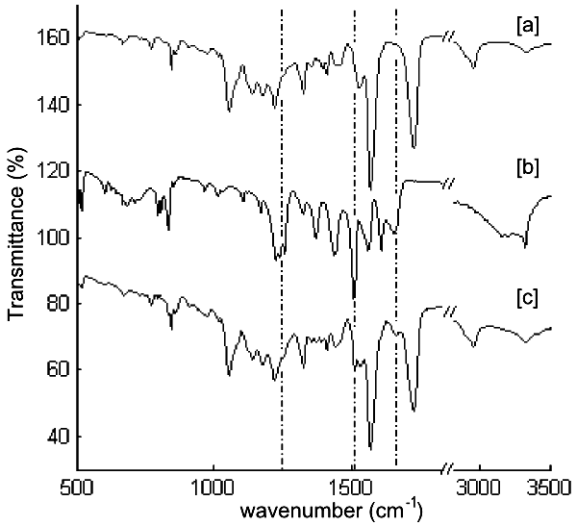

Figure 4.5. Partial FTIR spectra of (a) nitroplasticized Estane, (b) acetaminophen, and (c) the layered sample.

The absorbance peaks at approximately 1660, 1510, and 1260 cm^-1 all indicate the presence of acetaminophen in the layered specimen. Notably, there is no evidence of any residual ethanol in the acetaminophen, shown by the absence of the prominent ethyl C-O stretch which occurs at 1053 cm^{-1} in ethanol. This conclusion is further supported by the consistent relative intensity of the O-H stretching modes (~3200-3500 cm^{-1}) in bulk acetaminophen and the KBr film. Similarly, it can be verified that the polymer layer is free of residual solvent by the absence of a peak at 1366 cm^{-1} normally prominent in MEK (due to C-C-H bending involving the methyl group).

These results confirm that the sequential dip coating method produces structures containing the desired constituents in approximation of the composite formulation, and that the acetaminophen is not washed off during deposition of the polymer layer. The relative intensity of the polymer and acetaminophen spectral features indicates that a larger quantity of polymer is deposited than acetaminophen, which agrees with the modeled ellipsometry data. FTIR also confirmed the existence of acetaminophen beneath the plasticized polymer while ellipsometry was inconclusive. However, this technique does not allow for through-thickness spatial precision in indentifying chemical components.

4.3.3 Neutron Reflectometry

Reflectometry data were collected successfully for all the film samples. Reference samples of each film individually were measured and modeled first, with the resulting baseline parameters used to model the polymer-crystal layered samples. A typical reflectivity profile is shown in Figure 4.6 along with the corresponding theoretical fit.

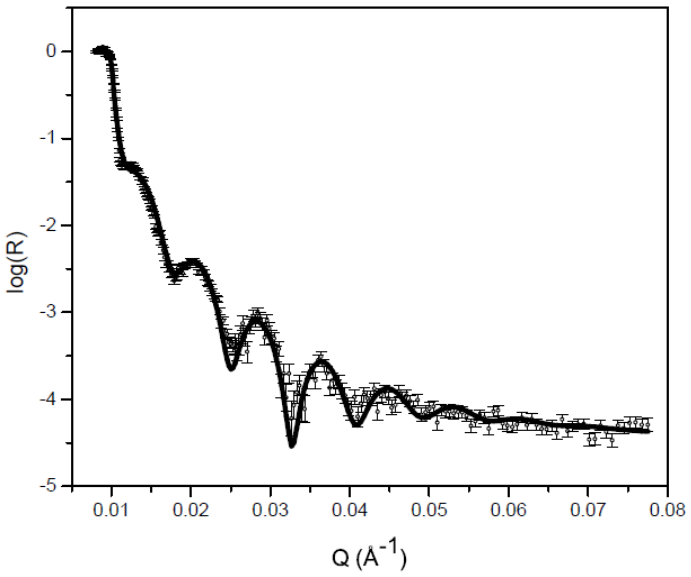

Figure 4.6. Reflectivity vs. momentum transfer vector Q for the sample with NP/Estane coating acetaminophen. Data points are shown by open circles with error bars indicating one standard deviation. The model fit is shown by the solid line.

The data fitting procedure described in the Experimental section was initiated for the reference samples by using theoretical SLD values and literature reports. The measured data compared well with literature reports for the standalone films. For the layered samples, the fitting method initially used a single box for each layer and a perfectly clean interface between each layer. Additional boxes were used to represent the mixing of the two layers, if necessary. The "roughness" of interphase boxes in these cases represents intermixing of the layers. The modeling results for the layered samples are shown in Table 4.3. Each sample was modeled with similar Si and SiO_2 layers, which are omitted in the table for brevity.

Table 4.3. Data fitting parameters for the composite NR samples along with the goodness of fit. The parameters for each individual component are italicized.

Sample	**Thickness (nm)**	**SLD ($x10^{-6}$ Å^{-2})**	**Roughness (nm)**	χ^2
NP/Estane	71	-	-	3.6
Concentrated NP	*7*	*2.01*	*0.5*	
Bulk polymer	*64*	*1.9*	*9.8*	
NP/Estane-acetaminophen	73	-	-	5.3
Acetaminophen	*2*	*0.72*	*0.7*	
Concentrated NP	*14*	*1.94*	*0.5*	
NP Estane	*57*	*1.9*	*4.0*	
Estane-acetaminophen	105	-	-	5.0
Acetaminophen	*3*	*0.66*	*1.0*	
Interphase 1	*12*	*0.95*	*2.0*	
Interphase 2	*30*	*1.13*	*8.0*	
Estane	*60*	*1.33*	*7.5*	
HPC-acetaminophen	39	-	-	0.1
Acetaminophen	*5*	*0.20*	*0.4*	
HPC	*34*	*0.71*	*2.1*	
HPC-sulfamerazine	43	-	-	3.0
Sulfamerazine	*5*	*1.23*	*1.0*	
HPC	*38*	*0.84*	*2.5*	

Comparison of the NR data with the ellipsometry results in Table 4.2 reveals further details of the film structure. NR confirms the thicknesses of the samples within about 10 nm, and shows layer mixing characteristics weakly suggested by ellipsometry. NR is considerably more useful in determining precise chemical structure of the layered samples. Modeling the results showed that the NP tends to concentrate at the substrate interface, consistent with previous observations of NP/Estane [33]. Thus the NP/Estane layers were best modeled with two boxes – a thin layer of concentrated NP coated with a layer of intermixed NP and Estane.

The SLD required for the model fit for acetaminophen is much lower than theory would predict. Because SLD is a function of chemistry and density, the most likely explanation is that the high roughness of the acetaminophen film lowers the effective density. The model assumes a box-shaped layer of complete homogeneity except for small surface roughness, so a very rough film with air filling the valleys between ridges of acetaminophen is modeled as a low density solid film. The validity of the interphase approach is thus in question as it is possible that the model results could be equally achieved by chemical intermixing or simply by Estane filling the corrugations. The SLD profile of the modeled system shows that both modes are present. Figure 4.7 shows the SLD profile of the Estane-acetaminophen system overlaying a schematic representation of the data.

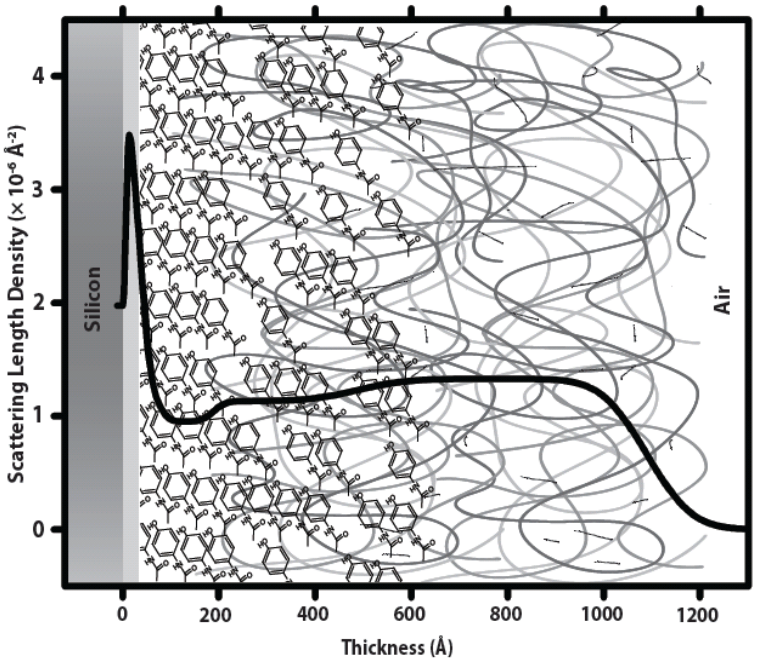

Figure 4.7. Scattering length density profile for the Estane-acetaminophen layered sample, showing a thin layer of acetaminophen (shown as drawings of acetaminophen molecules) intermixing with the polymer (shown as curved lines). Schematic depicts variations in chemistry as a function of thickness.

The sample in Fig. 4.7 consists of a thin native oxide layer coated with a 30Å film of solid acetaminophen with high surface roughness extending another 20Å or so before being coated by a thick polymer film. A definite chemical gradient exists between the two, as shown by the gradually increasing SLD between 200 and 600 Å in the figure. Some of this can be explained by polymer filling in the area between acetaminophen ridges, but considering the ellipsometry results, which limit the film thickness to at most 15nm, the remainder of the gradient can only be a result of acetaminophen migrating into the Estane. This is probably due to the presence of the MEK solvent during the dip coating process.

The NP/Estane does not explicitly show the same type of interface, illustrated in Figure 4.8. The plasticizer has such a high SLD that the presence of acetaminophen beyond 20Å into the sample is difficult to observe directly. The actual value of the SLD for the concentrated plasticizer in this sample is only 1.94×10^{-6} Å^{-2}, which is lower than the concentrated plasticizer without the presence of acetaminophen. Considering that acetaminophen has a much lower SLD than the plasticizer, and assuming that the heavily plasticized region of the polymer is similar in both samples, then the net lowering in the layered sample indicates acetaminophen has physically mixed with the plasticizer, and perhaps also dissolved into the polymer in a similar manner as shown in Fig. 4.7.

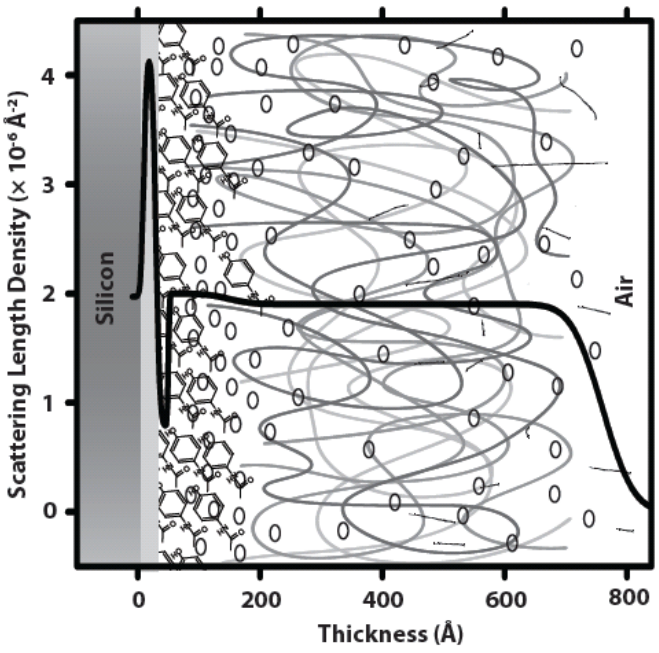

Figure 4.8. Scattering length density profile for the NP/Estane-acetaminophen layered sample, showing a thin layer of acetaminophen (shown as drawings of acetaminophen molecules) intermixing with the plasticizer (ovals) at the interface. The polymer is shown as curved lines. Schematic depicts variations in chemistry as a function of thickness.

Further insight into interface formation can be gained by examining the HPC-acetaminophen composite, shown in Figure 4.9. In this case, the polymer solvent was ethanol, in which acetaminophen is less soluble than it is in MEK. Much less of an interphase region was observed than in either Estane-based samples.

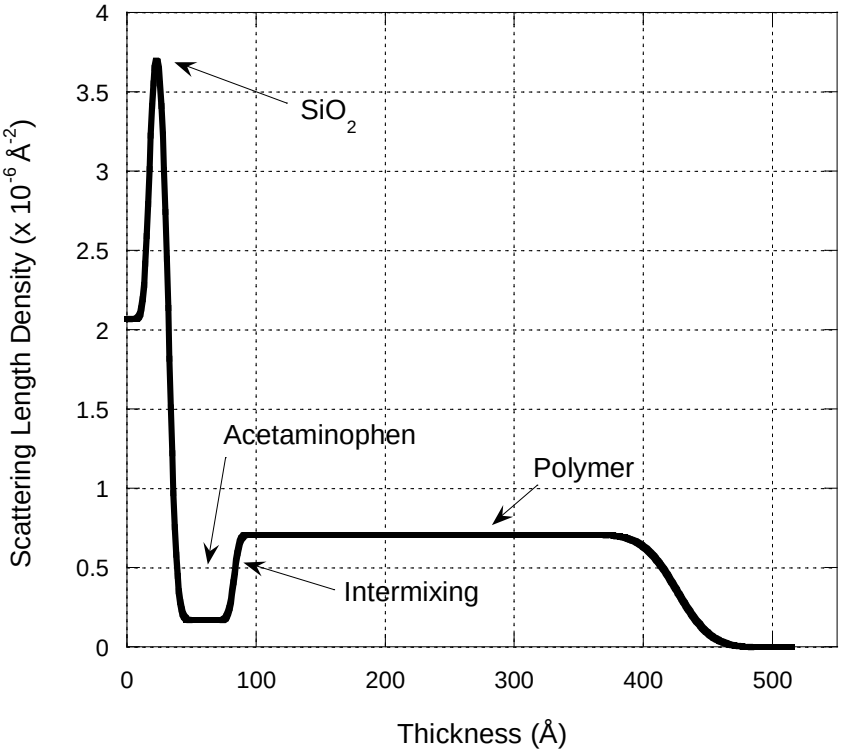

Figure 4.9. Scattering length density profile for the HPC-acetaminophen layered sample, showing chemistry as a function of depth into the sample. The region between plateaus of acetaminophen and polymer is interpreted here as an intermixing zone.

Fig. 4.9 reveals that acetaminophen does not form the same type of interface with HPC as it does with Estane. It should be noted that the size of the intermixing region is on the same scale as the intermixing zone predicted by one of the models in Table 4.2, about 20Å. Given the high roughness of the polycrystalline acetaminophen, as discussed earlier, it is likely that the majority

of this intermixing zone is simply physical intermixing rather than chemical bonding and dissolution.

The HPC-sulfamerazine composite showed similar behavior to HPC-acetaminophen, but the intermixing zone appeared to be approximately double the size in the sulfamerazine sample. The scattering length density profile is shown in Figure 4.10. However, the sulfamerazine also does not have an extensive intermixing zone, and in general the two composites are quite similar.

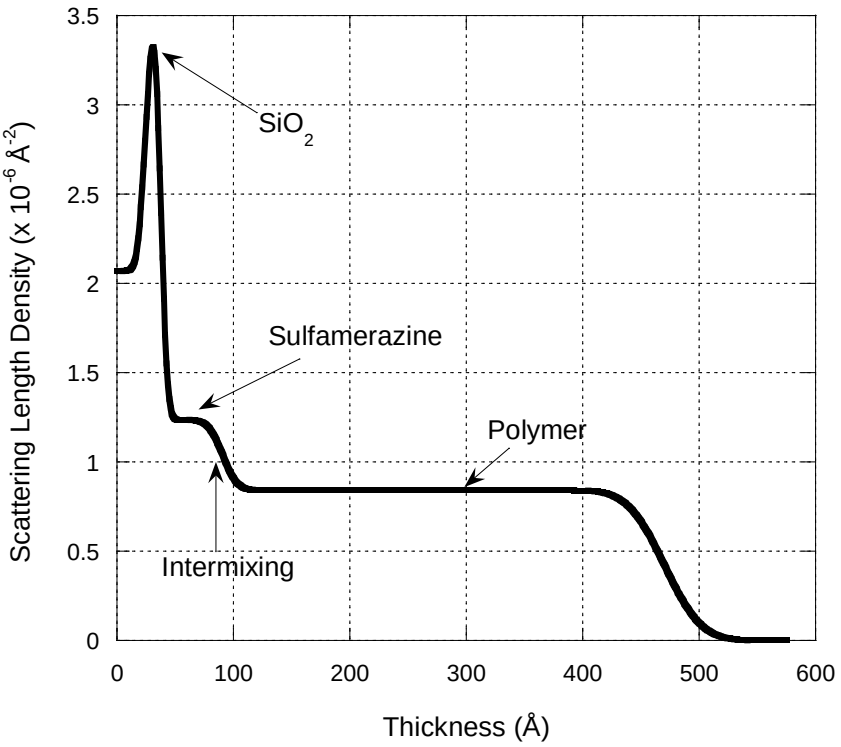

Figure 4.10. Scattering length density profile for the HPC-sulfamerazine layered sample, showing chemistry as a function of depth into the sample. The region between plateaus of sulfamerazine and polymer is interpreted here as an intermixing zone.

4.4. Discussion

Ellipsometry and neutron reflectometry appear to be excellent complementary techniques, with application of one to the other assisting in model development and analysis. Application of the ellipsometry results shown in Table 4.2 to the SLD information shown in Figs. 4.7 and 4.8 provide some interesting insight into the simulated PBX materials – acetaminophen coated with Estane with and without a plasticizer. While the intermixing region is similar in both samples, the interphase region is much smaller with the nitroplasticizer than in the Estane-acetaminophen sample. Ellipsometry results had shown definite intermixing behavior in the non-plasticized sample but little or no intermixing in the NP/Estane. In addition, ellipsometry conclusively limited the size of the pure acetaminophen layer beneath the polymer to 15nm at most, and more likely as thin as 6nm. Thus the remaining acetaminophen shown in Fig. 4.7 could only be a result of chemical dissolution and intermixing with the polymer.

By contrast, neither ellipsometry nor reflectometry identified significant acetaminophen dissolution into the NP/Estane. Several interpretations could be hypothesized but the most likely is that the acetaminophen film may have simply dissolved more quickly when dip coated with the plasticized polymer. This could either be a function of the time the sample was immersed in solution prior to deposition of the polymer film or be evidence of the effect of the plasticizer on solubility. Preliminary studies on the solubility of acetaminophen in both Estane-MEK and NP/Estane-MEK solutions have revealed some differences in dissolution behavior. It is probable that the nitroplasticizer is responsible for the difference in interfacial structure, though another possibility is that the presence of acetaminophen could be masked by the high SLD value of the bulk plasticized polymer. However, in this case there should have been at least a slight

fluctuation in the constant SLD of the polymer. Either way, a complex interphase region is observed in both the plasticized and non-plasticized layered samples. The observation of this interphase region is critically important for relating microstructure to mechanical properties, particularly in MEK-soluble explosives like HMX. The complexity of the interface shows that thermodynamic surface energy adhesion arguments are incomplete for these composites. Grain-scale models can use this type of information to more accurately reproduce experimentally observed PBX failure.

While the pharmaceutical composites showed much simpler interfacial structure, and were also similar to each other, a couple key observations should be noted. First, the sulfamerazine has a larger intermixing region in HPC than the acetaminophen despite the ellipsometry models suggesting acetaminophen should have more intermixing. Second, the SLD for the polymer is higher in the sulfamerazine case. Both cases are likely a function of solubility differences between acetaminophen and sulfamerazine in HPC-ethanol solutions. Roughness of the films could also play a role – if the sulfamerazine film was substantially rougher, for example, the interphase region would likely be larger.

Both PBX and pharmaceutical composites can benefit from using NR as a characterization tool. NR provides a way to study the relationship between processing and structure, exemplified here by the difference between Estane and NP/Estane at the acetaminophen interface. The structural causes for undesired mechanical behavior in such materials could be studied in detail with the techniques shown here and perhaps lead to optimization of formulation conditions for improved performance.

4.5. Conclusions

Understanding the interfacial behavior in a molecular composite is important for explosives and pharmaceutical materials. In this work, neutron reflectometry, infrared spectroscopy and ellipsometry have been utilized in concert to examine the interfacial structure of a model acetaminophen-Estane system. The roughness and solubility of the acetaminophen film contribute to the formation of an interphase region when coated with the polymer. Introduction of a plasticizing agent alters the structure of this interphase by concentrating at the interface. These results have important ramifications for the mechanical behavior and damage propagation models currently employed by the explosives community. These results may also be useful for similar organic crystal – polymer composites of pharmaceutical interest. This procedure for measuring interfacial properties of molecular composites provides a path for analyzing mechanical behavior and a link between processing and structure.

References

[1] I Krycer, DG Pope, JA Hersey. An evaluation of tablet binding agents part I. Solution binders. Powder Technol. 34 (1), 1983, 39-51.

[2] A Faure, P York, RC Rowe. Process control and scale-up of pharmaceutical wet granulation processes: a review. European Journal of Pharmaceutics and Biopharmaceutics. 52 (3), 2001, 269-77.

[3] C Bacher, PM Olsen, P Bertelsen, JM Sonnergaard. Compressibility and compactibility of granules produced by wet and dry granulation. Int J Pharm. 358 (1-2), 2008, 69-74.

[4] P York. Solid-state properties of powders in the formulation and processing of solid dosage forms. Int J Pharm. 14 (1), 1983, 1-28.

[5] K Gowthamarajan, GKP Kumar, NB Gaikwad, B Suresh. Preliminary study of Anacardium occidentale gum as binder in formulation of paracetamol tablets. Carbohydr Polym. In Press, Corrected Proof, 2010.

[6] J-H Guo, GW Skinner, WW Harcum, PE Barnum. Pharmaceutical applications of naturally occurring water-soluble polymers. Pharmaceutical Science & Technology Today. 1 (6), 1998, 254-61.

[7] T Cutt, JT Fell, PJ Rue, MS Spring. Granulation and compaction of a model system. III. Compaction properties of the granules. Int J Pharm. 49 (2), 1989, 157-61.

[8] S Jain. Mechanical properties of powders for compaction and tableting: an overview. Pharmaceutical Science & Technology Today. 2 (1), 1999, 20-31.

[9] G Perfetti, T Aubert, WJ Wildeboer, GMH Meesters. Influence of handling and storage conditions on morphological and mechanical properties of polymer-coated particles: characterization and modeling. Powder Technol. 206 (1-2), 2011, 99-111.

[10] E James. The Development of Plastic-Bonded Explosives. UCRL-12439-T. Livermore, CA: Lawrence Radiation Laboratory; 1965. p. 15.

[11] PJ Rae, SJP Palmer, HT Goldrein, JE Field, AL Lewis. Quasi-static studies of the deformation and failure of PBX 9501. Proc R Soc London, Ser A. 458 (2025), 2002, 2227-42.

[12] JK Dienes, QH Zuo, JD Kershner. Impact initiation of explosives and propellants via statistical crack mechanics. Journal of the Mechanics and Physics of Solids. 54 (6), 2006, 1237-75.

[13] HL Berghout, SF Son, CB Skidmore, DJ Idar, BW Asay. Combustion of damaged PBX 9501 explosive. Thermochim Acta. 384 (1-2), 2002, 261-77.

[14] JG Bennett, KS Haberman, JN Johnson, BW Asay. A constitutive model for the non-shock ignition and mechanical response of high explosives. Journal of the Mechanics and Physics of Solids. 46 (12), 1998, 2303-22.

[15] WC Davis, LG Hill. Joints, Cracks, Holes, and Gaps in Detonating Explosives. Twelfth Detonation Symposium: International Detonation Symposium; 2002.

[16] H Weiss. Adhesion of advanced overlay coatings: mechanisms and quantitative assessment. Surf Coat Technol. 71 (2), 1995, 201-7.

[17] JT Mang, RP Hjelm, EB Orler, DA Wrobleski. Small-Angle Neutron Scattering of a Solvent-Swollen Segmented Polyurethane as a Probe of Solvent Distribution and Polymer Domain Composition. Macromolecules. 41 (12), 2008, 4358-70.

[18] S Wu. Polymer Interface and Adhesion. New York: Marcel Dekker, Inc.; 1982.

[19] JD Yeager, AM Dattelbaum, EB Orler, DF Bahr, DM Dattelbaum. Adhesive properties of some fluoropolymer binders with the insensitive explosive 1,3,5-triamino-2,4,6-trinitrobenzene (TATB). J Colloid Interface Sci. 352 (2), 2010, 535-41.

[20] W Yan-Qing, H Feng-Lei. A micromechanical model for predicting combined damage of particles and interface debonding in PBX explosives. Mech Mater. 41 (1), 2009, 27-47.

[21] J Xiao, H Huang, J Li, H Zhang, W Zhu, H Xiao. Computation of interface interactions and mechanical properties of HMX-based PBX with Estane 5703 from atomic simulation. Journal of Materials Science. 43 (17), 2008, 5685-91.

[22] FPA Fabbiani, CR Pulham. High-pressure studies of pharmaceutical compounds and energetic materials. Chem Soc Rev. 35 (10), 2006, 932-42.

[23] B Singh, LK Chaturvedi, PN Gadhikar. A Survey on the Cyclotetramethylene Telranitramine(HMX) Defence Science Journal. 28 (1), 1978, 41-50.

[24] C Sun, DJW Grant. Influence of Crystal Structure on the Tableting Properties of Sulfamerazine Polymorphs. Pharm Res. 18 (3), 2001, 274-80.

[25] S Roy, KS Alexander, AT Riga, K Chatterjee. Characterization of physical mixtures and directly compressed tablets of sulfamerazine polymorphs: Implications on in vitro release characteristics. J Pharm Sci. 92 (4), 2003, 747-59.

[26] GG Zhang, C Gu, MT Zell, RT Burkhardt, EJ Munson, DJ Grant. Crystallization and transitions of sulfamerazine polymorphs. J Pharm Sci. 91 (4), 2002, 1089-100.

[27] KW Chau, PH Geil. Domain morphology in polyurethanes. Polymer. 26 (4), 1985, 490-500.

[28] GD Smith, D Bedrov, O Byutner, O Borodin, C Ayyagari, TD Sewell. A Quantum-Chemistry-Based Potential for a Poly(ester urethane). The Journal of Physical Chemistry A. 107 (38), 2003, 7552-60.

[29] ML Coote, DH Gordon, LR Hutchings, RW Richards, RM Dalgliesh. Neutron reflectometry investigation of polymer-polymer reactions at the interface between immiscible polymers. Polymer. 44 (25), 2003, 7689-700.

[30] M Geoghegan, RAL Jones, RS Payne, P Sakellariou, AS Clough, J Penfold. Lamellar structure in a thin polymer blend film. Polymer. 35 (10), 1994, 2019-27.

[31] Y Zhang, W Li, B Tang, S Ge, X Hu, MH Rafailovich, et al. Interfacial properties of elastomer blends as studied by neutron reflectivity. Polymer. 42 (21), 2001, 9133-41.

[32] TP Russell. On the reflectivity of polymers: Neutrons and X-rays. Physica B: Condensed Matter. 221 (1-4), 1996, 267-83.

[33] GS Smith, CB Skidmore, PM Howe, J Majewski. Diffusion, evaporation, and surface enrichment of a plasticizing additive in an annealed polymer thin film. J Polym Sci, Part B: Polym Phys. 42 (17), 2004, 3258-66.

[34] M Erber, A Khalyavina, KJ Eichhorn, BI Voit. Variations in the glass transition temperature of polyester with special architectures confined in thin films. Polymer. 51 (1), 129-35.

[35] G Nichols, CS Frampton. Physicochemical characterization of the orthorhombic polymorph of paracetamol crystallized from solution. J Pharm Sci. 87 (6), 1998, 684-93.

[36] J Guévremont, A Ajji, KC Cole, MM Dumoulin. Orientation and conformation in poly(ethylene terephthalate) with low draw ratios as characterized by specular reflection infra-red spectroscopy. Polymer. 36 (17), 1995, 3385-92.

[37] A Nelson. Co-refinement of multiple-contrast neutron/X-ray reflectivity data using MOTOFIT. J Appl Crystallogr. 39 (2), 2006, 273-6.

[38] DG Bucknall, JS Higgins, J Penfold, S Rostami. Segregation behaviour of deuterated poly(styrene-block-methyl methacrylate) diblock copolymer in the presence of poly(methyl methacrylate) homopolymer. Polymer. 34 (3), 1993, 451-8.

[39] S Ioan, D Macocinschi, D Filip, A Taranu. Specific refractive index increments of segmented poly(ester urethane)s. Polym Test. 21 (7), 2002, 757-62.

CHAPTER FIVE

MECHANICAL CHARACTERIZATION OF SIMULATED PLASTIC-BONDED EXPLOSIVE MATERIALS

This chapter presents results from two methods of mechanically characterizing the interface in the simulated plastic-bonded explosives previously examined in this dissertation. Nanoindentation was used because it is sensitive to small changes in mechanical properties even at the nano-scale and because the indenter tip pressing through polymer into crystal could be used to represent crystal-crystal interactions in actual formulations. An island delamination test was also used to study the effect of polymer properties on apparent adhesion strength.

5.1. Introduction

Mechanical deformation and failure of plastic-bonded explosives (PBX) is a critical area of research for the Department of Energy (DOE) and the Department of Defense (DOD). Typical crack propagation under applied loading proceeds along the interface between explosive crystals and the polymer binder [1-3]. This delamination of crystals from the polymer is a potential concern for off-normal (e.g. unintentional) deflagration and detonation of the explosive [4, 5]. Deformation and delamination result in regions of local anisotropy which can change the detonative properties of the PBX [6] and result in hot spot formation under relatively mild mechanical or thermal insult [7-9]. Thus the interaction between crystals and the binder is not only responsible for mechanical stability during normal use but also for sensitivity in off-normal use. The interface between the two materials is of critical importance but has not been extensively examined historically.

Previous chapters in this dissertation have examined the chemistry of the interface, focusing on thermodynamic interaction (Chapter 3) and interface / interphase structure (Chapter 4). While the results have been instructive, mechanical characterization of the interface would be directly applicable to failure and damage models currently employed by the explosives community. Ideally, the difference in interfacial chemistry between Estane-acetaminophen and nitroplasticized (NP) Estane-acetaminophen discovered by neutron reflectometry would be verified by a mechanical characterization. Such mechanical data would complement the structural information and result in a coherent picture or model of damage and delamination at the nano-scale.

In this chapter, nanoindentation is used to probe the mechanical properties of idealized PBX materials – specifically, acetaminophen single crystals coated with approximately 400 nm of polymer. Nanoindentation is a well-characterized technique for probing mechanical properties of materials on the micro-to-nano scale. Indentation has been applied in particular to interfacial characterization in traditional composites [10] and elastically-mismatched film systems [11-13], as well as for elastic modulus and hardness information in complex anisotropic materials like the explosive cyclotrimethylene trinitramine (RDX) [14]. Figure 5.1 schematically describes the two benefits of indenting the acetaminophen-polymer samples. First, the hard indenter tip pressing through the thin polymer and into the acetaminophen crystal is an analogue for crystal-polymer-crystal interaction which occurs in the pressed PBX composites under compressive loading. Second, the micron-scale sharpness of the indenter tip may be able to sense the interphase regions which were observed with neutron reflectometry.

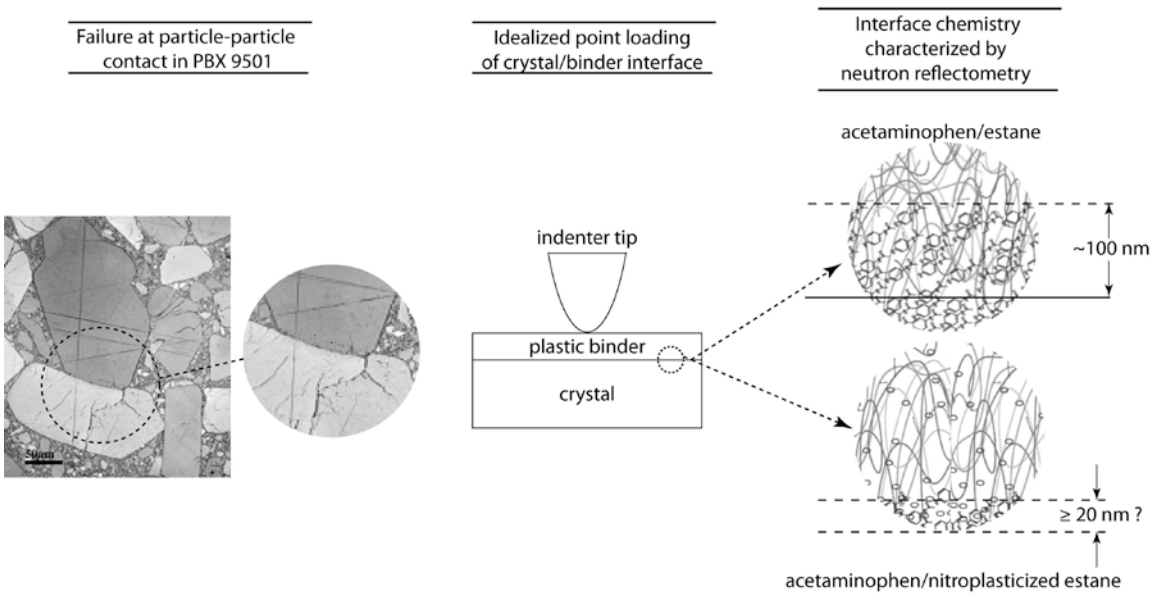

Figure 5.1. Schematic of how nanoindentation can be used to understand crystal-crystal interactions in an idealized manner, and how it can potentially sense a difference in interfacial properties between the two Estane-acetaminophen composites characterized in Chapter 4.

While small-scale mechanical deformation events have important ramifications for hot spot formation and crack initiation, macro-scale mechanical properties are critical for PBX manufacturing and application. Quality control in production, machinability, and pellet compaction may all be affected by deformation and crack propagation. In addition, aging due to fatigue and thermal cycling may be affected by macroscopic cracking and deformation. The island delamination test first outlined by Lu et al. is proposed to investigate macro-scale adhesion. Figure 5.2 shows a schematic of the test.

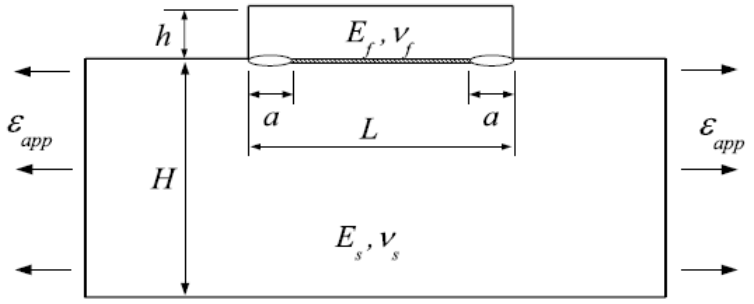

Figure 5.2. Schematic of island delamination test [15]

The crucial test parameters for calculating adhesion are all shown in Figure. 5.2. *H* and *h* are the thicknesses of substrate and island respectively, *L* is the length of the island, *E* is the elastic modulus, υ is the Poisson's ratio, and ε is the applied strain. It should be noted that the original purpose of Lu's paper was to identify the critical island size for delamination, not to measure the interfacial toughness. Indeed, no literature has been found which uses this test to experimentally characterize the bimaterial interface. The prospect of developing Lu's theory into a viable test which can be compared to more traditional methods is very intriguing. The main advantage is that the island or crystal experiences little to no strain, making the test advantageous for brittle crystalline materials such as acetaminophen or RDX.

5.2. Experimental

5.2.1 Sample preparation

The samples were prepared in ways quite similar to experimental methods previously in this dissertation. Single crystals of acetaminophen were grown from saturated water solutions as in Chapter 2. Crystals which appeared flat under 500x optical inspection were glued to stainless steel pucks for indentation. After the glue dried, the crystals were dip-coated with either

NP/Estane or Estane in a similar manner to the samples in Chapter 4. The solutions were somewhat more concentrated than before, now 10% by weight in methyl ethyl ketone in each case, in order to produce thicker films from dip-coating. Ellipsometry was used to measure the film thickness on the samples as described in Chapter 4. At least four days lapsed between dip-coating and indentation measurements in order to give the films sufficient time to dry.

5.2.2 Nanoindentation

Nanoindentation was performed on an MTS NanoXP (MTS Systems Corp., Knoxville, TN) in the continuous stiffness measurement (CSM) mode. A general review of nanoindentation as related to molecular crystals can be found in Ramos et al [16], while the CSM method is addressed by Oliver and Pharr [17]. Briefly, the CSM applied slowly increasing cyclic loading, allowing for stiffness and hardness measurements to be taken nearly continuously during penetration of the tip into the sample. The stiffness (*S*) of the sample is given by equation 5.1,

$$S = \frac{dP}{dh} = \beta \frac{2}{\sqrt{\pi}} E_{eff} \sqrt{A} \qquad (1)$$

where *P* is the load, *h* is the displacement, *A* is the contact area between the tip and the sample, β is a dimensionless constant approximately equal to unity, and E_{eff} is the effective elastic modulus. Note that dP/dh is measured during the unloading portion of the curve as the material elastically recovers [17]. E_{eff} is a function of the tip and sample elastic properties (defined earlier) and is given by Equation 5.2.

$$\frac{1}{E_{eff}} = \frac{\left(1 - \nu_{sample}^2\right)}{E_{sample}} + \frac{\left(1 - \nu_{indenter}^2\right)}{E_{indenter}} \qquad (2)$$

For these indentation experiments, both Berkovich and cube corner tip geometries were used, though the focus in this chapter is on the 10μm radius cube corner.

5.2.3 Island Delamination and Digital Image Correlation

The island delamination test samples consisted of polymer dog bones bonded to a glass island or an acetaminophen crystal. The bonding was accomplished by partially dissolving the polymer with an appropriate solvent. The polymers chosen were NP/Estane and Kel-F 800, a fluoropolymer studied in some detail in Chapter 2. Kel-F is several orders of magnitude stiffer than Estane and was chosen instead of Estane to give a larger range of polymer properties to test.

Bonded samples were spray painted on one side with black paint to provide a matrix for the test. Each individual spot was tracked during tensile testing with a camera to provide local strain information. This technique is known as digital image correlation (DIC) and is explained in detail by Liu et al [18].

5.3. Results and Discussion

5.3.1 Composite Modulus and Hardness Measured with Indentation

CSM allows for continuous measurement of mechanical properties during the indent. This allows for determination of elastic modulus and hardness as a function of depth for each indent, which is useful for non-homogeneous materials such as a film-substrate system. Figure 5.3 compares the elastic modulus of Estane and plasticized Estane films as a function of indenter contact radius and displacement into the sample, while Figure 5.4 compares the hardness of the two samples. Both films were approximately 420nm thick, and indentation was performed with a cube corner tip to various target depths in the samples. The contact radius is plotted along with the

displacement into the sample and is found by assuming the indenter has a circular cross section. Thus the calibrated contact area is equal to the quantity of the contact radius squared times pi.

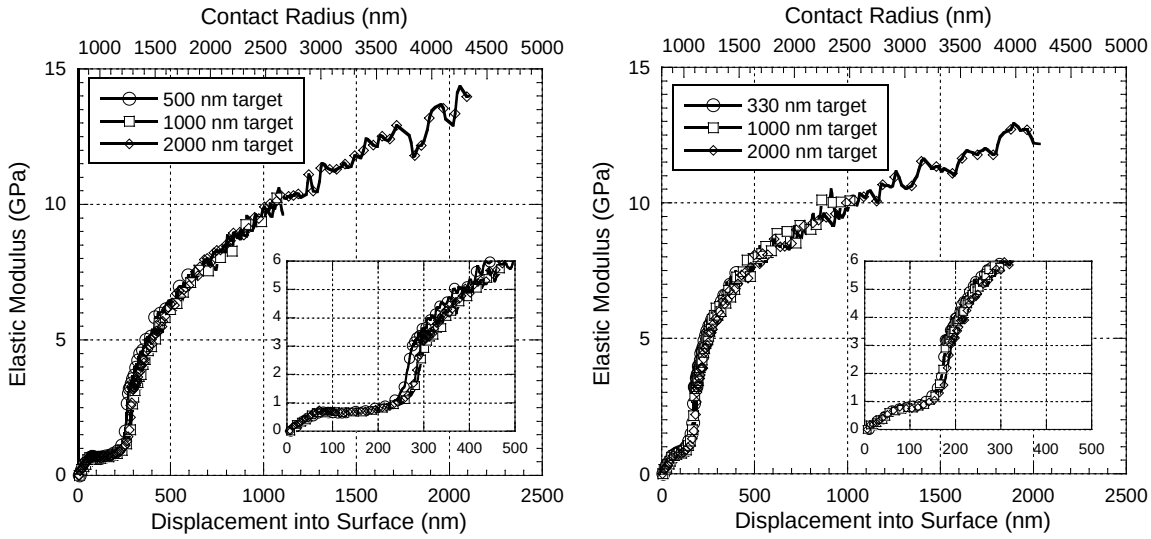

Figure 5.3. Elastic modulus as a function of indentation depth and contact radius for Estane (a) and plasticized Estane (b) coating acetaminophen, with inset magnification of region of interest.

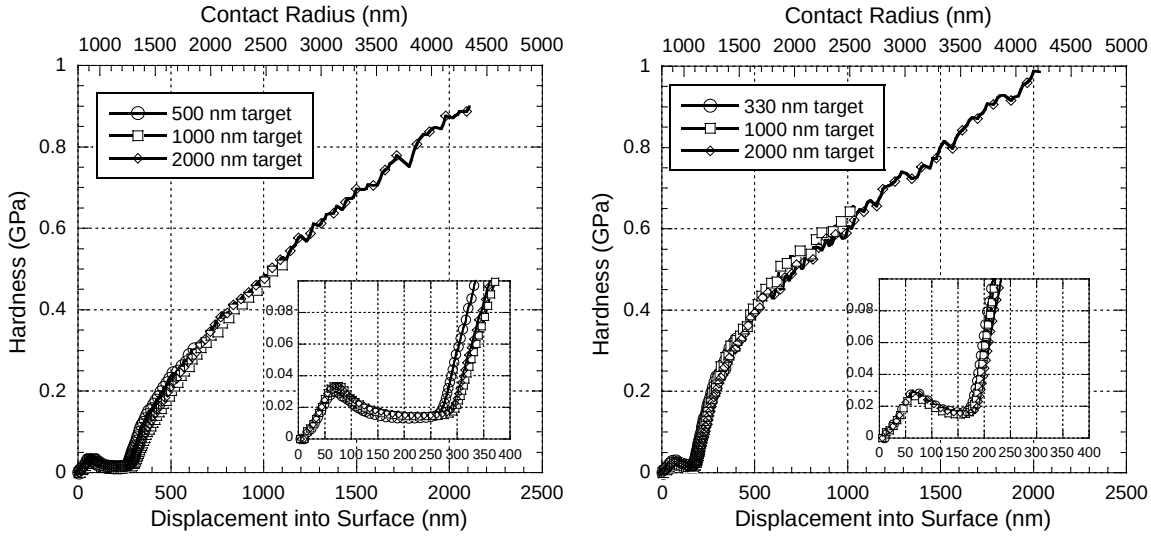

Figure 5.4. Hardness as a function of indentation depth and contact radius for Estane (a) and plasticized Estane (b) coating acetaminophen, with inset magnification of region of interest.

Some general observations are immediately apparent and will be explained in order of increasing displacement into the film. First, all samples showed a small increase in modulus and hardness up to approximately 50 nm. This is almost certainly an artifact of the indentation software and the tip calibration rather than true data. In fact, the data is probably not reliable until 100 nm displacement. After an initial soft and compliant plateau, both composites showed dramatic increases in mechanical properties as a function of depth into the sample. Recalling that the films are nearly identical in thickness, the difference in depth of the initial plateau between the two samples may be meaningful. It is possible, however, that this is only due to the high compliance of the NP/Estane, and results from the tip not sensing enough resistance to indentation to trigger the surface detection algorithm in the software. The sharp increase in mechanical properties at the end of the plateau results from the tip sensing the stiff acetaminophen substrate. All indents for a given sample appeared to sense the substrate at the same rate, but comparing the two samples to each other is instructive. The 2000 nm indents for the Estane-acetaminophen and NP/Estane-acetaminophen sample are shown in Figure 5.5.

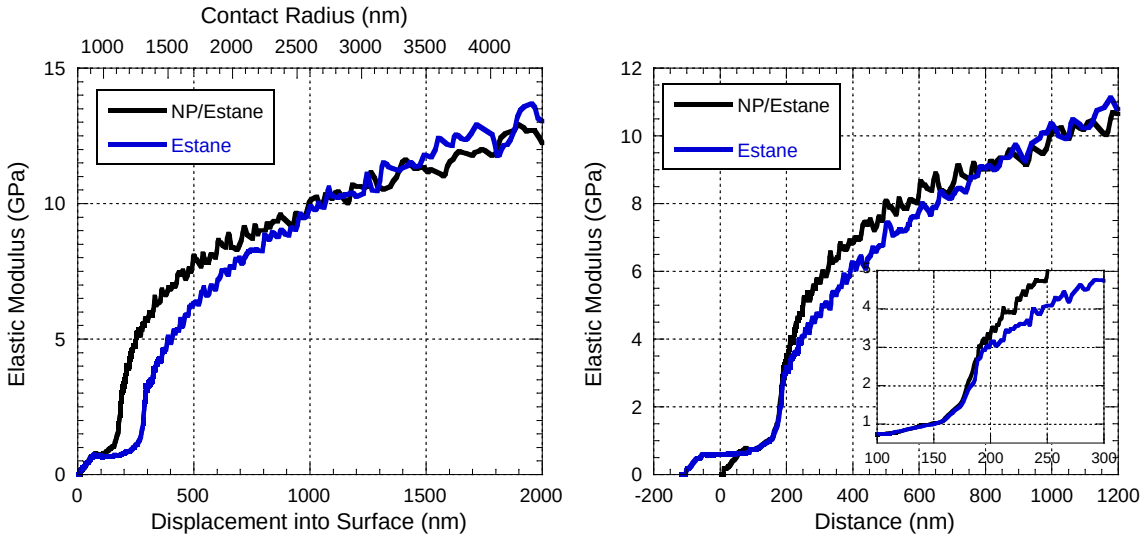

Figure 5.5. Elastic modulus of composites re-plotted from Figs. 5.3a and 5.3b (a), and plotted again with the Estane curve artificially offset to match initial increase in modulus (b). The region of interest is magnified and is inset in (b).

The slope of the increase in elastic modulus (as well as the hardness) is steeper for the NP/Estane. This is readily observed in Fig. 5.5b in particular, where the raw Estane data has been offset to match initial substrate sensing with the NP/Estane. The steeper slope indicates that the tip is sensing the acetaminophen substrate more quickly in the NP/Estane composite. There are two possible explanations for this behavior when the neutron reflectometry results are taken into account: 1) the plasticizer in the NP/Estane makes the NP/Estane-acetaminophen interface stiffer or 2) the Estane interaction with the acetaminophen makes the Estane-acetaminophen interface more compliant. Noting the unlikelihood of the plasticizer concentrating at the interface resulting in a stiffer composite, the most probable explanation is that the Estane effectively softens the apparent surface of the acetaminophen. More precisely, the large and diffuse interface in the

Estane-acetaminophen sample distributes applied loads more effectively than the small and sharp interface in the NP/Estane composite.

5.3.2 Optical microscopy of residual deformation after indentation

Like the quantitative indentation data, polarized light microscopy reveals differences in deformation behavior between the two samples. Using polarized light to characterize these materials is extremely useful because contrast can be high between the amorphous polymer and optically active crystals. Further, since the polymers are thin, damage to the crystalline substrates is easy to observe. Figure 5.6 shows optical microscopy images with bright field, dark field, and polarized light, while also providing qualitative information about the indentation of plasticized Estane on acetaminophen. The indents shown in the figure were targeted for 2000 nm depth.

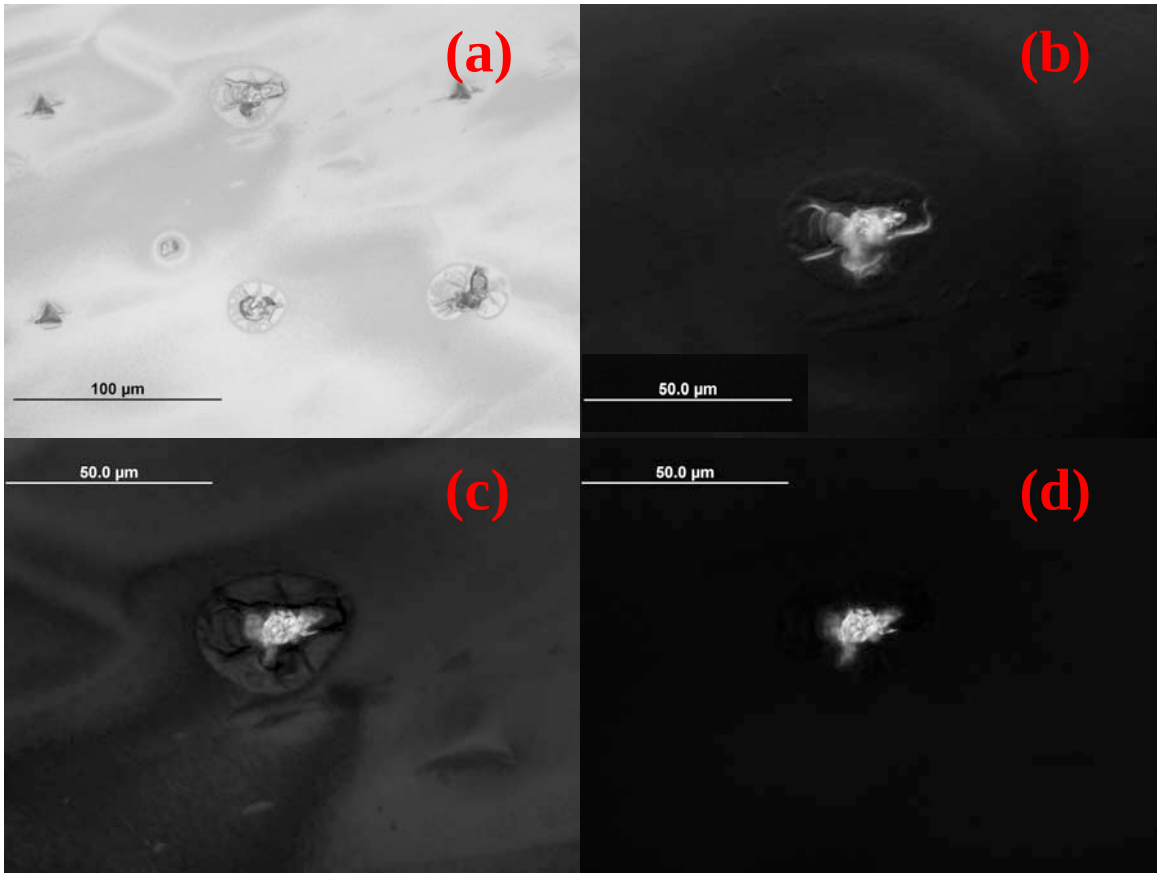

Figure 5.6. Post-indentation microscopy of NP/Estane-acetaminophen. Lower magnification (50x) bright field imaging of several indents (a) and 100x magnification of top center indent in (a) with dark field imaging (b), one level of polarization (c), and a different polarization which negates polymer contribution (d). Contours in the polymer are indicative of thickness variation, except for in (b) where the large faint ring is an image artifact. The blisters surrounding some indents indicate delamination of the polymer from the acetaminophen.

Fig. 5.6a shows several indents in the plasticized polymer film. All six of the observed indents show cracking of the substrate, an unsurprising result of indenting to a depth of approximately 1600 nm into the substrate. Some of the indents also show a blister, or a region of polymer

apparently pulled up from the surface. The top center indent in Fig. 5.6a is shown with several imaging modes in Fig. 5.6b-d. Dark field imaging emphasizes surface asperities, while the two polarizations can either enhance (Fig. 5.6c) or negate (Fig. 5.6d) the polymer's contribution to reflected light.

Figure 5.7 shows the indentation deformation on the non-plasticized Estane-acetaminophen. It should be noted that the films are approximately the same thickness, and indentation was performed to the same depth with the same indenter tip.

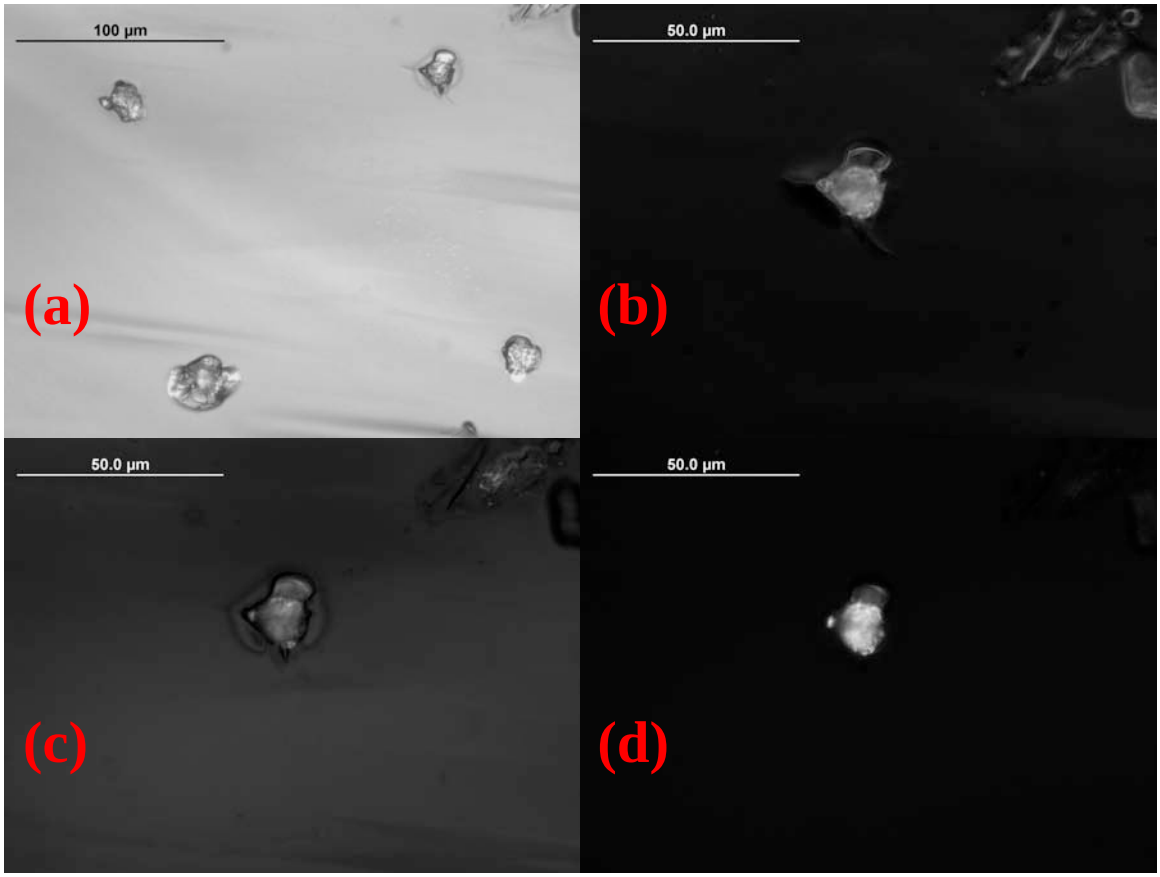

Figure 5.7. Post-indentation microscopy of Estane-acetaminophen. Lower magnification (50x) bright field imaging of several indents (a) and 100x magnification of top right indent in (a) with dark field imaging (b), one level of polarization (c), and a different polarization which negates polymer contribution (d). In contrast to the plasticized Estane film, little to no blister impression is observable.

Figs 5.6 & 5.7 are typical indentation images, and the delamination behavior in each is quite repeatable. While not every indent in the NP/Estane sample produced large blisters in the film, indicating that delamination may be a somewhat random event, not one indent in the non-plasticized Estane resulted in blister formation to a larger extent than shown in Fig 5.6.

Indentation was also performed with a Berkovich tip to investigate whether the delamination required a certain activation zone. The cube corner is a sharper tip than the Berkovich, and so projects a different stress field ahead of the tip [19-21]. The conical tip is self-symmetric, and indentation studies on bare acetaminophen have shown that the symmetry of the indenter tip can play a large role in crack formation. Figure 5.8 shows a polarized light micrographs of the Berkovich impressions. Note the large amount of polymer deformation immediately surrounding the indent.

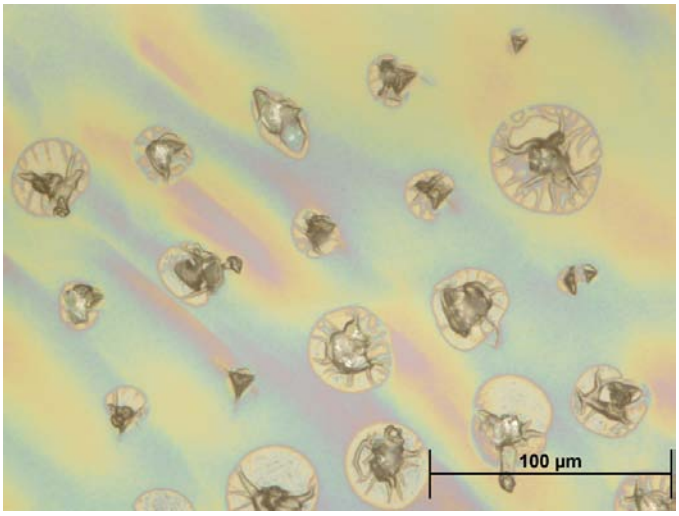

Figure 5.8. Polarized light micrographs of Berkovich indents to 2000nm in the 400nm plasticized Estane film.

\

In general, the quantitative observation of indentation impressions reinforce the indentation data and neutron reflectometry results. The Estane sample, which has a large, diffuse interface that tends to dissipate energy more rapidly, shows less (or no) polymer delamination. Meanwhile, the sharp and small interfacial region in the NP/Estane sample tends to allow delamination quite easily under applied loading. This has important implications for sensitivity, hot spot formation and crack initiation in PBX materials.

5.3.3 Initial Results from Island Delamination Testing

Preliminary results from island delamination testing of glass bonded to Kel-F 800 are shown in Figure 5.9.

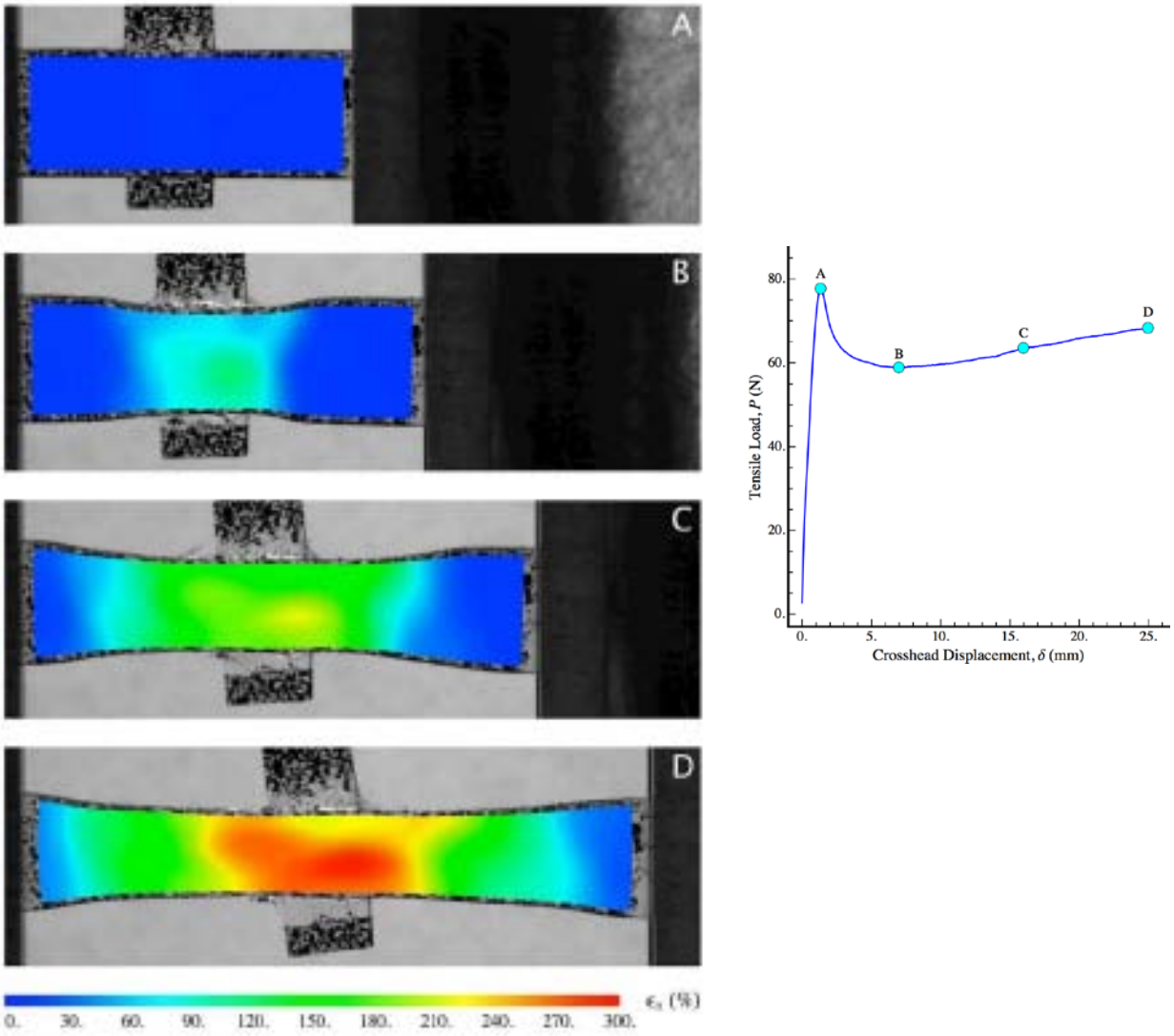

Figure 5.9. Tensile strain along the longitudinal direction mapped over photographs of the Kel-F 800-glass sample at specified points in the loading history. The load-displacement curve is shown to the right, with the labeled points corresponding to the strain maps.

Kel-F 800 is a relatively stiff polymer with an expected tensile modulus of 960 MPa [3]. Estane has a modulus of approximately 10 MPa, and NP/Estane is approximately 1 MPa, meaning Kel-F is ~1000x stiffer than NP/Estane. The strain map for the Kel-F test shown above tends to look much like the strain distribution for a regular tensile test. The bonding of the glass does not appear to affect the deformation of the polymer at all. By contrast, Figure 5.10 presents the DIC results from NP/Estane bonded to acetaminophen, and does show unusual deformation behavior.

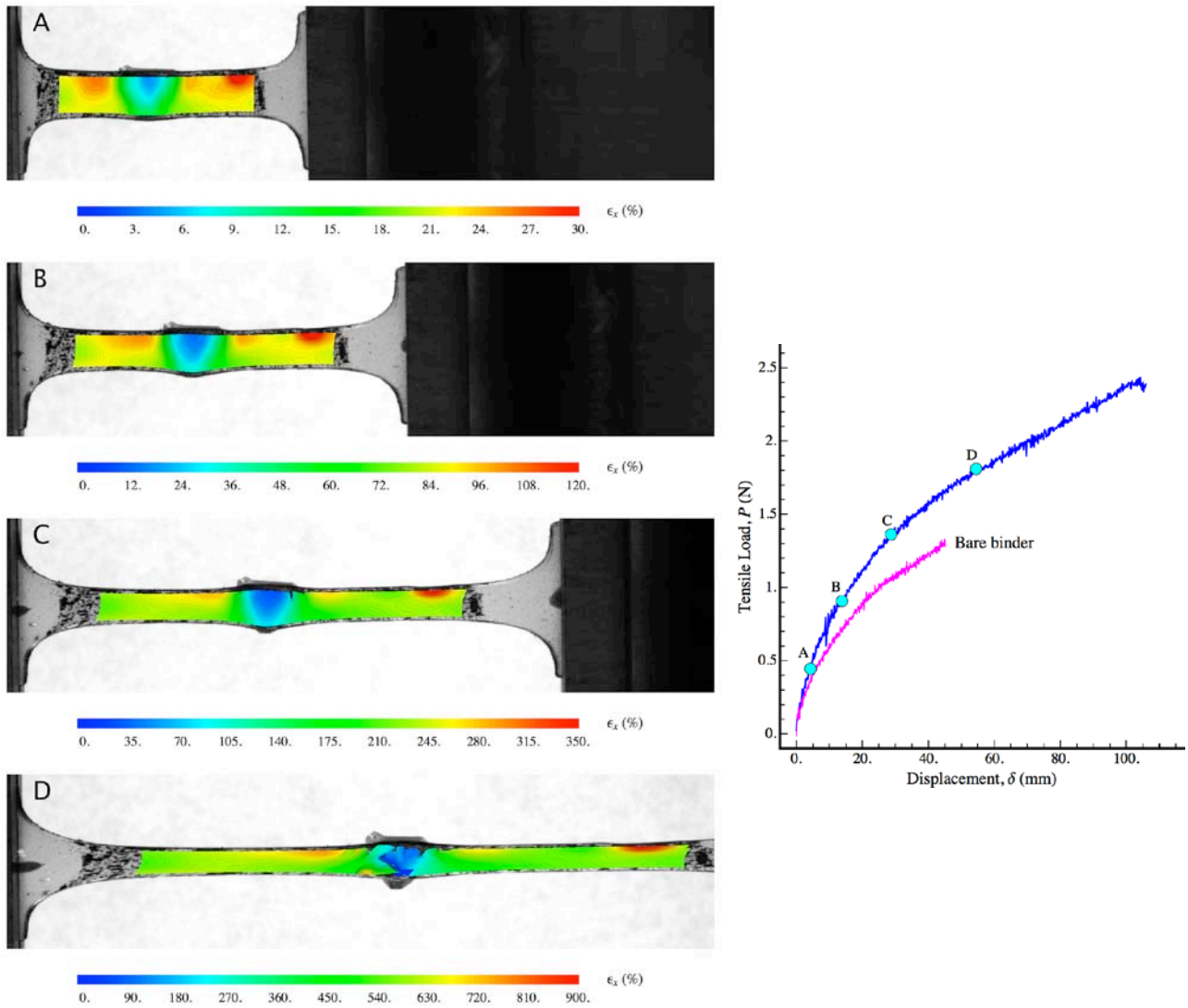

Figure 5.10. Tensile strain along the longitudinal direction mapped over photographs of the NP/Estane-acetaminophen sample at specified points in the loading history. Note the triangular shape of the crystal and its effect on the strain distribution in the center of the sample. The load-displacement curve is shown to the right, with the labeled points corresponding to the strain maps.

The acetaminophen, which is an order of magnitude stiffer than the polymer, appears to strengthen the polymer. This is evidenced by the low strain in the center of the sample. Note that the strain color scale is adjusted for each image – use of only one strain scale shows the advancement of a particular zone of a given strain across the face of the acetaminophen over time. For example, a movie composed of multiple strain images would show a 10% strain band in the same shape as the acetaminophen crystal moving from the edges of the crystal to the center over time. It is quite probable that one of these strain bands represents the critical strain for delaminating the sample. Following the test to 150% sample strain (overall, not local, as determined by sample dimensions and cross-head speed), observation of the sample indicated the acetaminophen crystal had completely delaminated.

In comparison to the glass-Kel-F composite, a few questions remain to be answered. Was the test truly representative of the interfacial nature of the respective materials, or were other factors more important? Such factors could be the relative elastic mismatch (glass-Kel-F has a much higher mismatch), the shape of the bonded island (rectangular interfacial area vs. triangular), the percent crystallinity of the Kel-F polymer (unknown but likely >20%), or inconsistencies in sample preparation. While many details must be worked out before extensive use of this test can begin, the advantages and possibilities of the test are clear.

5.4 Conclusions

Nanoindentation of acetaminophen-polymer composites simulated particle-particle crack initiation though polymer binder in PBX materials and revealed several insights into crack initiation and crystal delamination. For a given film thickness, indenter tip and indentation depth,

the Estane film delaminates to a lesser extent than the NP/Estane, and the indenter tip senses the substrate more slowly than in NP/Estane. Delamination only occurs when the substrate has been substantially cracked. However, plastic deformation is evident even at low loads, and the stress-absorbing nature of the polymer is clear from elastic modulus measurements. The contrast in interfacial chemistry between the two composites is the most likely explanation for the delamination and mechanical property differences. In addition, the island delamination test also revealed unintuitive mechanical response in simulated PBX composites and shows promise as an analytical tool for future use. A convenient method for evaluating the usefulness of the island delamination test would be to compare Estane to NP/Estane bonded with acetaminophen. Any differences in behavior between these two samples would provide a further link between interfacial structure and mechanical behavior. In both mechanical characterization methods presented here, an understanding of the interfacial chemistry provides key insight into interpretation of mechanical behavior, and these methods should be applied to actual PBX formulations.

References

[1] PJ Rae, HT Goldrein, SJP Palmer, JE Field, AL Lewis. Quasi-Static Studies of the Deformation and Failure of β-HMX Based Polymer Bonded Explosives. Proceedings: Mathematical, Physical and Engineering Sciences. 458 (2019), 2002, 743-62.

[2] SJP Palmer, DM Williamson, WG Proud. Adhesion Studies between HMX and EDC37 Binder System. AIP Conference Proceedings. 845 (1), 2006, 917-20.

[3] SJP Palmer, JE Field, JM Huntley. Deformation, Strengths and Strains to Failure of Polymer Bonded Explosives. Proc R Soc London, Ser A. 440 (1909), 1993, 399-419.

[4] AM Mellor, DA Wiegand, KB Isom. Hot spot histories in energetic materials. Combust Flame. 101 (1-2), 1995, 26-8.

[5] HL Berghout, SF Son, BW Asay. Convective burning in gaps of PBX 9501. Proceedings of the Combustion Institute. 28 (1), 2000, 911-7.

[6] HL Berghout, SF Son, CB Skidmore, DJ Idar, BW Asay. Combustion of damaged PBX 9501 explosive. Thermochim Acta. 384 (1-2), 2002, 261-77.

[7] JK Dienes. Frictional Hot-Spots and Propellant Sensitivity. Materials Research Society. Boston, MA1984. p. 373-81.

[8] FP Bowden, AD Yoffe. Initiation and Growth of Explosion in Liquids and Solids. Cambridge, UK: Cambridge University Press; 1952.

[9] WC Davis, LG Hill. Joints, Cracks, Holes, and Gaps in Detonating Explosives. Twelfth Detonation Symposium: International Detonation Symposium; 2002.

[10] S-L Gao, E Mäder. Characterisation of interphase nanoscale property variations in glass fibre reinforced polypropylene and epoxy resin composites. Composites Part A: Applied Science and Manufacturing. 33 (4), 2002, 559-76.

[11] MJ Cordill, NR Moody, DF Bahr. The effects of plasticity on adhesion of hard films on ductile interlayers. Acta Mater. 53 (9), 2005, 2555-62.

[12] DF Bahr, JW Hoehn, NR Moody, WW Gerberich. Adhesion and acoustic emission analysis of failures in nitride films with a metal interlayer. Acta Mater. 45 (12), 1997, 5163-75.

[13] TD Nguyen, JD Yeager, DF Bahr, DP Adams, NR Moody. Nanoindentation of Compliant Substrate Systems: Effects of Geometry and Compliance. J Eng Mater Technol. 132 (2), 2010, 021001-7.

[14] KJ Ramos, DE Hooks, DF Bahr. Direct observation of plasticity and quantitative hardness measurements in single crystal cyclotrimethylene trinitramine by nanoindentation. Philosophical Magazine. 89 (27), 2009, 2381 - 402.

[15] N Lu, J Yoon, Z Suo. Delamination of stiff islands patterned on stretchable substrates. International Journal of Materials Research. 98, 2007, 717-22.

[16] KJ Ramos, DF Bahr. Mechanical behavior assessment of sucrose using nanoindentation. J Mater Res. 22 (7), 2007, 9.

[17] WC Oliver, GM Pharr. Measurement of hardness and elastic modulus by instrumented indentation: Advances in understanding and refinements to methodology. J Mater Res. 19 (1), 2004, 3-20.

[18] C Liu, DG Thompson. Macroscopic crack formation and extension in pristine and artificially aged PBX 9501. 14th International Detonation Symposium. Coeur d'Alene, ID2010.

[19] DJ Morris, SB Myers, RF Cook. Sharp probes of varying acuity: Instrumented indentation and fracture behavior. J Mater Res. 19 (1), 2004, 165-75.

[20] D Morris, R Cook. Radial Fracture During Indentation by Acute Probes: I, Description by an Indentation Wedging Model. International Journal of Fracture. 136 (1), 2005, 237-64-64.

[21] D Morris, A Vodnick, R Cook. Radial Fracture During Indentation by Acute Probes: II, Experimental Observations of Cube-corner and Vickers Indentation. International Journal of Fracture. 136 (1), 2005, 265-84.

CHAPTER SIX

SUMMARY AND CONCLUSIONS

This chapter presents an overview of the dissertation and summarizes the important discoveries.

6.1 Microstructural Characterization

While certain aspects of the microstructure of plastic-bonded explosive (PBX) materials have been well-characterized in the past, the research in this dissertation provided new insights. The high-speed synchrotron x-ray phase contrast imaging (PCI) study showed simulated, idealized composites could be studied at micron-level detail at microsecond exposure times. Synchrotron PCI had an effective source size many times larger than traditional laboratory sources, such as absorption radiography, providing higher contrast and effective resolution with no doping requirements even for low-Z materials. Inclusion of a dopant was not necessary for contrast but did reveal a different structure (i.e. structure of molding prills rather than crystals). The feasibility of dynamic study at high strain rates was demonstrated by measuring signal-to-noise ratios in static conditions and calculating the ratios for shorter exposure times and various beam profiles. The response of preexisting microstructure to shock loading should now be studied for these materials. Void nucleation and collapse, fracture delamination, and grain boundary / interface deformation may be studied with high temporal and spatial resolution. The general applicability of synchrotron PCI to other low-Z composites was also demonstrated.

The interfacial structure of several simulated plastic-bonded explosive composites was also studied in great detail. The ellipsometry and neutron reflectometry (NR) investigations provided

complementary interface / interphase information and could easily be applied to PBXs or pharmaceutical composites. NR provides a way to study the relationship between processing and structure, exemplified in this dissertation by the difference between Estane and NP/Estane at the acetaminophen interface. The roughness and solubility of the acetaminophen film contribute to the formation of an interphase region when coated with the polymer, but introduction of a plasticizing agent alters the structure of this interphase by concentrating at the interface. These findings were consistent with previous observations in the literature, both for plasticizer migration and for crystal dissolution in the presence of polar solvents, but additionally proved that many assumptions made in PBX mechanical behavior and damage propagation models are incomplete. NR is a powerful tool that investigates surface and interfacial structure at the nano-scale and should provide substantial information of use to the modeling community once applied to actual PBX formulations.

6.2 Linking Structure and Chemistry to Mechanical Properties

A series of binder candidates were evaluated for their adhesive interactions with several molecular crystals by measuring their surface energies with contact angle methods. The candidates were fluoropolymers with some degree of fluorine-hydrogen substitution and were intended for formulations involving the high explosive TATB. For comparison, the non-fluorinated PBX 9501 binder, NP/Estane, was evaluated as well. The surface and thermomechanical properties of the binders were studied systematically by varying copolymer compositions, but no strong correlations of the surface energies with backbone structure were found to exist across the series. By using the measured values of the surface energy of

acetaminophen, HMX, RDX and TATB, the work of adhesion of the binders was determined for a variety of scenarios. This parameter has implications for both processing (polymer wetting the crystal during formulation) and for composite failure. For example, the commonly observed failure mode of crystal-binder crack propagation indicates that adhesion is critical for composite durability. However, strong differences in wetting or adhesive properties between the binder candidates were not found. Other parameters, such as thermal or mechanical properties, were shown to be more important for determining which candidate should be used in a given formulation. All binders were found to exhibit similar surface properties to the PBX 9502 binder, Kel-F 800, and therefore may be sensible choices for substitution in PBX formulations. Of all the candidates, Oxy 461 and NP/Estane might be expected to show slightly improved adhesive strength to the molecular crystals of interest.

In contrast, the interfacial structure and chemistry of acetaminophen-polymer film systems was found to play a large role in mechanical properties of simulated composites. Nanoindentation of acetaminophen-polymer composites simulated the particle-particle crack initiation which is likely to occur in PBX materials under compression. The indentation revealed several insights into crack initiation and propagation at the crystal-binder interface as well as general deformation behavior. The NP/Estane film showed extensive deformation and delamination when compared to the Estane, and the indenter tip senses the substrate more quickly than for Estane. Interfacial crack initiation (i.e. polymer delamination) is driven by substrate cracking, which likely results in a complex stress state at the interface. However, plastic deformation is evident even at low loads, and the stress-absorbing nature of the polymer is clear from elastic modulus measurements.

The contrast in interfacial chemistry between the two composites is the most likely explanation for the delamination and mechanical property differences. The large, diffuse interphase found in the Estane-acetaminophen sample appeared to absorb or distribute stress more effectively than the small and sharp NP/Estane-acetaminophen interphase. The implications of these results for composite fracture toughness, sensitivity and explosive performance will be discussed in the next section. In addition to nanoindentation data, the island delamination test revealed unintuitive mechanical response in simulated PBX composites and shows promise as an analytical tool for future use. A future comparison of Estane-acetaminophen to NP/Estane-acetaminophen would be particularly instructive. Based on the indentation and NR results, it is possible to predict that the Estane-acetaminophen samples would exhibit better adhesion and therefore higher fracture toughness than the NP/Estane samples.

6.3 Future Applications to PBX Formulations and Similar Composites

The goal of this project was to develop a methodology for characterizing the microstructure of plastic-bonded explosives (PBX) and similar molecular composites, and to relate such structure to mechanical properties, with particular attention to material failure. The proposed methodology has been tested on simulated PBX composites and the viability of applying similar characterization to PBXs has been demonstrated. It may be instructive to consider the application of the simulated PBX results from this dissertation to actual formulations, PBX or otherwise, with the assumption that HMX or other molecular crystals may exhibit similar solubility and mechanical behavior to acetaminophen.

Consider the implications of inhomogeneities within a molecular composite, as covered in detail in Chapter 1. The composite must exhibit mechanical stability over a range of mechanical and thermal conditions, so strength and fracture toughness are important. Capping or other pharmaceutical tablet failure can delay production or, worse, result in unintended drug release profiles as drug release is a function of dissolution in a fluid and cracks cause the available surface area to change. In PBX materials, inhomogeneities can result in formation of hot spots in off-normal conditions, resulting in a more sensitive explosive. During intentional use of explosives, inhomogeneities can change the detonation front or reactive burn and result in non-useful and, at worst, unpredictable detonations. The mechanical and structural characterization of Estane-acetaminophen and NP/Estane-acetaminophen presented in this work thus allow for some conclusions on the importance of the interface.

Fracture toughness conclusions must consider the following factors: 1) the nature of the interface (e.g. a diffuse, well-adhered interface increases toughness); 2) the mechanical properties of the binder (e.g. higher compliance increases toughness); and 3) the relative amount of interfacial area, which is a function of particle size, shape, and weight percent in the formulation. Estane provides a much tougher interface with acetaminophen than NP/Estane does, but NP/Estane is approximately two orders of magnitude more compliant (modulus of 0.1 GPa compared to 10 GPa for Estane). For highly loaded formulations such as PBX 9501 (95 wt% HMX), the large amount of interfacial area probably favors use of Estane as a binder if the goal is to increase fracture toughness.

However, this does not mean that Estane formulations will be less sensitive than NP/Estane formulations. Consider the processing of PBX materials. The agglomerates are pressed into pellets at high pressure to minimize differences in density throughout the composite. The compression likely results in crack initiation from the faceted crystal edges coming into contact through the binder. A material with a relatively weak interface, in this case a formulation with NP/Estane, should propagate that crack along the interface because delamination is energetically favorable. A formulation using Estane, with a tough interface, might instead propagate the crack through the brittle crystal. Cracks within crystals are suspected to be extremely favorable for hot spot formation, and so use of Estane as a binder in PBX 9501 might shift the failure mode from delamination to crystal cracking and result in a more sensitive explosive. In pharmaceutical materials, no such safety issues exist, but changing the failure mode of the tablet may still have consequence for tabletability and dissolution profiles.

Perhaps the most important PBX implication of the dissimilar delamination behavior in the two composites is that the detonation front will be very different between the two and will be a function of the pre-existing microstructure. Crystal-crystal cracking from processing conditions will likely result in NP/Estane delamination in various areas of the PBX. Such delamination was not observed in the Estane composites, and so the NP/Estane composites probably have a much higher proportion of small volumetric inhomogeneities if all other processing parameters are equal. Similar inhomogeneities such as pores, voids, bubbles, or inclusions have all been shown to deleteriously affect the detonation, and it is reasonable to predict that a mildly stressed NP/Estane PBX would behave much less predictably than an equivalent Estane PBX during a

shock event. Future studies should investigate this scenario to validate the methodology presented over the course of this dissertation.

Most of the materials studied in this dissertation have direct similarities to PBX formulation materials. Outside of the various safety concerns with transporting high explosives to experiment sites, there is no practical reason why the characterization methodology cannot be applied to any number of PBX materials. Neutron and x-ray studies have been performed in some capacity in certain explosive materials previously. Ideally, these explosives can now be studied in a comprehensive manner to link formulation parameters to structure and properties, across multiple length scales and even during high-speed dynamic events. Even if experimentation with explosives is delayed due to safety concerns, the information gathered in this dissertation is directly applicable to existing PBX damage models with only limited assumptions required. Overall, this dissertation presents a comprehensive methodology to link structure to properties for PBXs and similar materials in an effort to fundamentally understand current experimental results and to design safer and more effective composites in the future.